NTNU

Department of Hydraulic and

Environmental Engineering

## M.Sc. in Hydropower Development

## Master Thesis

# Short term Distributed Hydrological Modelling of Gaula Catchment

Submitted by:

**Aynalem Tassachew Tsegaw**

**June 2010**

# FORWARD

This report, which is entitled "Short term Distributed Hydrological Modelling of Gaula Catchment", is submitted to the Department of Hydraulic and Environmental Engineering at the Norwegian University of Science and Technology, as a partial fulfillment of the requirements of the Master of Science in Hydropower Development.

The author hereby declares that the work presented in this report is his own and significant notes and figures obtained from outside has been mentioned.

Aynalem Tassachew Tsegaw

June 2010

Trondheim,

Norway

# ACKNOWLEDGMENT

I would like to thank my advisor Associate Professor Knut Tore Alfredsen for his direction, assistance, guidance, sound suggestions & recommendations from the inception to the completion of my work.

I also wish to thank my supervisor Yisak Sultan Abdela (PHD candidate at NTNU) who has helped me a lot in many ways for the execution of my work.

I would like to express my gratitude to Dr. Kiflom Belete and Mrs Hilbørg Sandvic, at the Hydraulic and Environmental Engineering Department at NTNU, for their continuous support and guidance during my study at NTNU.

**NTNU**
**Norwegian University of**
**Science and Technology**

**Faculty of Engineering**
**Science and Technology**
**Department of Hydraulic and**
**Environmental Engineering**

M.Sc. THESIS IN

HYDROPOWER DEVELOPMENT

Candidate: Aynalem Tassachew Tsegaw

Title: Short term Distributed Hydrological Modelling of Gaula Catchment.

# 1 BACKGROUND

Short term hydrological simulation with time resolution of one hour or less can be important to capture flow events in small catchments. The purpose of this assignment is to tryout the new developments to the LANDPINE model allowing for using TOPMODEL runoff generation and distributed runoff generation. The preliminary test will be carried out using gauge IDW interpolation, gauge simulated and radar based precipitation input data.

# 2 MAIN QUESTIONS FOR THE THESIS

1. Prepare the catchments, sub-catchments and stream networks from digital data. Compute the properties for the stream reaches (slope, length and channel width) that are to be used in the routing computation. Prepare necessary input maps for the LANDPINE model. All input data should be clearly documented in the thesis text including data sources.
2. Compute the topographic index of the study site. Determine the TOPMODEL 'm' parameter for the sub-catchments that is to be used in the simulation.
3. Together with the advisor select a number of short events that is to be simulated in the model. For each selected event, the distributed precipitation input should be prepared for the model. The criteria for selection events should be included in the thesis.
4. Calibrate the model for gauge IDW interpolation, gauge simulated and radar precipitation data. Initially manual calibration should be used, but as the candidate gets familiar with the model and the parameter automatic routines can be employed. The calibration method and result should be documented clearly in the text. The difference between the simulations with radar and gauge precipitation should be discussed in the thesis.

# 3 SUPERVISION, DATA AND INFORMATION INPUT

Associate Professor Knut Alfredsen will be responsible for the work, and PhD student Yisak Sultan Abdella the main supervisor of the thesis work and assist the candidate to make relevant information available.

Discussion with and input from colleagues and other research or Engineering staff at NTNU, SINTEF, power companies or consultants are recommended. Significant inputs from others shall, however, be referenced in a convenient manner.

The research and engineering work carried out by the candidate in connection with this thesis shall remain within an educational context. The candidate and the supervisors are therefore free to introduce assumptions and limitations, which may be considered unrealistic or inappropriate in a contract research or a professional engineering context.

## 4 REPORT FORMAT AND REFERENCE STATEMENT

The thesis report shall be in the format A4. It shall be typed by a word processor and figures, tables, photos etc. shall be of good report quality. The report shall include a summary, a table of content, lists of figures and tables, a list of literature and other relevant references and a signed statement where the candidate states that the presented work is his own and that significant outside input is identified.

The report shall have a professional structure, assuming professional senior engineers (not in teaching or research) and decision makers as the main target group.

The summary shall not contain more than 450 words it shall be prepared for electronic reporting to SIU. The entire thesis may be published on the internet as full text publishing through SIU. Reference is made to the full-text-publishing seminar during NORADS winter-seminar. The candidate shall provide a copy of the thesis (as complete as possible) on a CD in addition to the A4 paper report for printing.

The thesis shall be submitted no later than 28th of June 2010.

Trondheim 19th of January 2010

_____

Knut Alfredsen

Associate Professor

Department of Hydraulic and

Environmental Engineering at NTNU

# EXECUTIVE SUMMARY

Testing and trying out of the applicability and utility of watershed hydrological models in different; catchment sizes, hydro-geologic conditions, soil conditions and with different time resolutions is necessary for a range of spatial scales to assess the utility of these models in water shade management means like flood protection, land slide prevention, erosion control etc. The main purpose of this thesis is to tryout TOPLAND hydrological model, i.e. the new developments to the LANDPINE model allowing for using TOPMODEL distributed runoff generation, with different precipitation input methods. It focuses on the simulation of precipitation events with time resolution of one hour. Short term time resolution event simulations are important to capture flow events in small and large catchments; since these events are responsible for local flood, land slide etc., especially in areas where they are strongly localized. The model simulation has been carried out using three different precipitation input methods; gauge IDW interpolation, gauge simulated and radar based precipitation data for the selected hourly events of 2006 (27-07-2006 00:00 to 29-07-2006 23:00) and 2009 (19-07-2009 05:00 to 25-07-2009 20:00).

2009 Event

The 2009 event is characterized by high peak and uniformly distributed event. For the bias corrected radar precipitation, the objective method of result comparison showed an excellent correspondence between observed and simulated flows with NS ($R^2$) of 0.98, correlation ($R^2$) of 0.98 and PBIAS of 0.48% at the calibration point (Gaulfoss). The bias corrected radar precipitation also showed a very good performance of the model at the interior uncalibrated gauging stations with average values of NS ($R^2$) 0.85, correlation ($R^2$) 0.93 and PBIAS 16.6% of the HugdalBru, Lillebudal and Eggafoss gauging stations. The gauge IDW interpolation and gauge simulated precipitation input methods also showed a very good performance of the model both at the calibration and internal uncalibrated gauging stations.

2006 Event

The 2006 event is characterized by low peak and unevenly distributed (localized) event. The bias corrected radar precipitation is the only precipitation input method that made possible for calibration of the model. The objective method of result comparison showed a very good result for NS ($R^2$) of 0.96, correlation ($R^2$) of 0.97 and PBIAS of 5.1% at the calibration point (Gaulfoss). At the internal uncalibrated gauging stations, the correlation and PBIAS showed a good performance with average correlation ($R^2$) of 0.77 and PBIAS of 21.3% and a poor average NS ($R^2$) of 0.3.

# TABLE OF CONTENTS

# LIST OF FIGURES

# LIST OF TABLES

## LIST OF ABBREVIATIONS

| | |
|---|---|
| amsl | above mean sea level |
| Corr. | Correlation |
| DEM | Digital Elevation Model |
| DInf. | Multiple flow direction |
| Dist. | Distance |
| Fac | Flow accumulation |
| Fdr | Flow direction |
| Fig. | Figure |
| HBV | Hydrologiska Byråns vattenbalansavdelning (Hydrological Bureau Waterbalance-section) |
| ID | Identification number |
| IDW | Inverse Distance weighting |
| MRC | Master Recession Curve |
| NS | Nash Sutcliff Index |
| rc | Recession curve |
| Sca | Specific Catchment area grid |
| SCS | Soil conservation service |
| SINTEF | The Scientific and Industrial Research at Norway-Trondheim |
| U/s | Upstream |
| UTM | Universal Transverse Mercator System |

# 1. INTRODUCTION

## 1.1 BACKGROUND

Nowadays different hydrologists over the world have been working on developing new hydrological models or improve the existing ones to simulate the watershed hydrology efficiently. As mentioned by Singh (1995) and Singh and Frevert (2002a, b), this has resulted in a large number of hydrologic models, and many more are likely to emerge in the near future. These models are generally classified as either lumped models like HBV or distributed like LANDPINE and TOPMODEL. The main difference between these model classes is that lumped models do not take into account the spatial distribution of the water shade parameters, such as soil, land use and topography; while the distributed models have the capacity to disaggregate watersheds into discrete units and assign different physical parameter values for each unit. Lumped models require less data and are generally easier to use compared to distributed models. However, distributed models are now known to more accurately represent temporal and spatial patterns in hydrological processes. The most widely and thrust hydrological models are distributed models together with the Geographical Information System (GIS) which enhances the capability to parameterize these distributed models. GIS enables linking large spatially related data sets and to account for the spatial variation of model parameters and processes at any resolution (Liu 1999; Beven 2000). **Fig.1** shows general steps involved in hydrological model formulation.

## 1.2 OBJECTIVE

Many models developed so far are unable to simulate short term events which are highly localized especially when the density of raingauges is poor. This thesis uses TOPLAND (physically distributed hydrological model) to simulate hourly events using gauge, gauge simulated and radar precipitation of which one of the few publications in the application of such models.

Early warning with the use of either gauged, gauge simulated or radar precipitation observation and hydrologic models is crucial for minimizing flood and flood related hazardous. The potential advantage of using gauge precipitation is that it gives more accurate data than radar precipitation especially when there is high density of rain gauges for large sized study area. The use of gauge precipitation is limited when the density of the gauge stations is poor; the spatial and temporal resolution of the event is high, i.e. in the order of kilometers and hours and when the event is strongly localized. Because of its potential to resolve precipitation at small time and space scales, radar precipitation is important especially for small basins prone to flash flooding and complex terrain.

The main objectives of this thesis work are summarized as follows:

- To tryout the applicability of TOPLAND hydrological model in handling hourly distributed precipitation events by selecting typical precipitation events.
- To assess the extent of the applicability of different precipitation input methods, i.e. gauge IDW interpolation, gauge simulated and radar to the TOPLAND hydrological model.
- To examine how the model is applicable in prediction flows at interior uncalibrated discharge gauging station using different precipitation input methods.
- To assess the applicability of the model in handling short term events which are highly localized.

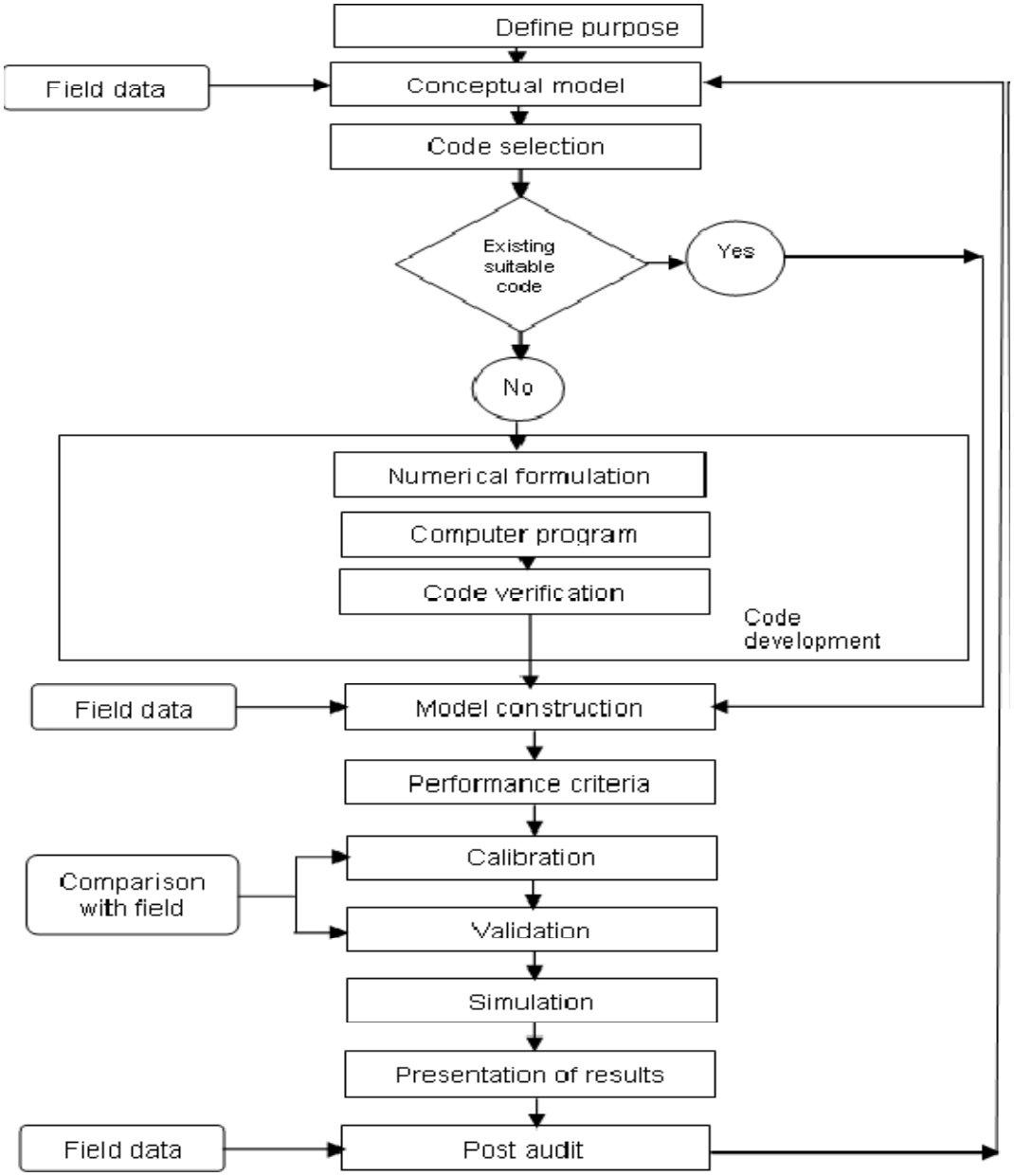


**Figure 1: Steps in hydrological model formulation (Refsgaard, 2000)**

# 2. TOPLAND HYDROLOGICAL MODEL

## 2.1 TOPLAND MODEL OVERVIEW

TOPLAND hydrological model is an integrated version of two independent hydrological models and routing component; TOPMODEL (Kirkby 1979; Beven et al., 1986a, b) that controls the soil hydrology and LANDPINE (Rinde, 1998) that controls the surface hydrology. The processes in TOPLAND model can be classified into two groups, i.e. the process with in the grid cell and those between grid cells. The processes within a grid cell can be simulated grid cell by grid cell, and the interaction between grid cells is not to be dominant and the movement of water between grid cells is simulated by the routing component of the model. **Fig.3** shows the structure of the TOPLAND model; and the descriptions of LANDPINE and TOPLAND are discussed below.

### *2.1.1 DESCRIPTION OF LANDPINE*

The distributed hydrological model LANDPINE is developed by Trond Rinde to study the impacts of land use changes have on runoff generation. The development of this model was a part of 3-years research programme, called HYDRA, whose main objectivities was to study how human activities may affect flood regimes in rivers (Rinde, 1998). The project was initiated and funded by the Norwegian Government after the country suffered the biggest flood of these century in the spring of 1995. The simulation framework within which LANDPINE was implemented is called PINE (Rinde, 1998). The two basic requirements on which the development of this model were based are:

**(1)** Explicit representation of the catchment characteristics that will change if land use is changed and which are relevant with respect to runoff and **(2)** Not requiring more input data than what is generally available for operational modeling in Norway, i.e. only precipitation and temperature data.

The LANDPINE hydrological model explicitly accounts for interception in high and low vegetation, storage of water on the ground surface, evapotranspiration, accumulation and melting of snow, infiltration, retention of water in the soil, and generation of surface runoff and outflow from the soil in a distributed manner. The modeling concept on which the representation of these hydrological processes is based on is a grid–mesh partitioning of the catchment area. But water movement in rivers and outflows from water reservoirs are described by the use of an aggregated response function similar to the one used in the lumped hydrological model like HBV.

TOPLAND model uses groundwater, water movement in rivers and outflow from reservoirs in a distributed manner by integrating TOPMODEL into LANDPINE.

### *2.1.2 DESCRIPTION OF TOPMODEL*

TOPMODEL (Topography-based hydrological model) is a conceptual hydrological model (developed as complete hydrological model originally by Beven and Kirkby, 1979; Beven et al., 1986a, b) that can be used to reproduce the hydrological behavior of catchments in a distributed or semi-distributed way, in particular the dynamics of surface or subsurface contributing areas. It is based on some simple approximate hydrological theory but recognizes that, because of the lack of measurements in internal state variables and catchment characteristics, the representation of the internal hydrological responses of the catchment must necessarily be functional while introducing the minimal number of parameters to be calibrated (Kirkby, 1975; Beven, 1989a).

Numerous field studies have indicated that surface runoff in wet regions, where the precipitation intensity is low and the soil infiltration capacity is high, is mainly produced by saturation excess runoff (Dunn flow). This means that the spatial distribution of soil moisture storage will result in different surface runoff production. Even though there are many surface runoff models based on the saturation excess runoff mechanism, only a few models takes the topography influence on the spatial distribution pattern of soil moisture into consideration and in turn on runoff production. TOPMODEL is one of such kind of models, which fully takes the influence of topography on soil moisture and groundwater table over a catchment into consideration. By using the prescribed topography index of a catchment and average water storage deficit calculated in the drainage, the model can directly estimate spatial distribution of the ground water table and local water storage deficit in the unsaturated zone, and in turn predict the portion of area in the catchment where saturation excess runoff will happen. The model has the advantage of a few parameters with a good physical meaning (Beven and Kirkby, 1979; Beven, 2000).

This thesis will contribute the implementation of TOPMODEL with LANDPINE that modifies the original LANDPINE root zone moisture routine and describes the ground water outflow and surface runoff in rivers, which were provided as input to lumped response routine consisting of two linear thanks in the original LANDPINE model, in a distributed manner.

The basic assumptions in conceptualization of TOPMODEL are;

**I**. The dynamics of the saturated zone can be approximated by successive steady state representation, i.e. there is a saturated zone in equilibrium with a steady recharge rate over an upslope contributing area.

**II**. The hydraulic gradient of the saturated zone can be approximated by the local topographic index of Beven, $\boldsymbol{ln(a/\tan\beta)}$.

**III**.The distribution of the downslope transmissivity ($\boldsymbol{T}$) with depth is an exponential function of storage deficit or depth to the water table, i.e. $\boldsymbol{T = T_0 e^{-D/m}}$;

Where $\boldsymbol{T_0}$ is the lateral transmissivity when the soil is fully saturated and $\boldsymbol{D}$ is the local storage deficit below saturation expressed as water depth and $\boldsymbol{m}$ is the TOPMODEL parameter.

## 2.2 PROCESSES INVOLVED IN TOPLAND

### *2.2.1 HIGH VEGETATION COMPONENT*

High vegetation is represented in the model in terms of five parameters: $LAIMAX$, the maximum seasonal leaf area index, $LAIMIN$, the minimum seasonal leaf area index, $laicap$,the specific interception capacity per unit leaf area; $VEGCOV$, the percentage of high vegetation cover over the land; and $VEGHGT$, which is the height of the vegetation stand. For the high vegetation, interception capacity and potential evaporation are calculated along with actual values for these responses. Precipitation that is not intercepted is considered as through fall to the ground.

#### 2.2.1.1 Interception Capacity

The interception capacity of the high vegetation, $HINTCAP$, is calculated as:

$$HINTCAP = [LAIMAX * laicap] * VEGCOV * VEGCOR * SESCOR \quad \text{(Eq. 2.1)}$$

$VEGCOR$ Accounts for the fact that a stand may not be fully grown and $SESCOR$ accounts for the seasonal variation in the canopy cover. Depending on the vegetation height, $VEGCOR$ varies between 0.0 and 1.0 according to the equation:

$$VEGCOR = \frac{VEGHG}{dveghgt} \quad \begin{cases} max = 1.0 \\ \\ min = 0.0 \end{cases} \quad \text{(Eq. 2.2)}$$

$dveghgt$ is a parameter which represents the default height for fully-grown trees. $VEGCOR$ = 0.0 represents a situation where the forest has been removed, while $VEGCOR$ = 1.0 represents a fully grown stand. $SESCOR$ may vary from $LAIMIN/LAIMAX$ to 1.0 and is calculated on the basis of accumulated degree days above a given threshold temperature, $tvlow$.

The equation for calculating $SESCOR$ is:

$$SESCOR = \sum \frac{TEMP - tvlow}{tvsum} \quad \begin{cases} \max = 1 \\ \\ \min = \frac{LAIMIN}{LAIMAX} \end{cases} \qquad \text{(Eq. 2.3)}$$

The degree days start to accumulate when the temperature rises above $tvlow$.Then $SESCOR$ attains its maximum value when the accumulated degree days reaches or rises beyond a value given by the parameter $tvsum$.

### 2.2.1.2 Potential Evaporation

Potential evaporation (POTET) is calculated from monthly average values for potential evaporation per day which are provided as input to the model. These values refer to average climatic conditions, and a standardized surface type. To account for possible deviation from their normal values during simulation runs, the values are corrected for deviation between the actual temperature and the long-term monthly mean by linear function for $TMPCOR$, given by the following equation.

$$TMPCOR = 1.0 + etmp * (TEMP - temp_{mnd}) \qquad \text{(Eq. 2.4)}$$

$etmp$ is the dependency of potential evaporation on temperature deviation from the long - term monthly mean, $temp_{mnd}$.

To represent the reduction of $POTET$ with increase in air humidity, a reduction factor, $PRCCOR$, is used. During time steps with precipitation, $PRCCOR$ is set lower than unity, whereas it is unity for time steps without precipitation. Potential evaporation rates can also be adjusted for deviations in wind speed s from their monthly means by applying wind correction factor (WNDCOR).

$$WNDCOR = 1.0 + kwnd * wind \qquad \text{(Eq. 2.5)}$$

$kwnd$ is a factor for the dependency of potential evaporation on wind speed deviation from the long-term monthly mean wind speed.

Potential evaporation also dependent on the vegetation height since the exchange of air masses generally occurs more efficiently high above the ground than close to it. High vegetation therefore leads to higher potential evaporation than low vegetation. This effect is dealt with an adjustment factor, $HGTCOR$, which accounts for changes in potential evaporation for deviations of $VEGHGT$ from $dveghgt$.

$$HGTCOR = 1.0 + ehgt * (VEGHGT - dveghgt) \Big| min = 1.0 \quad \text{(Eq.2.6)}$$

$ehgt$ is the dependency of potential evaporation on $VEGHGT$ deviation from $dveghgt$. The final equation for potential evaporation computation from a single cell is:

$$POTET = ep_{mnd} * TMPCOR * HGTCOR * WINDCOR * PRCCOR \quad \text{(Eq.2.7)}$$

Where $ep_{mnd}$ is the input of monthly average potential evaporation for each month.

### 2.2.1.3 Actual Interception and Evaporation

Actual evaporation from interception in high vegetation, AEH, is taken as the potential evaporation rate multiplied by the VEGCOV and a correction factor which accounts for reduction in evaporation if the intercepted precipitation is in the form of snow. This factor, SNWCOR, is set to either unity for time steps with temperature higher than $tx$ or to $eredsnw$ (<1.0) for time steps with temperature lower than $tx$. In each time step, incoming precipitation, PREC, is used to fill up the interception storage, HINT, which is depleted by the actual evaporation (AEH).When the interception capacity is reached, excess precipitation forms throughfall (TRUFAL) to the ground or the snow surface. The equations for the above processes are given below.

$$AEH = POTET * SNWCOR * VEGCOV \Big| \begin{matrix} \max = HINT \\ \\ \min = 0.0 \end{matrix} \quad \text{(Eq. 2.8)}$$

$$HINT_i = HINT_{i-1} + PREC - TRUFAL - AEH \quad \begin{cases} \max = HINT\ CAP \\ \min = 0.0 \end{cases} \qquad \text{(Eq. 2.9)}$$

$$TRUFAL = PREC - (HINTCAP - HINT) \quad \begin{cases} \\ \min = 0.0 \end{cases} \qquad \text{(Eq. 2.10)}$$

### *2.2.2 SNOW*

If local air temperature is lower than the rain/snow threshold, the throughfall from high vegetation goes to increase the snow layer. If the temperature is higher, the through fall instead goes to increase the liquid water in the snow, or, if no snow is present, it passes on to the lower interception storage. In each grid cell, the snow distribution is assumed to be linear. A distribution factor, $snwdst$, is then used to specify the relative magnitudes of the maximum and minimum storage values in the cell.

If the distribution factor is set to unity, the snow pack ($SNWPCK$) becomes homogeneous. If it is equal to 2.0, the maximum value, $MAXPCK$, becomes twice the average value, and the minimum value, $MINPCK$, becomes zero. If it is higher than 2.0, only partial snow cover will be simulated.

Snow melt,SNWMLT, is calculated on the basis of actual air temperature, TEMP, a threshold for melting, $ts$, and a melt factor, $tx$, according to the degree day principle.

$$SNWMLT = cx * (TEMP - tx) * SNWCOV,\ TEMP \geq tx \qquad \text{(Eq. 2.11)}$$

In forested and partly forested areas the melt factor is reduced. This is represented by a reduction factor, $cxred$, which causes reduced melt intensity and there by delayed snow melting in forested areas compared to open land. If air temperature is lower than the melt threshold, refreezing of liquid water, SNWFRZ, in the snow is calculated through the use of the parameter, $cfr$, which accounts for the fact that refreezing occurs at a much lower rate than melting.

$$SNWFRZ = cfr * cx * (tx - TEMP) * SNWCOV,\ TEMP < tx \quad \text{(Eq. 2.12)}$$

Snowmelt, as well as refreezing, is assumed to be homogeneous across the snow surface. Melted snow is added to the liquid water content in the snow, SNWWAT. A separate parameter, $lwmax$, specifys the maximum relative amount of such water that can be withheld in the snow. If the relative amount becomes larger than this fraction, the excess forms outflow from the snow, SNWOUT. Through fall on the snow-free parts contributes directly to SNWOUT. The equations for the above processes are given below.

$$SNWPCK = SNWPCK + SNWPRC - SNWMLT + SNWFRZ \quad \text{(Eq. 2.13)}$$

$$SNWWAT = SNWWAT + RAINPRC + SNMLT - SNWFRZ - SNWOUT \quad \text{(Eq. 2.14)}$$

Where; SNWPRC/RAINPRC = precipitation in the form of snow/rain

$$SNWOUT = [SNWWAT - lwmax * SNWPCK] \left| \begin{array}{l} + \ RAINPRC * (1.0 - SNWCOV) \\ min = 0.0 \end{array} \right. \quad \text{(Eq. 2.15)}$$

### *2.2.3 LOW VEGETATION AND LAND SURFACE COMPONENT*

The leaf area index for low vegetation, $LAILOW$, is the only parameter separately defined for the low vegetation. Similar to the high vegetation, interception storage is also computed for the low vegetation. The interception capacity, $LINTCAP$, computation is based on the same principle used in $HINTCAP$ computation except for the fact that it is lumped together with a wetting storage for the land surface, $SRFSTR$ , for simplicity.

$$LINTCAP = [LAILOW * laicap] * SESCOR + SRFSTR \quad \text{(Eq. 2.16)}$$

The lumped storage is filled by outflow from the snow routine. When the storage capacity is exceeded, excess water will go to the soil, TOSOIL. Potential evaporation for this storage is taken as the potential evaporation that was calculated for the high interception storage, reduced according to the actual evaporation that has already occurred in the high interception

storage, AEH. Actual evaporation from the lower storage, AEL, is assumed to occur at a potential rate as long as water is left in the storage. The equations within this routine are given below.

$$LINT_i = LINT_{i-1} + SNWOUT - TOSOIL - AEL \begin{cases} max = LINTCAP \\ \\ min = 0.0 \end{cases} \quad \text{(Eq. 2.17)}$$

$$TOSOIL = SNWOUT - (LINTCAP - LINT) \begin{cases} \\ \\ min = 0.0 \end{cases} \quad \text{(Eq. 2.18)}$$

$$AEL = (POTET * SNWCOR - AEH) * [1.0 - SNWCOV] \begin{cases} max = LINT \\ \\ min = 0.0 \end{cases} \quad \text{(Eq. 2.19)}$$

### *2.2.4 SOIL COMPONENT*

Throughfall and unsatisfied potential evaporation, $E_p$, from the interception component serve as the forcing for the soil component, which represents the root zone, unsaturated zone and saturated zone. Beven et al.; (1995a) indicated that two formulations that have been adopted in the past TOPMODEL applications have assumed that the unsaturated flows are essentially and have been expressed in terms of drainage flux from the unsaturated zone. Neither of the formulation presented by Beven et al. (1995a) limit the infiltration capacity, possibly due to the historical association of TOPMODEL with the saturation excess rather than the infiltration excess runoff generation mechanisms.

The state variable $S_r$ quantifies the depth of water held in the soil root zone for each model element and is calculated using the following equation.

$$\frac{dS_r}{dt} = I - AET_s - q_v \quad \text{(Eq. 2.20)}$$

Where $I$ is the infiltration rate; $AET_s$, Actual soil evapotranspiration rate; $q_v$ is the drainage rate or recharge to the saturated zone store from the soil store. The infiltration rate, $I$, is limited to be less than the infiltration capacity, $I_c$.

### 2.2.4.1 Root Zone Component

The root zone is the upper layer of soil to the depth below which roots can no longer extract water. In TOPLAND model, root zone is characterized by $S_{rz}$ , $S_{rmax}$ and $S_{rzini}$ . Where $S_{rz}$ , root zone storage (variable state), $S_{rmax}$, maximum available root zone storage $S_{rzini}$, initial root zone storage. Refer to **Fig.2** for illustration.

### 2.2.4.2 Unsaturated Zone Component

The basic soil structure illustrated in **Fig.2** is used to accommodate one method of different unsaturated zone process descriptions. One formulation that has been adopted in past TOPMODEL applications assumes that the root zone store for each topographic index value is depleted only by evapotranspiration, and that water is added to the unsaturated zone drainage store only once the root zone reaches the field capacity. The drainage is assumed to be essentially vertical and a drainage flux per unit area $(qv)$ is calculated for each topographic index class expressed in terms of storage deficit, Beven and Wood (1983) suggested that a suitable functional form for the vertical flux $qv$ at any point *i* is;

$$q_v = {S_{uz}}/{D_i * t_d} \qquad \text{(Eq. 2.21)}$$

Where $S_{uz}$ is storage in unsaturated (gravity drainage) zone, $D_i$ is the local saturated zone deficit due to gravity drainage, and dependent on the depth of the local water table . Parameter $t_d$ is a time constant, expressed as a mean residence time for vertical flow per unit of deficit. Equation 2.21, is the equation of a linear store but with a time constant $\{D_i t_d\}$ that increases with increasing depth to the water table.

TOPLAND uses TOPMODEL's calculation method of actual evapotranspiration, $E_a$ , as a function of potential evapotranspiration, $E_p$ , and root zone moisture storage for cases where $E_a$ can not specified directly. In the Topmodel description of Beven (1991a), evaporation is allowed at the full potential rate for water draining freely in the unsaturated zone and for predicted areas of surface saturation. When the gravity drainage zone is exhausted, evapotranspiration continue to deplete the root zone store at the rate $E_a$, given by;

$$E_a = E_p \frac{S_{rz}}{S_{rmax}} \quad \text{(Eq. 2.22)}$$

Where the variables $S_{rz}$ and $S_{rmax}$ are root zone storage and maximum available root zone storage respectively. If some effective root zone depth $S_{rz}$ can be assumed, $S_{rmax}$ can be estimated approximately by trial and error.

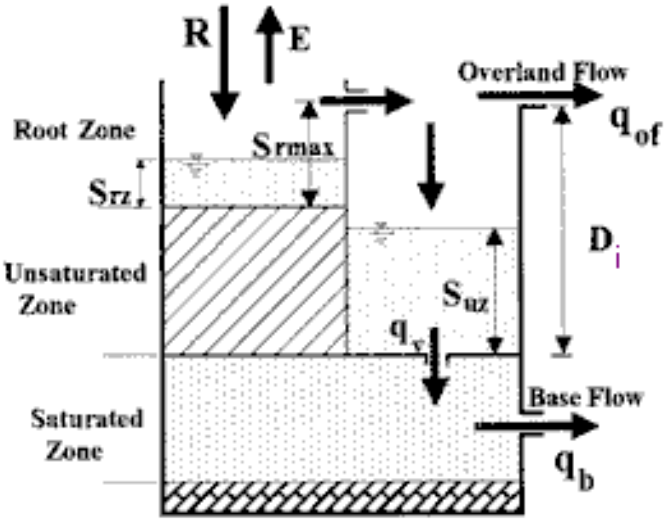


**Figure 2 : The basic soil component (Hydrological Sciences, Kuniyoshi Takeuchi, August 1999)**

### 2.2.4.3 Saturated Zone Component

The saturated zone component is modeled using the TOPMODEL assumptions of saturated hydraulic conductivity decreasing exponentially with the depth and saturated lateral flow driven by topographic gradient (Beven and Kirkby 1979); Beven et al. 1995). Two important parameters are soil profile lateral transmissivity, $T_0$ , and the sensitivity parameter, m, characterizing the decrease of hydraulic conductivity with depth.

The outflow from the saturated zone per unit area is given by;

$$q_b = T_o e^{-\gamma} e^{-D_{mean}/m} \quad \text{(Eq. 2.23)}$$

The total out flow from a give catchment area $A$ is given by;

$$Q_b = A T_o e^{-\gamma} e^{-D_{mean}/m} = Q_o e^{-D_{mean}/m} \quad \text{(Eq. 2.24)}$$

$\gamma$ is the spatial average of topographic index, $ln\left({}^{a}/_{tan\beta}\right)$ and given by the following equation;

$$\gamma = \frac{1}{A}\sum_{i=1}^{n} Ai\ ln\,{}^{a}/_{tan\beta} \qquad \text{(Eq. 2.25)}$$

Where, $T_o\ is$ Saturated transmissivity at the surface , $q_b$ is out flow from saturated zone, m is TOPMODEl parameter that controls the rate of decline of hydraulic conductivity with increasing storage deficit, $Q_o$ is outflow from saturated zone when the soil is fully saturated, $D_{mean}$ is the spatial average of the depth to the water table quantifying the basin average soil moisture deficit and serving as a state variable for the saturated zone component.

The saturated zone state equation is given be;

$$\frac{\mathrm{dD_{mean}}}{\mathrm{dt}} = -q_v + T_o e^{-\gamma} e^{-D_{mean}/\mathrm{m}} \qquad \text{(Eq. 2.26)}$$

$q_v$ is the recharge to the saturated zone.

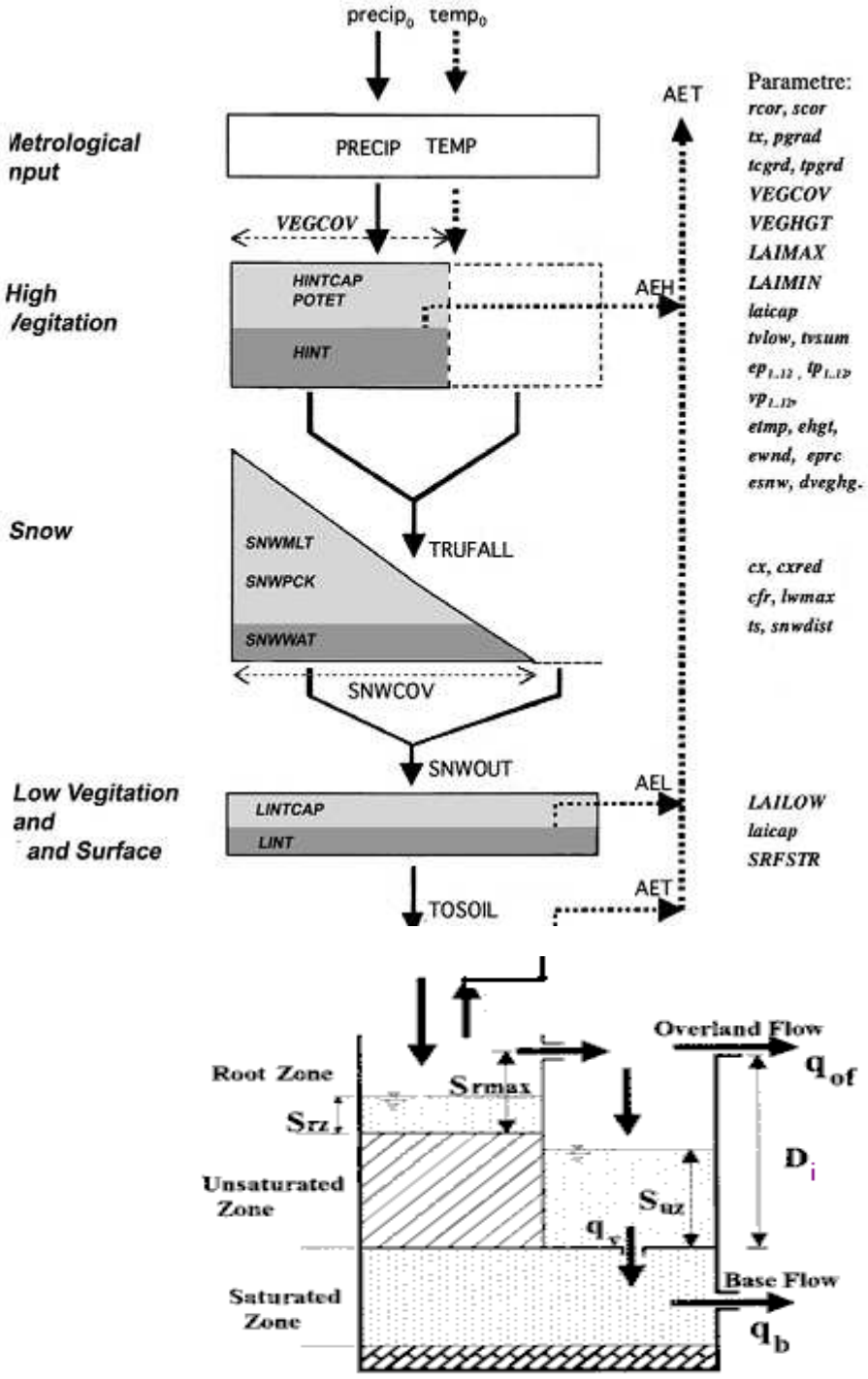


**Figure 3: TOPLAND model structure for a grid cell processes**

### *2.2.5 ROUTING COMPONENT*

Since the precipitation intensity at Norway is low and the soil has high infiltration capacity, the infiltration excess flow is omitted from the model. Therefore, there are only two sources of runoff from each sub-catchments;

1. Saturation excess runoff ( $q_{0f}$) from excess precipitation on variable source saturated areas as determined from topographic index.

2. Runoff from saturated zone drainage ( $q_b$ )

The routing component of TOPLAND hydrological model is described by;

**I**. Overland flow routing for the saturated excess flow ( $q_{0f}$) which is controlled by delay velocity, fraction of saturated areas and the distance to the nearby stream. This is a distributed outflow and is delayed in reaching the nearby stream due to the time taken by sub basin travel.

**II**. Runoff from saturated zone drainage which is lumped output of the sub-catchment at each time step.

**III**. Kinematic routing also called stream routing component for the combined flow of saturated zone and saturated excess flow which is controlled by the kinematic wave routing parameters.

Once in the stream, a kinematic wave routing algorithm, a nonlinear solution with initial estimation from linear solution (Chow, et al., 1988) is used to route flow through the network. Sub-catchment inputs to the channel network are assumed to occur laterally along the stream. **Fig.4** illustrates a rough sketch of stream routing mechanism for TOPLAND model.

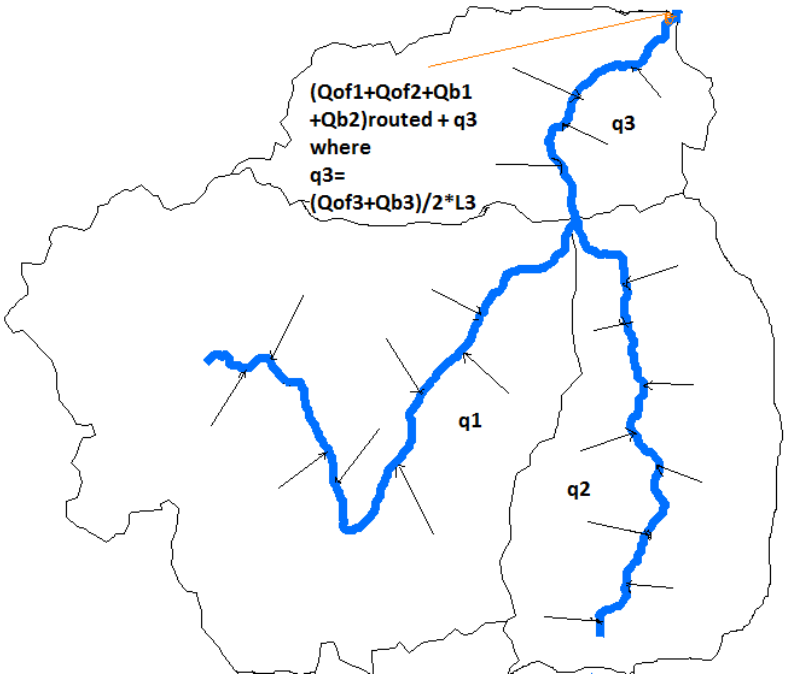


**Figure 4: Stream routing mechanism for TOPLAND hydrological model**

The basic kinematic wave routing equations are continuity and momentum.

$$\frac{\partial Q}{\partial x} + \frac{\partial A}{\partial t} = q \qquad \text{Continuity equation} \qquad \text{(Eq. 2.27)}$$

$$A = \alpha Q^{\beta} \qquad \text{Momentum equation} \qquad \text{(Eq. 2.28)}$$

$$S_o = S_f \qquad \text{Assumption} \qquad \text{(Eq. 2.29)}$$

Where $q$ is lateral inflow to the stream; $A$, flow cross sectional area; $Q$, discharge; $\alpha$ and $\beta$ kinematic wave routing coefficients; $S_o$ *and* $S_f$ are bed and energy slopes respectively.

The parameters used in the kinematic wave channel network routing are Manning's roughness number, top width, length of each stream segment, slope and kinematic wave routing coefficients. Length and slope are determined from the GIS based upon the digital Elevation Model (DEM). Channel width has been determined from semi-field measured data and from basic assumption that states, top width is directly proportional to the upstream contributing

area. The parameters are explained in detail under section-2 of this paper. **Fig.5** shows schematics of the physical processes represented by the TOPLAND modeling system.

The stream text file for routing component includes; grid ID of sub catchments, bed slope, kinematic routing parameters, top width, initial discharge, initial observed discharge, number of sections, upstream sub-catchments, manning's number, length of each section.

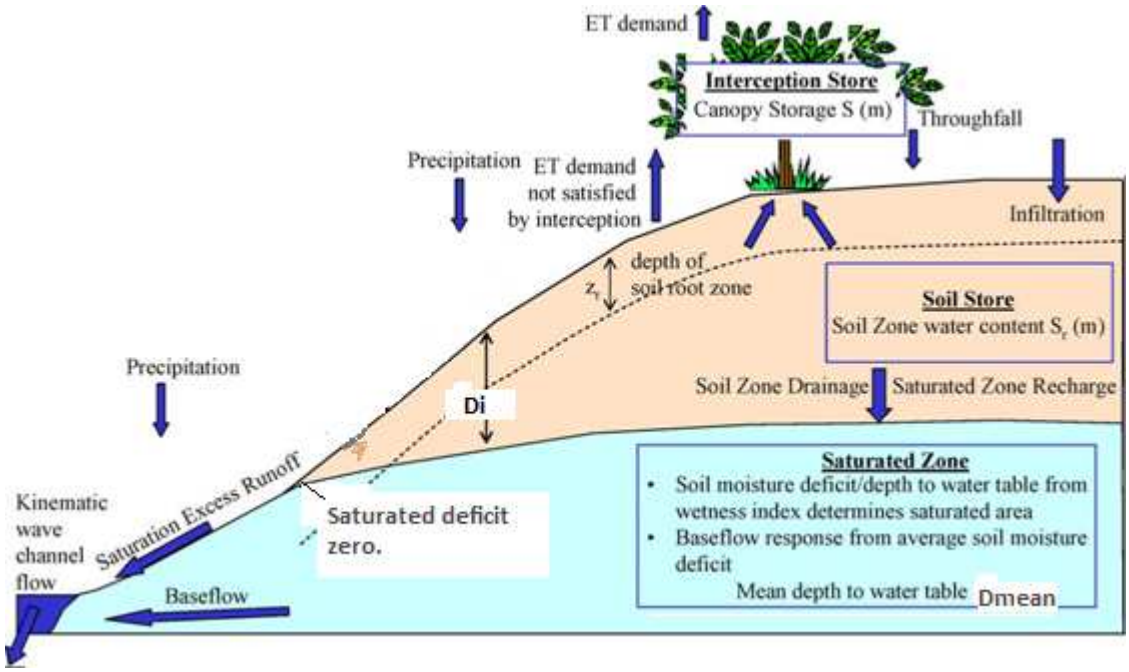


**Figure 5: Schematic sketch of the physical processes represented by the TOPLAND modelling system.** *(Modified from C.Bandaragoda et al. / Journal of Hydrology 298 (2004) 178-201)*

# 3. APPLICATION TO THE GAULA CATCHMENT

## 3.1 DESCRIPTION OF THE STUDY AREA

The study catchment, Gaula catchment upstream of Gaulfoss gauging station, has an area of 3094.74km$^2$. It is located at the South and West of the city of Trondheim in SørTrodlag County, Norway with latitude and longitude coverage of 62$^0$38' to 63$^0$7' N and 9$^0$53' to 11$^0$47' E respectively. Norway has a total catchment area of 324 000 km$^2$ (NVE.no) of which Gaula catchment comprises 0.95% of it. **Fig.6** shows the location of the Gaula catchment in SørTrodlag. The outlet of the study catchment is at Gaulfoss discharge gauging station, which is used as the calibration point.

The Gaula River, which runs through three municipalities (Holtålen, Midtre-Gauldal and Melhus), is regarded by many as the best salmon river in Europe and even in the world. It runs through an area full of contrasts; from high mountain plateaus through canyons and forests to the gentler, wider and rich agricultural land near the Trondheim fjord. It is also one of the longest salmon rivers in Norway being 85 kilometers (53 miles) from the moth at Øysanden to Eggafoss (waterfall).

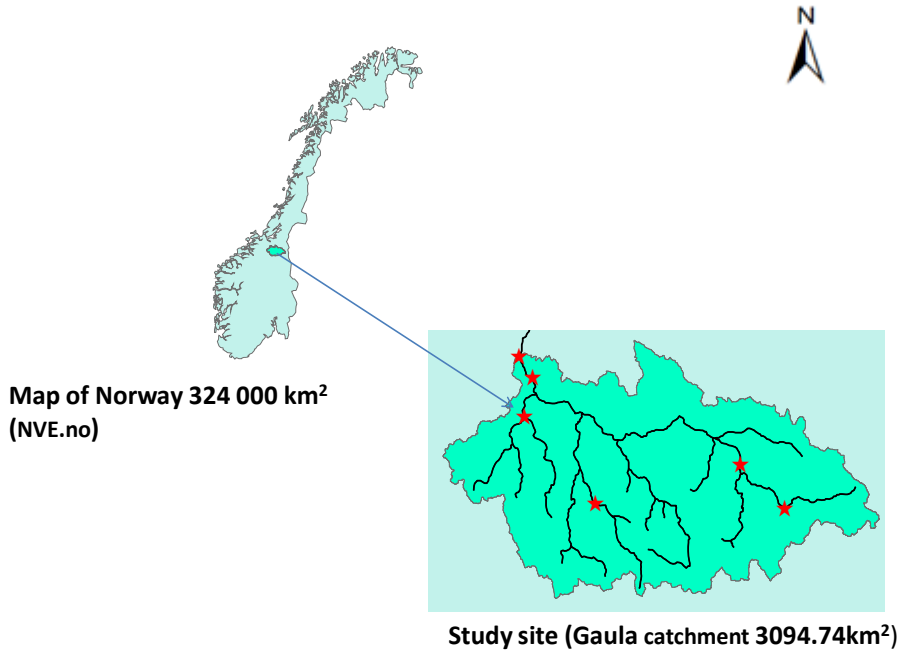


**Figure 6 : Location of the Study Site**

## 3.2 MODEL PARAMETERIZATION AND DATA NEEDS

### *3.2.1 DIGITAL ELEVATION MODEL*

The characteristic of large sized catchment like Gaula can be generated effectively with the help of GIS technologies. GIS offers the potential to increase the degree of spatial details of the study area, which hydrologic models have not modeled previously (Maidment, 1992). For this paper, Arc GIS Desktop - Arc Info have been used. The basic framework of Arc GIS desktop includes; arc map, arc catalog and arc toolbox. To generate catchment characteristics and digital maps; that include information of land use, slope, sub catchment boundaries; and to develop individual data layers for each of those attributes, arc hydro and spatial analyst tools, TauDEM and Idrisi softwares are mainly used. For the study watershade, 25m*25m DEM resolution, obtained from the department of Hydraulic and Environmental Engineering at NTNU, has been used initially for analysis and aggregated to 50m*50m DEM due to computer memory and runtime limitations. **Fig.7** shows the 50m DEM with topography variation of 53m at outlet to 1325m up the mountains.

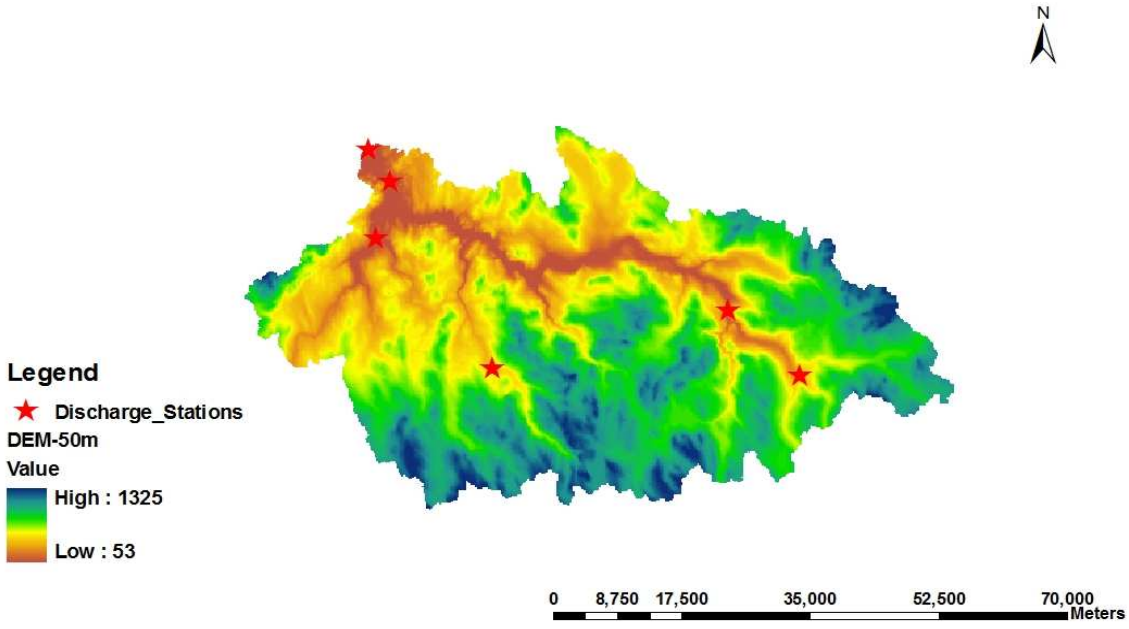


**Figure 7 : 50m DEM of Gaula catchment**

### *3.2.2 HYDRO-METEOROLOGICAL INPUT DATA*

Hydro-meteorological data are input model variables as time series. The main hydro-meteorological input data for TOPLAND model include; hourly precipitation, temperature and discharge. Gauge and radar precipitation data obtained from Norwegian meteorological institute (Met.no) and gauge simulated precipitation obtained from SINTEF- Energy section, has been used for the study.

#### 3.2.2.1 Precipitation Input Methods

Three different precipitation input methods has been used to tryout the TOPLAND hydrological model for handling short term distributed events. **Fig.8** shows sample of different precipitation input methods, i.e.

I. Gauge IDW precipitation input method
II. Conditional gauge simulated precipitation input methods
III. Bias corrected radar precipitation input methods

**Gauge precipitation input method**

In this method, precipitation is imported to the model as records of point measurements from two rain gauge stations, Sokendal and Kotsøy. The point measurements have been interpolated by Inverse Distance Weighting (IDW) to produce precipitation distribution over the catchment. Precipitation values are adjusted for difference between local surface elevation (pixel elevation) and the elevation of the measurement site. A single linear precipitation gradient, *pgrad,* is used for adjusting the precipitation. The model can handle data from more gauge stations but only the above mentioned gauge stations are within the catchment and with hourly data for 2008 and 2009 years.

**Conditioned gauge simulated precipitation input methods**

The conditioned simulation is based on a stationery space-time model incorporating an advection which enables a temporal autocorrelation and a realistic evolution of the spatial rainfall structure with time aggregation. All parameters used in this model are fitted using rainfall time series for four years (2006 – 2009). The rainfall simulation is conditioned by several punctual rain gauge values. Similarly to the kriging method, the conditioned simulation respects exactly the data. For one rainfall past event, each output resulting from the conditioned rainfall simulation will represent one probable rainfall scenario. Each rainfall output has an equal probability to occur.

**Bias corrected radar precipitation input methods**

Quantitative use of weather radar precipitation estimates is not a straightforward due to a variety of gross errors affecting the observations (Wilson and brandes, 1979; Joss and Waldvogel, 1990). For C-band radars at mid-latitudes, the most important ones are non-uniform vertical profile of reflectivity (VPR), variability of the drop size distribution (DSD), and attenuation due to strong precipitation intensity. At longer ranges the height of observation will increase and in the presence of a significant VPR gradient this will typically result in an underestimation of the accumulated precipitation (Joss and waldvogel, 1990; Koistinen, 1991).

Since nowadays amean-field bias adjustment algorithm is widely used, this method has been used to reduce the gross errors in radar-based precipitation estimates. The bias-adjusted precipitation estimates are calculated hourly from the uncorrected precipitation estimates.

$$\check{R}(i,j) = {R(i,j)}/{F} \qquad \text{(Eq. 3.1)}$$

Where $\check{R}(i,j)$ and $R(i,j)$ represent the bias-adjusted accumulation and uncorrected accumulation, repectivelly, of the pixle at the image coordinates (i, j). $F$ is calculated by the following formula.

$$F = \frac{\sum_{n=1}^{N} R\,(i_n, j_n)}{\sum_{n=1}^{N} G_n} \qquad \text{(Eq. 3.2)}$$

Where $(i_n, j_n)$ are the image coordinates of rain gauges n and N is the number of available rain gauges $(G_n)$. Twenty five raingauges within a radius of 75 km has been used for bias correction of radar precipitation. **Appendix 1 and 2** presents the bias correction factors for 2006 and 2009 events respectively.

**I.Gauge Inverse Distance Weighting (IDW) precipitation input on 20-07-2009 18:0**

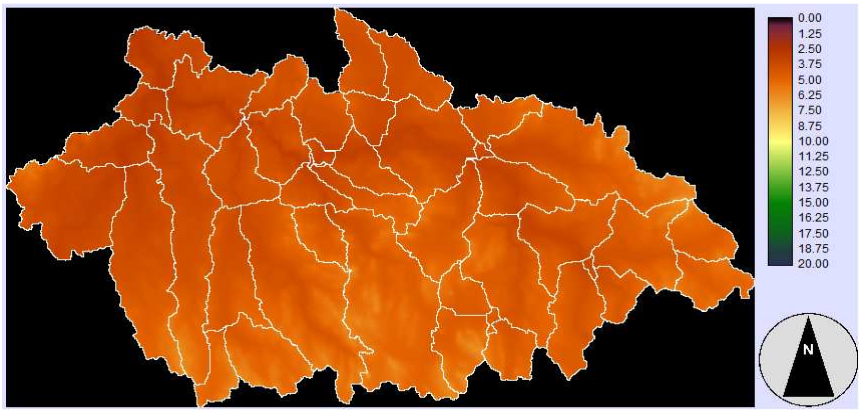


**II.Gauge simulated precipitation input on 20-07-2009 18:00**

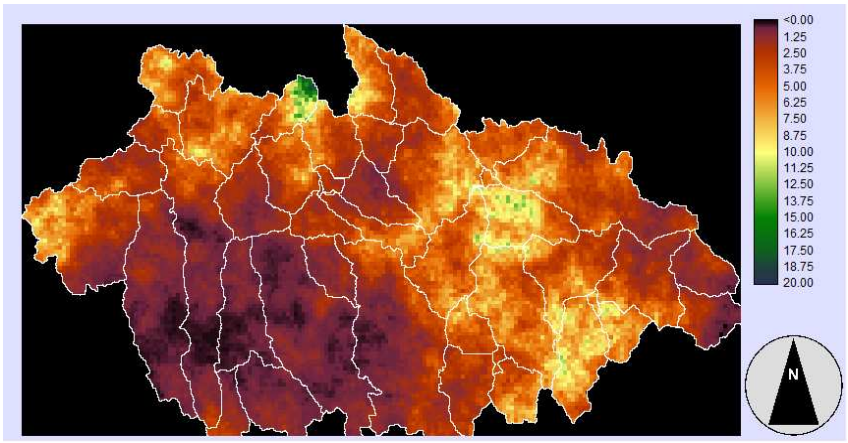


**III. Bias uncorrected radar precipitation input on 20-07-2009 18:00**

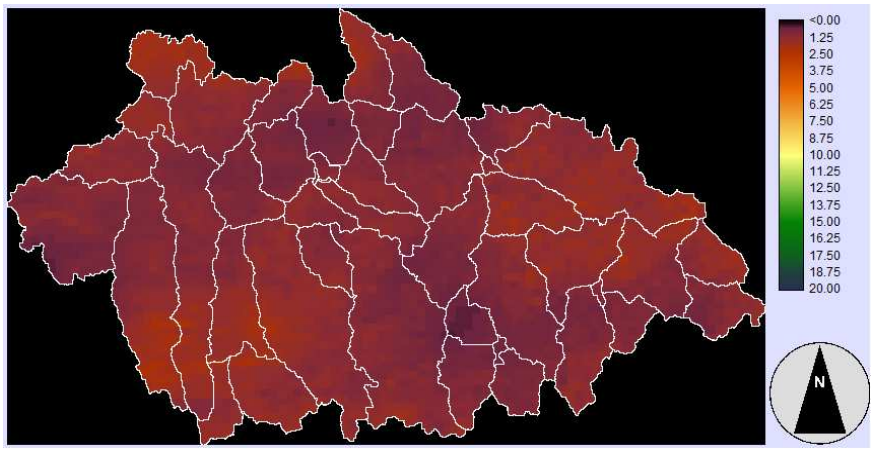


**Figure 8: Sample of different precipitation input methods for 2009 event**

#### 3.2.2.2 Temperature, Wind speed and Discharge

Temperature data is imported to the model as a lumped input from three gauge stations. Since the discharge gauging stations have temperature measurements and to have a representative data for the catchment, temperature data from HugdalBru, Lillebudal and Eggafoss discharge gauging stations has been used for gauge simulated and bias corrected precipitation input methods. For gauge IDW interpolation method, the precipitation gauging stations has been used for temperature also. Temperature is adjusted for difference between local surface elevation and the elevation of the measurement site.

Observed hourly discharge data and wind speed is imported to the model as a lumped input from a single gauging station that is located at calibration point (Gaulfoss). The input hourly discharge data at the calibration point and interior uncalibrated gauging stations was obtained from Norges Vassdrags-og energy direktorat (NVE.NO). The observed hourly discharges from the interior gauging stations have been used to assess the performance of the model at these stations. The UTM coordinates of the discharge and raingauge stations are presented in **Table 1 & 2** and refer to **Fig.9** for the locations of discharge and meteorological gauging stations.

**Table 1: Location of discharge gauging stations.**

| Discharge gauging stations | Easting (m) | Northing (m) | Elevation amsl (m) |
|---|---|---|---|
| Gaulfoss | 562052 | 6998272 | 53.00 |
| Hagabru | 564969 | 6993669 | 61.50 |
| Hugdalbru | 563147 | 6985547 | 139.50 |
| Lillebudal | 578900 | 6966845 | 518.00 |
| Eggafoss | 611013 | 6975227 | 297.00 |
| Killingidal | 620855 | 6965818 | 475.75 |

**Table 2: Location of interior hourly rain gauge stations**

| Rain gauge stations | Easting (m) | Northing (m) | Elevation amsl (m) |
|---|---|---|---|
| Sokendal | 559804.142 | 6980956.498 | 299 |
| kotsøy | 578719.501 | 6984288.896 | 127 |

### *3.2.3 WATERSHED, SUB-CATCHMENTS AND STREAM NETWORK DELINEATION*

Before starting to do any hydrological modeling; streams, watersheds and sub-catchments have to be delineated and some basic watershed properties such as area, slope, flow length, and stream network density have to be obtained. The processing of DEM to delineate watershed, sub-catchments and stream network is referred to us terrain pre-processing. Arc hydro has been used for watershed, sub-catchments and stream network delineation. The results has been used to create input files for the model that includes; stream link grid, sub-catchments etc.

The first step that has been done in sub-catchment, watershed and stream network delineations is to carry out raw DEM processing using arc hydro for two cases, i.e. starting from DEM reconditioning to watershed for with agree method and from fill sinks to watershed for without agree method. The second step is clipping out the flow direction grid of the first step by the water shade of the Gaulfoss gauging station.

The third step is carrying out sub-catchment, watershed and stream network delineations starting from clipped flow direction grid to drainage point. The last step is repeating steps one to three for both cases (with agree DEM and without agree DEM) for 1% of maximum accumulated flow, because in arc-hydro catchment is breakdown into sub catchments based on stream network target.

Stream network and sub-catchments are compared for both cases to see how the variation is between the existing stream and DEM created streams (with and without burning over the existing streams). **Fig.10** shows comparison of stream networks. The results are similar except minor differences and the 1% of maximum accumulated flow as threshold for stream delineation without agree method have been selected for stream network delineation because this is suggested as appropriate for the TOPLAND topographic index calculation and size range of sub-catchments. **Fig.9** shows sub-catchments and stream network delineated using arc-hydro tool. **Appendix-3** presents stream and sub-catchment properties generated using arc-hydro.

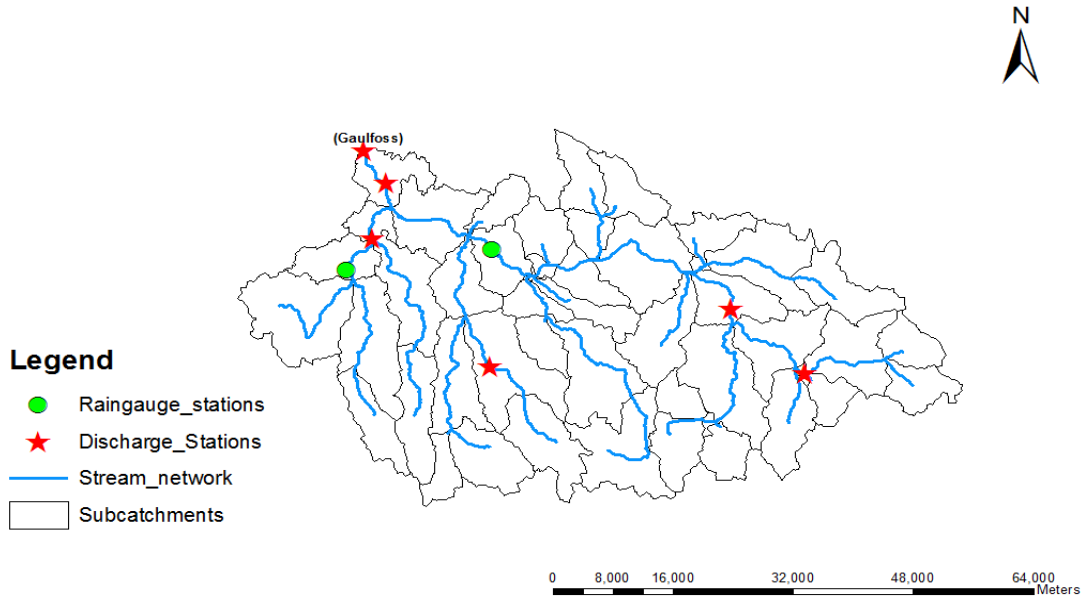


**Figure 9 : Sub -Catchments and Stream networks delineated using arc hydro tool**

Using arc-hydro tool, the total number of sub-catchments delineated was forty five. Further sub division of large sub-catchments has been carried out by writing small script, so that unrealistic model output from such large sub-catchments will be more reliable and accurate. The total numbers of sub-catchments, used for the preparation of the model input data, are fifty.

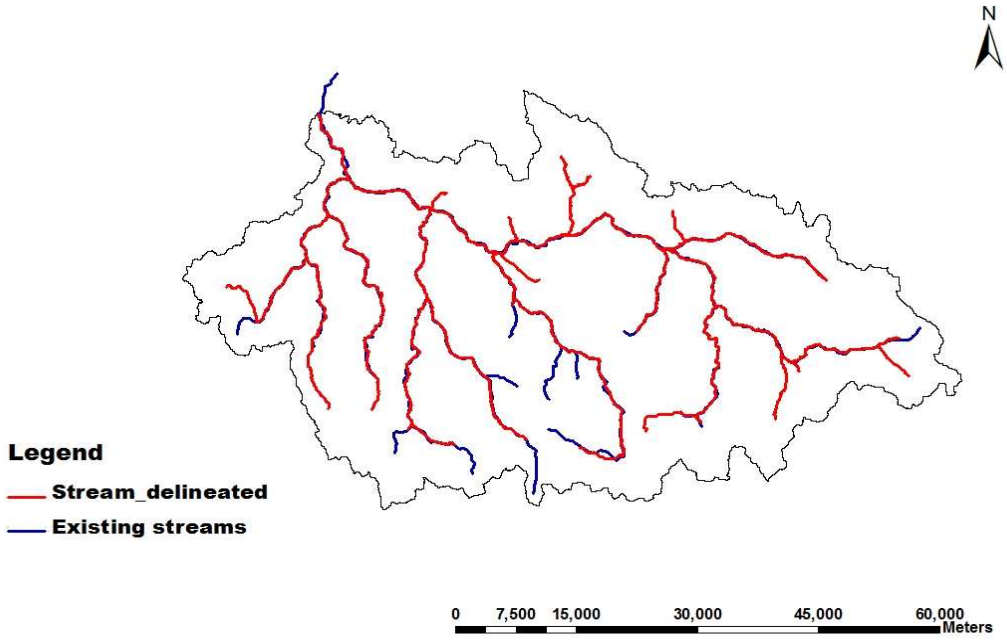


**Figure 10 : Stream network comparison**

Watersheds from the interior gauging stations have been delineated using point watershed delineation function of arc-hydro tool. These watersheds are important; to estimate TOPMODEL parameter 'm', to see the distribution of events with in the sub-catchment using area ratio method, and to use these gauging stations as validation of the model. **Table 3.3** presents watershed areas of the gauging stations in the Gaula catchment and **Fig.11** shows the sub-catchments from interior gauging stations.

**Table 3:** ***Watershed areas for the gauging stations***

| Gauge Stations | Gaulfoss (outlet) | HagaBru | Hugdalbru | Lillebudal | Eggafoss | Killingidal |
|---|---|---|---|---|---|---|
| Area($km^2$) | 3094.74 | 3068.203 | 557.761 | 168.944 | 668.370 | 224.1 |

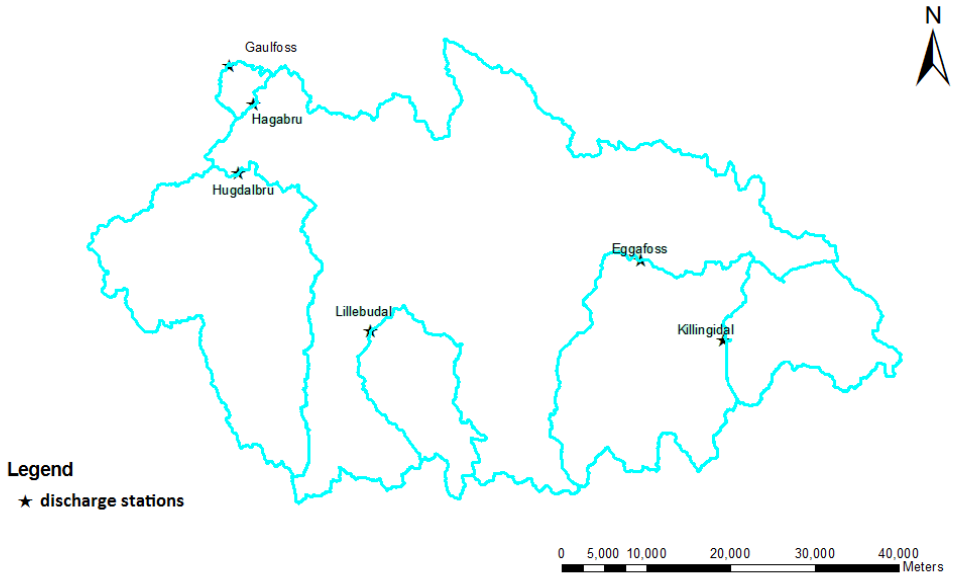


**Figure 11 : Watersheds to the discharge gauging stations**

### *3.2.4 STREAM REACH PROPERTIES ESTIMATION*

For many catchments, especially large ones like Gaula, it is inappropriate to assume that all runoff reaches the catchment outlet within a single time step. In such cases, some routing of model output is required and therefore it is important to determine stream reach properties used for routing that include bed slope, length and top width of the streams.

**Slope**

To determine the distributed channel routing parameter ($\alpha$) and Kinematic wave celerity ($c_k$ ) in a channel, slope of the channel is an important input parameter. See the following equation how $s_o$ is used in estimating $c_k$ by relating continuity and momentum equation.

$$c_k = \left(\frac{\sqrt{S_o}}{n}\right)\left(\frac{5}{3}\right) Y^{2/3} \qquad \text{(Eq. 3.3)}$$

Where, $Y$ is depth of flow and $n$ is Manning's number.

A common problem of digital elevation model analysis is to determine slope of the river bed in one dimension, which is the requirement for kinematic routing. This is because of river grid squares, where the actual river bed width is much less than the grid size (50m). Bed slope of the river has been analyzed in two methods.

The first method is determining slope of each pixels in the DEM by using the function in spatial analyst - surface analysis-slope and then extracting using stream link. But the way that this function calculates slope does not agree with the kinematic wave routing assumptions (the flow characteristics like depth and velocity are considered to vary in the longitudinal direction of the channel) and therefore another method has been adopted.

The second method (which is taken as reasonable and used for analysis) is extracting the raw and fill DEM by writing small script of python using stream link, flow direction and flow accumulation grids. After the extraction of the DEM, the length of the stream reach is calculated manually considering the flow direction value and plotted against the DEM value to see the stream profile in a longitudinal direction.

Since the slope of each stream varies from upstream to downstream end, average slope has been taken.

$$Average\ Slope = \frac{Upstream\ end\ DEM - Downstream\ end\ DEM}{Length\ of\ the\ stream} \qquad \text{(Eq. 3.4)}$$

It has been also cheeked that slope estimation by the second method (slope of slope line from fill DEM) gives the same result as the slope calculation using arc-hydro function (Watershed processing-longest flow path parameters-flow path parameters from 3D Line). The results of some selected streams slope for 50m DEM obtained by the second method are presented in **Fig.12**.

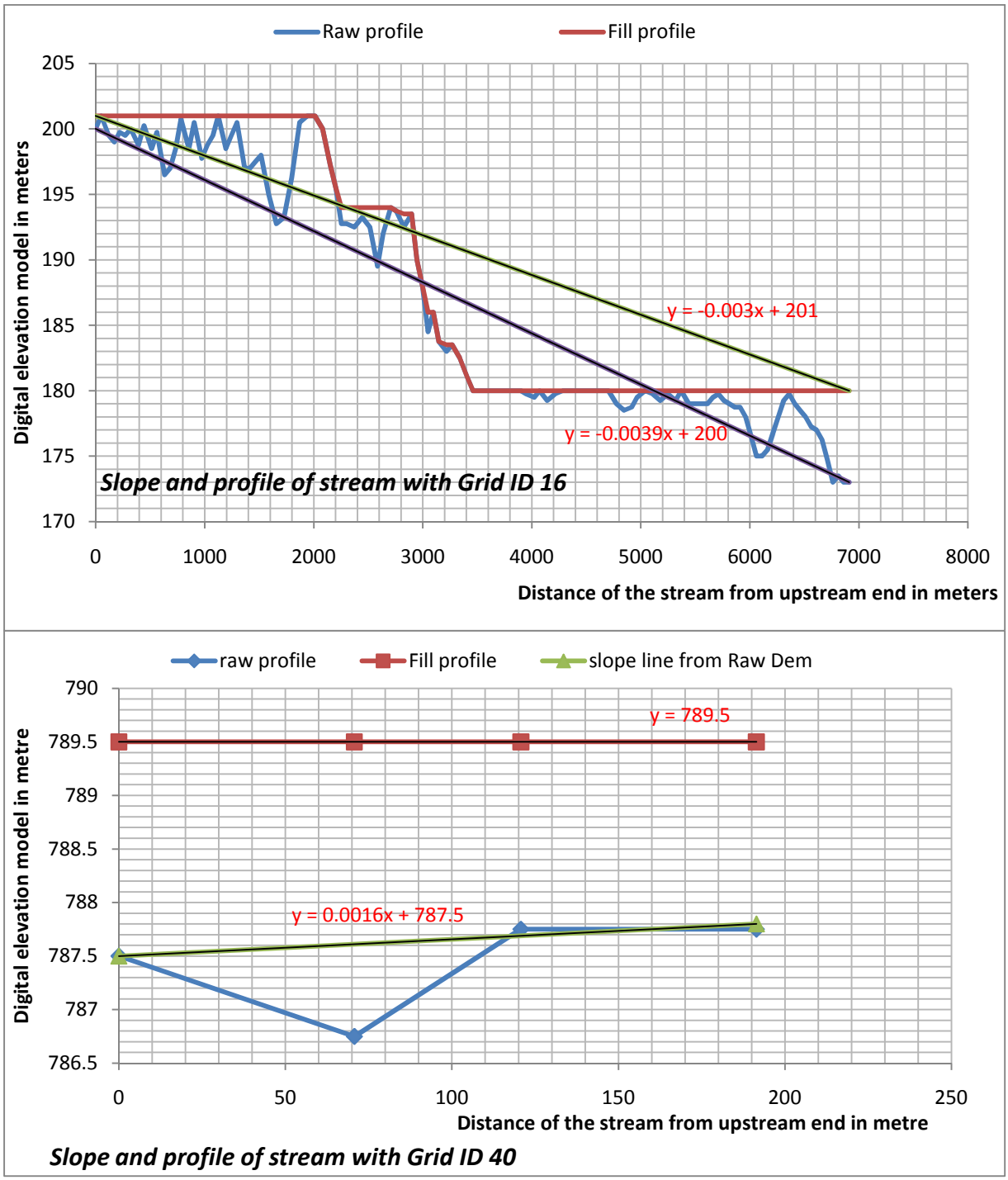


**Figure 12 : Longitudinal profile and slope of some selected streams**

As it is observed from stream with Grid ID 40, slope of some streams are zero for fill DEM and negative for raw DEM (with arc hydro stream generation method) which is not true in reality. Therefore, the minimum positive slope value has been assigned for zero slope streams.

**Top width**

Like the slope of the channel, top width of the channel ($B$) is important to determine the distributed channel routing parameter ($\alpha$). See the following equation how $B$ is used in estimating $\alpha$ by relating continuity, momentum and manning's equation.

$$\alpha = \left[\frac{nB^{2/3}}{\sqrt{S_o}}\right]^{0.6} \quad \text{(Eq. 3.5)}$$

The top width of the channel has been analyzed in two methods. One is from the theoretical assumptions and the other is from semi-field measurement.

**Method one**

The following assumptions have been made for computation of top width of the stream channels:

**I.** The shape of cross section of the river is similar throughout the stream network. Since the shape of the cross section at the outlet is nearly parabolic (shown in **Fig.13**), the following equation can be developed.

$$B_i = a_o^{1/bo+1}[(b_o + 1)A_i]^{b_o/b_o+1} \quad \text{(Eq. 3.6)}$$

$b_o, and\ a_o$ are constants determined from the stage-discharge relationship and cross sectional profile closest to Gaulfoss gauging station. The cross sectional profile data is presented in **Appendix 4**.

**II**. Channel forming flow is a known function of drainage area.

$$\frac{Q_i}{Q_o} = \frac{A_i}{A_o} \quad \text{(Eq. 3.7)}$$

**III**. Cross sectional area is a known function of stream order.

$$\frac{A_i}{A_o} = R_L^{(K\,i-Ko)/Ko} \quad \text{(Eq. 3.8)}$$

Where *i* denote any upstream cell and subscript *o* the value at the outlet, $R_L$ is Horton's length ratio and $K$ is stream order.

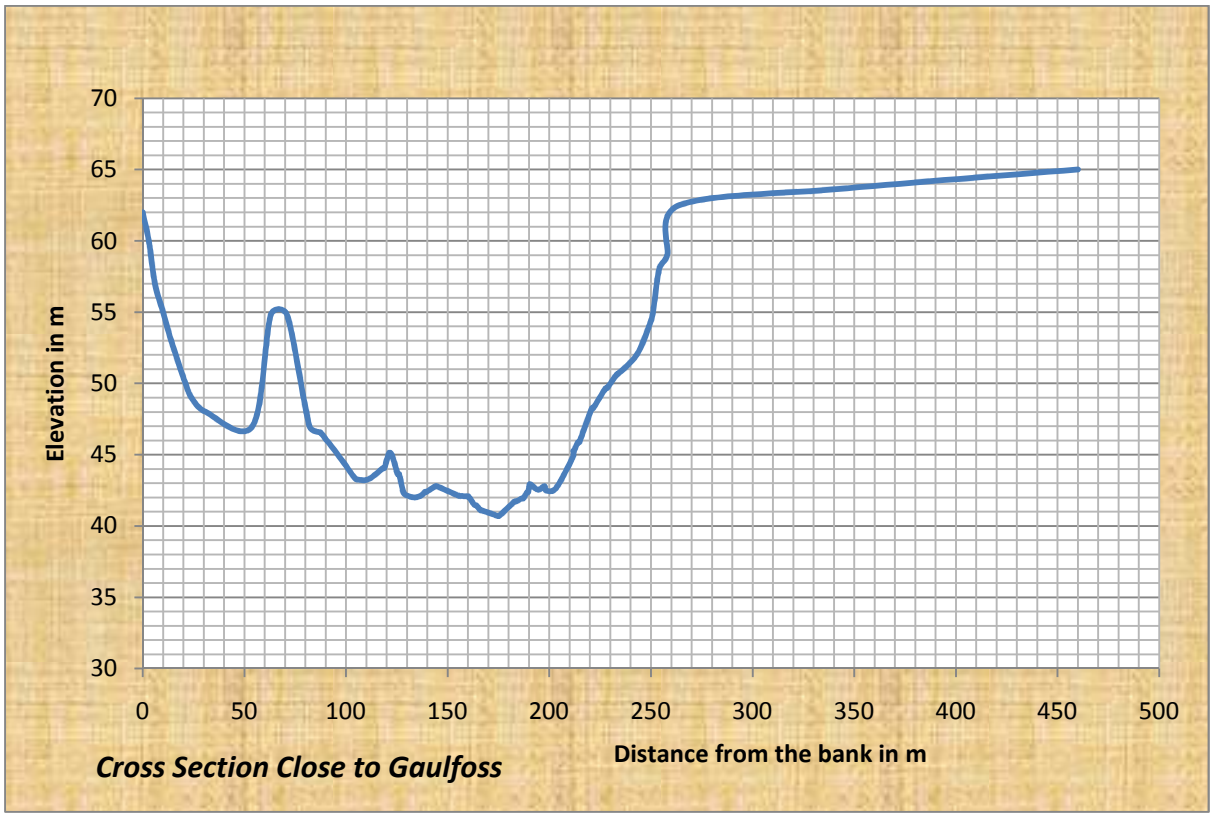


**Figure 13 : Cross section of the Gaula river close to Gaulfoss gauging Station**

Combining the stage discharge curve and the cross-section of the river, the relationship between top width and flow area has been developed (**Table 4**), and shown in **Fig.14**. From the graph of **Fig.14**; $a_o$ =60.7 , $b_o$=0.47.

**Table 4: Discharge, cross sectional area and top width relationship close to Gaulfoss gauging station**

| Average height above stage of zero discharge (m) | Discharge Q ($m^3/s$) | Top width (m) | Cross sectional area ( $m^2$) |
|---|---|---|---|
| 2 | 58.24 | 114 | 228 |
| 3 | 107.6 | 124 | 372 |
| 4 | 177.2 | 134 | 536 |
| 5 | 269.8 | 140 | 700 |
| 6 | 388 | 145 | 870 |
| 7 | 534 | 150 | 1050 |
| 8 | 711.1 | 159 | 1272 |
| 9 | 920.7 | 169 | 1521 |
| 10 | 1165 | 173 | 1730 |
| 11 | 1417 | 176 | 1936 |
| 12 | 1675 | 180 | 2160 |
| 13 | 1957 | 244 | 3172 |
| 14 | 2225 | 247 | 3458 |
| 15 | 2482 | 250 | 3750 |
| 16 | 2779 | 253 | 4048 |
| 17 | 3032 | 254 | 4318 |
| 18 | 3325 | 255 | 4590 |
| 19 | 3661 | 259 | 4921 |

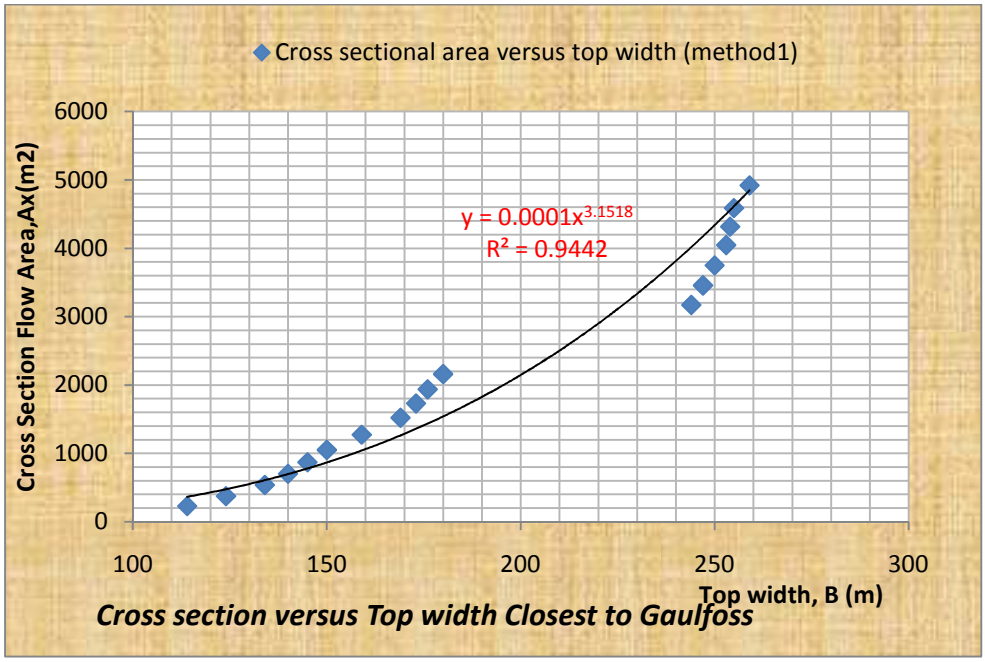


**Figure 14: Relationship between cross sectional area and top width using assumptions**

**Method two**

Since equation of the third assumption in the method one is rough, i.e. it needs detail investigation to set appropriate equation to the study water shade, a preliminary field measurement has been carried out and a simple relationship (needs detail measurement to set appropriate relationship) developed between discharge versus top width of the Gaula river. **Fig.15** illustrates the simple relationship from field measurements of gauging stations. Data for the field measurements is presented in **Table 5.**

**Table 5:Top width and discharge data from field measurement**

| **Location** | Q ($m^3/s$) | B (m) |
|---|---|---|
| Gaulfoss | 428 | 70 |
| Eggafoss | 130.5 | 28 |
| Lillebudal | 22 | 24 |
| Hugdal | 64 | 27 |
| Killingal | 15 | 19 |
| ID 5 | 364 | 53.2 |
| ID19 | 316 | 46 |

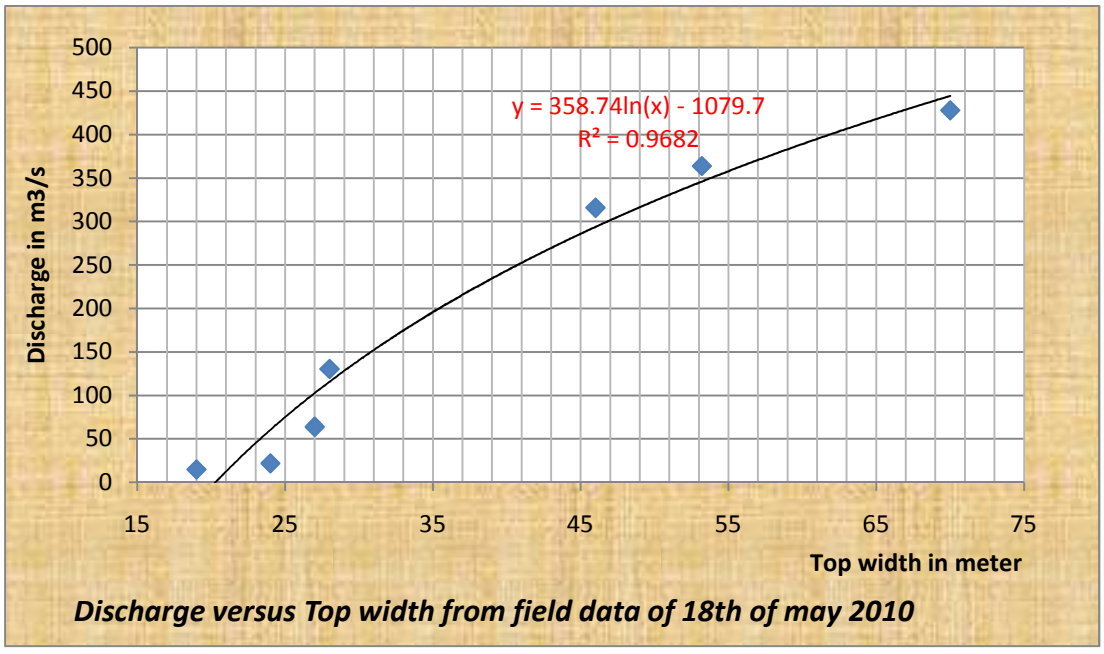


**Figure 15: Simple relationship between discharge and top width using field easurements**

Since the first method of top width estimation overestimates the top width very much, the second method has been used to compute the top width of the model input. As a wide channel assumption is used in kinematic routing, mean discharge of the simulation period is selected for the computation.-

**Length**

The solution of the kinematic wave equation specifies the distribution of the flow as a function of distance x along the channel and time t. To determine the outflow hydrograph at the downstream end of the stream channel, we have to know the length and then the number of sections of each stream. The length of the streams have been calculated using two methods and both of them gave as the same result. The first method is directly reading the attribute tables of the drainage line output of the arc- hydro analysis.

The second method (semi-manual method) is extracting the flow direction grid of the stream using the stream link grid by writing a small script of python and calculating manually by assigning appropriate length to each flow direction. For 1, 4, 16 and 64 flow direction values, the length is equal to the DEM size whereas for 2, 8, 32 and 128 flow direction values it is $\sqrt{2}$ times the DEM size because they are diagonal ( refer to **Table 6**).

Both methods of the result gave the same result and also they used as a cross check. The analysis for stream with grid ID 40 is presented in **Table 6.**

**Table 6: Manual method of stream length calculation for stream with Grid ID 40**

| Raw | | | | | Fill | | | | |
|---|---|---|---|---|---|---|---|---|---|
| Fac | Fdr | DEM | Cell to cell dist. (m) | Leng. from u/s end (m) | Fac | Fdr | DEM | Cell to cell dist. (m) | Leng. from u/s end (m) |
| 12560 | 2 | 787.5 | 70.71 | 0 | 12560 | 2 | 789.5 | 70.71 | 0 |
| 12641 | 1 | 786.75 | 50.00 | 70.71 | 12641 | 1 | 789.5 | 50.00 | 70.71 |
| 12644 | 2 | 787.75 | 70.71 | 120.71 | 12644 | 2 | 789.5 | 70.71 | 120.71 |
| | | 787.75 | | 191.42 | | | 789.5 | | 191.42 |
| Total | | | | 191.42 | Total | | | | 191.42 |

## *3.2.5 DIGITAL INPUT MAPS FOR TOPLAND MODEL*

### 3.2.5.1 General Description

Distributed input maps are prepared as digitized maps with a network of raster cells. Raster digital input maps for TOPLAND model is generally divided into two, i.e. distributed non-initial state parameter maps and distributed initial state maps. For the preparation of most of

the distributed and initial state maps, land use and vegetation maps obtained from Norwegian Forest & landscape (Formerly NIJOS), has been used. IDRISI software has been used for the preparation of input files and remapping. Vegetation map works as basins for vegetation height, cover, type and leaf area index. Land use as basis for field capacity, surface storage, infiltration and leaf area index of low vegetation.

TOPLAND hydrological model uses LANDPINE and TOPMODEL coding system for the preparation of required digital maps.

**I. Distributed initial state maps**

Distributed initial state maps describe the characteristics of the catchment just before the start of simulation and change in their value during each time step in simulation period, i.e. they vary both spatially and timely. Distributed initial maps include; initial soil saturation denoted by *INITIALSOLSAT*, initial snow coverage *( INITIALSNWCOV)*, initial free water in snow pack (*INITIALSNWWAT*), initial accumulated temperature (*INITIALACCUTMP*), and initial snow pack denoted by (*INITIALSNWPCK*).

**II. Distributed non-initial state parameter maps**

Distributed non-initial state input parameter maps vary spatially within the catchment. Once they determined, they are constant from the beginning to the end of the simulation period. Distributed parameter maps for TOPLAND model include; land use maps (*LANDUSE)*, high vegetation cover (*VEGCOV*), type of vegetation e.g. leaf, needle, mixed(*VEGTYP*), average height of trees (*VEGHGT*), leaf area index maximum (*LAIMAX*), leaf area index of low vegetation (*LAILOW*), leaf area index minimum (*LAIMIN*), surface storage (*SRFSTR*), infiltration capacity (*INFCAP*), field capacity (*FLDCAP*), elevation (*ELEVATION*), flow direction (*FLOWDIR*), stream link (*STREAM*), sub catchment (*SUBCAT*) and topographic index (*TI*).

**Land Use/Land Cover (*LANDUSE)***

The classification and representation of the land use/land cover characteristics of the catchment is required as input to the model for defining the catchment boundary and differentiating lakes (water bodies) from land with any other type of cover. This differentiating is necessary since the hydrological processes considered for computation are not the same for a lake and a land with or without vegetation. Though it is not directly useful in the model computation process, TOPLAND uses LANDPINE system that requires further classification system for land surfaces. This classification is used as a reference for driving other input parameters describing vegetation.

The LANDPINE land use classification system with the corresponding codes assigned is given in **Table 7.**

**Table 7 : LANDPINE coding system for land use**

| Code | Description |
|---|---|
| 0 | Outside catchment. Defines catchment boundary. It has 0 values outside the catchment boundary. |
| 1 | lake |
| 2 | Areas with forest removed |
| 3 | New growth forest |
| 4 | Marsh |
| 5 | Forest |
| 6 | Mountain/bare rock |
| 7 | Farmland |
| 8 | Urban |
| 9 | Low vegetation – mountainous |

**Vegetation Type (VEGTYP)**

The map representing the types of vegetation within the catchment is not directly used for computation purposes within the model. By integrating with the corresponding land use map, it is used in estimating relevant vegetation parameters. This is because varies vegetation parameters are normally specified in literatures for particular land use and vegetation types.

The LANDPINE vegetation type classification system with the corresponding codes assigned is given in **Table 8.**

**Table 8 : LANDPINE Coding system for VEGTYP**

| Code | Description |
|---|---|
| 100 | Needle trees |
| 200 | Mixed trees |
| 300 | Trees with broad leaves |

**High and Low Vegetation**

It is very important to define the High and Low Vegetation types within the particular land cover types. These are derived from the land use and the vegetation type maps already prepared. This definition is important since different vegetation parameters used by the model are specifically assigned for the high and low vegetation.

**Vegetation Cover (VEGCOV)**

Vegetation map represents the percentage coverage of the high vegetation and varies depending on the type of land use. It is utilized for the computation of rainfall interception and evapotranspiration from high vegetation.

**Vegetation height (VEGHGT)**

The height of trees influences the evapotranspiration from vegetated land. In order to simulate this dependency properly, the variation of the vegetation height over the catchment is represented by this map.

**Leaf area index (LAI)**

Leaf area index (LAI) is broadly defined as the amount of leaf area in a canopy per unit ground area. This dimensionless parameter indicates the average density of vegetation covering the ground. Since precipitation interception is substantially determined by the vegetation surface, LAI is utilized in the computation of interception capacity.

**Soil parameters**

The soil parameters that are required by the model for the evapotaranspiration and runoff computation are surface storage (SRFSTR), infiltration capacity (INFCAP), field capacity (FLDCAP) and the initial soil saturation (INITIALSOLSAT). Surface storage determination are based on representative values given by the LANDPINE coding system for major land cover types is presented in **Table 9.** Infiltration capacity estimates are based on standard values given the by the SCS hydrologic soil group classification system and presented in **Table 10.**

**Table 9: Surface storage values for different land use systems**

| Value (mm) | Description |
|---|---|
| 0 | Lake |
| 0.1 | Bare Rock |
| 0.5 | Soil Surface |
| 2.0 | Marshes |

**Table 10 : SCS hydrologic soil group classification**

| Soil group | Description (Texture) | Infiltration Capacity (mm/day) |
|---|---|---|
| A | Sand, or sandy loam | 180-270 |
| B | Silt loam or loam | 90-180 |
| C | Sandy clay loam | 30-90 |
| D | Clay loam, silty clay loam, sandy clay or clay | 0-30 |

### 3.2.5.2 Application to Gaula Catchment

**ELEVATION**

The elevation map for Gaula catchment is extracted from the 50m x 50m resolution DEM of the area. Refer to **Fig.7** for elevation map of Gaula catchment.

**LNDUSE**

The land use of Gaula catchment is mainly composed of mountainous/bare rock, coniferous forest, deciduous forest, marsh, mixed forest, anna jorddekt fastmark, and Grunnlendt mark. The land use map is prepared from digitalized land use maps obtained from Norwegian Forest & landscape (Formerly NIJOS). The codes used for specification are adopted from **Table 7.**

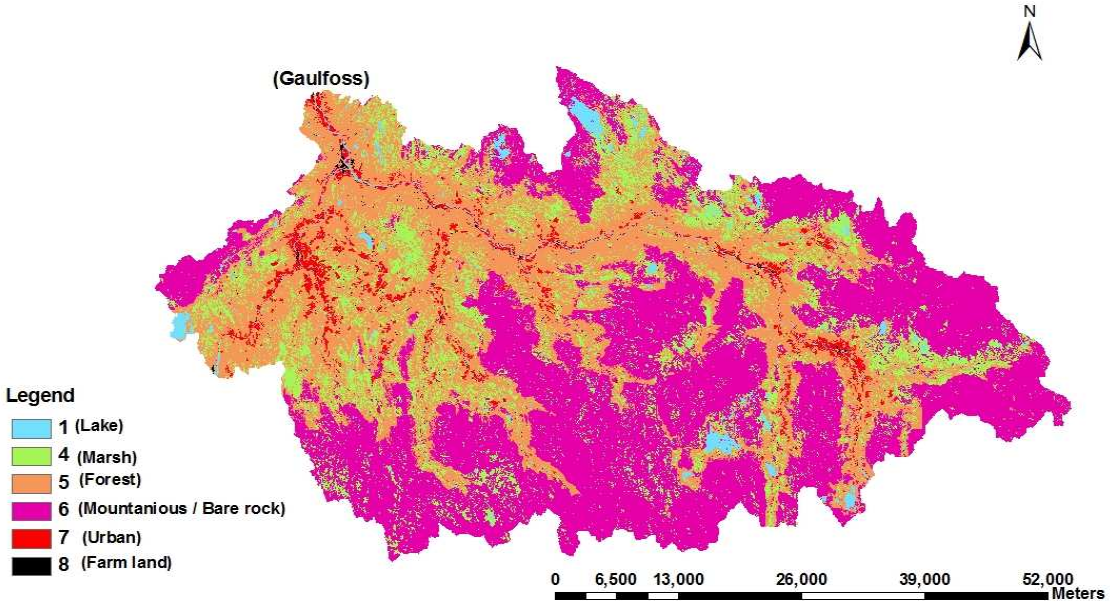


**Figure 16 : Re-classified land use map of the study catchment**

**VEGCOV**

The percentage vegetation cover values for the forests of Gaula are estimated using the following empirical equations categorized based on Bonitet values.

*High Bonitet*

$$VEGCOV = 62.963127 + 0.102046 * VUPRHA - 0.000171 * VUPRHA^2 \qquad \text{(Eq. 3.9)}$$

*Low Bonitet*

$$VEGCOV = 22.628106 + 0.310853 * VUPRHA - 0.000422 * VUPRHA^2 \quad \text{(Eq. 3.10)}$$

*Medium Bonitet*

$$VEGCOV = 35.980247 + 0.20525210 * VUPRHA - 0.000250 * VUPRHA^2 \quad \text{(Eq. 3.11)}$$

Where $VUPRHA$ = volume without bark in $m^3$ per ha.

The above equations give vegetation coverage values of 40%, 54% and 74% for the forests with low, medium and high Bonitet values respectively. Since there is no Bonitet values provided for marshes and other land use types like cultivated land and built up areas, a value of 10 % is assigned for marshes and a value of 5 % is assigned for mountainous/bare rock land uses. Vegetation cover value of 0% is assigned for lakes and water bodies.

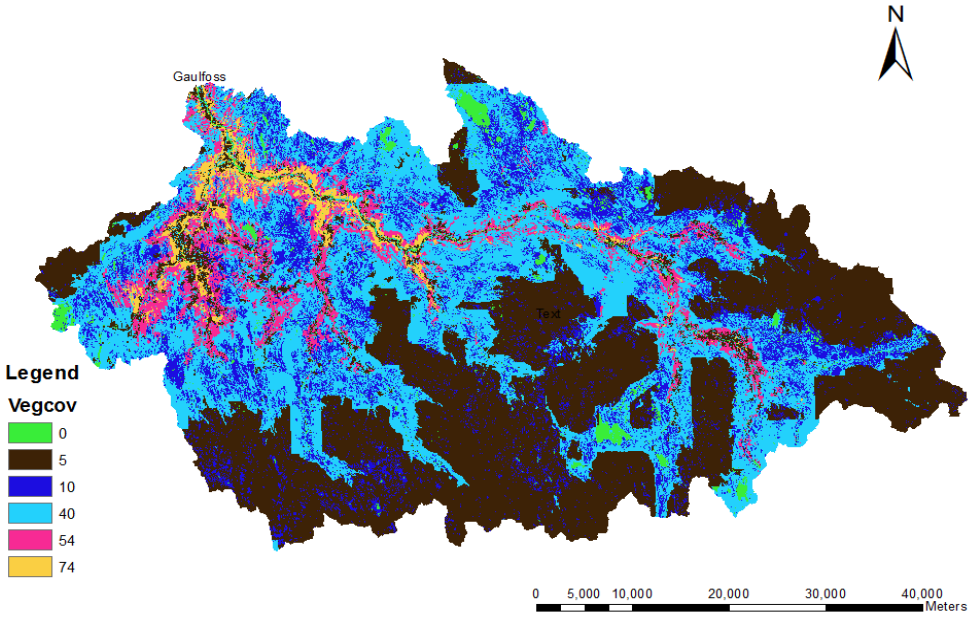


**Figure 17: Vegetation cover map of the study catchment**

**VEGTYPE**

The map representing the vegetation type in the catchment is prepared based on digitized maps available and prepared in the same fashion as the land use maps. The whole catchment is dominated by mountainous/barerock, needle trees with higher density to the forest areas and much lighter density for the marshy areas. Conversion to the TOPLAND system is made using the LANDPINE conversion system and presented in **Table 8**.

Since the map representing the types of vegetation within the catchments is not directly used for computation purposes within the model and assuming that Gaula catchment is dominated by needle trees, all the vegetation type has been assumed to have a value of 100 for simplicity.

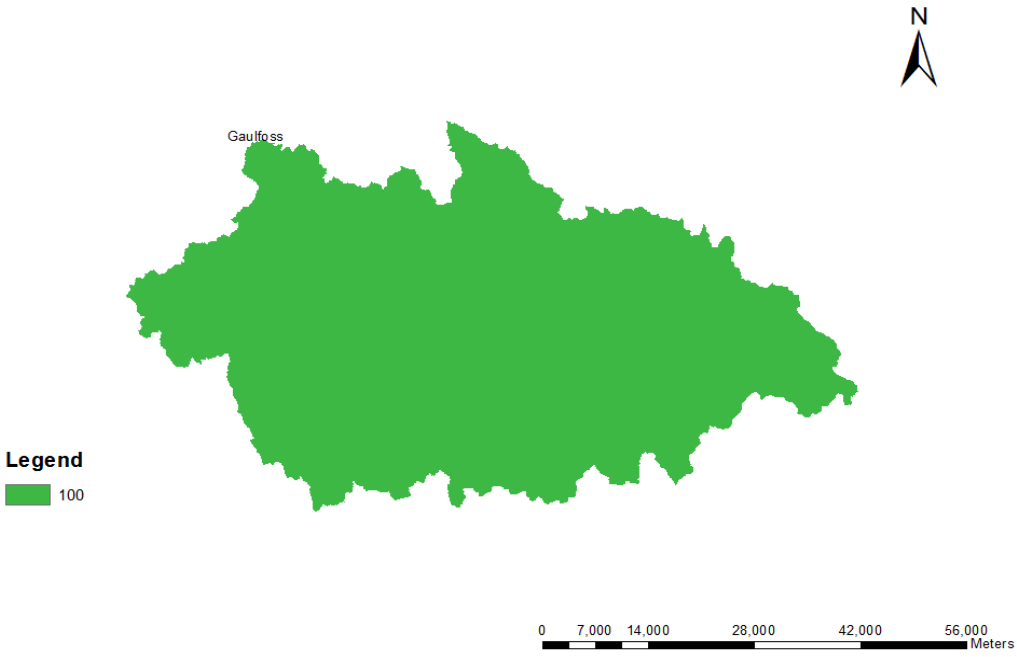


**Figure 18: Vegetation type map of the study catchment**

**VEGHGT**

The heights of the needle trees for the study catchment are computed from a set of empirical equations developed within the HYDRA project (Grønlund et al, 2000). These equations are categorized according to Bonitet values.

Low Bonitet

$$OH = 10.535277 + 0.056626 * VUPRHA - 0.000080076 * VUPRHA^2 \quad \text{(Eq. 3.12)}$$

Medium Bonitet

$$OH = 9.764838 + 0.0675535 * VUPRHA - 0.000090347 * VUPRHA^2 \quad \text{(Eq. 3.13)}$$

High Bonitet

$$OH = 8.416540 + 0.076589 * VUPRHA - 0.000095159 * VUPRHA^2 \quad \text{(Eq. 3.14)}$$

$VUPRHA$ = *volume without bark in* $m^3$ *per ha.*

$OH$ = *overheight in m*

For High and Medium Bonitet

$$MH = 0.00413 * OH^2 + 0.8822 * OH - 1.573 \quad \text{(Eq. 3.15)}$$

For Low Bonitet

$$MH = 0.00266 * OH^2 + 0.9297 * OH - 1.111 \quad \text{(Eq. 3.16)}$$

$MH$ = mean height in m

The mean height ( $MH$) is assumed to represent the average height of the needle trees for the corresponding Bonitet values. Accordingly, mean height of 12 m is taken for all vegetation types in the Gaula catchment.

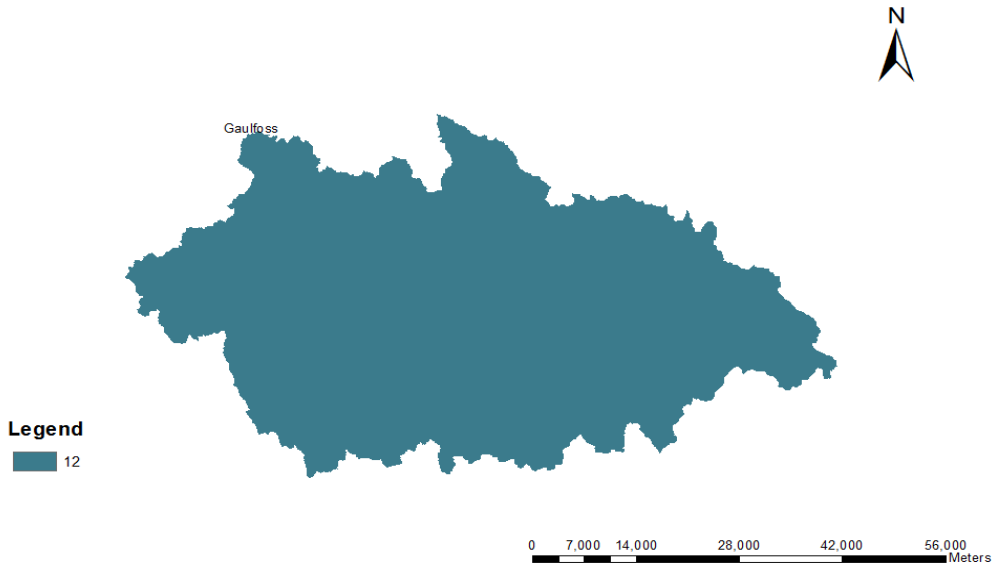


**Figure 19: Vegetation height map of the study catchment**

**LAIMAX and LAIMIN**

Since the simulation of this model is for hourly events that will last for hours or few days but not a season, seasonal variation is not so much important. But the model requires it as input. The LAIMAX values are computed from a set of empirical equations developed within the hydra project. These equations are categorized according to Bonitet values.

High Bonitet

$$G = 12.648458 + 0.080741 * VUPRHA - 0.000085535 * VUPRHA^2 \quad \text{Eq. 3.17)}$$

Medium Bonitet

$$G = 6.885102 + 0.141683 * VUPRHA - 0.000179 * VUPRHA^2 \quad \text{(Eq. 3.18)}$$

Low Bonitet

$$G = 4.377573 + 0.166735 * VUPRHA - 0.000285 * VUPRHA^2 \quad \text{(Eq. 3.19)}$$

Where G = projected area in $m^2$ per ha

High Bonitet

$$LAIMAX = 0.243737 * G + 0.262616 \quad \text{(Eq. 3.20)}$$

Medium Bonitet

$$LAIMAX = 0.243477 * G + 0.067787 \quad \text{(Eq. 3.21)}$$

Low bonitet

$$LAIMAX = 0.221806 * G + 0.308468 \quad \text{(Eq. 3.22)}$$

As computed from the above equations, the $LAIMAX$ values assigned for the needle trees with high, medium and low Bonitet values are 5.6, 4.8 and 3.3. For other land use types, a low Bonitet value, i.e. 3.3 have been assigned. For lakes and water bodies, a value of 0 has been assigned. According to the LANDPINE system, the $LAIMIN$ values for needle trees are estimated from the following relationship.

$$LAIMIN = 0.80 * LAIMAX \quad \text{(Eq. 3.23)}$$

The corresponding $LAIMIN$ values for the $LAIMAX$ values of 3.3, 4.8 and 5.6 are 2.6, 3.8 and 4.5 respectively.

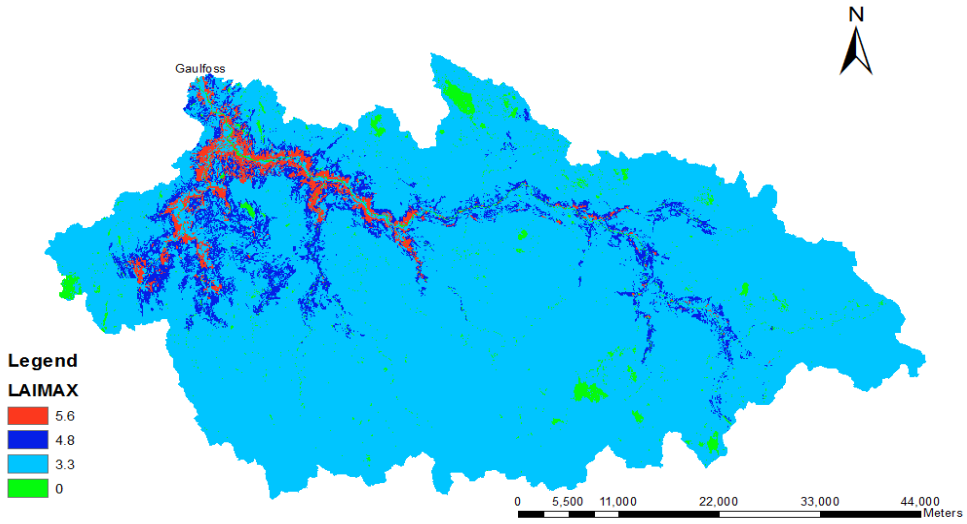


**Figure 20: Maximum leaf area index map for high vegetation**

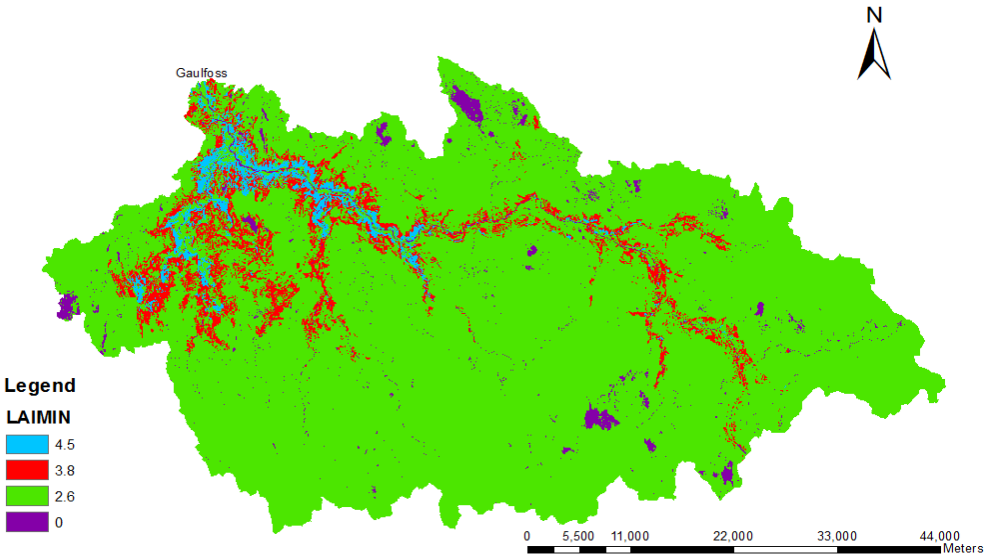


**Figure 21: Minimum leaf area index map for high vegetation**

**LAILOW**

The leaf area index of low vegetation (LAILOW) is taken from the default values used by the landpine code system as given in **Table 11**. The seasonal variation of LAILOW is controlled by one of the calibration parameters, *rwlailw*.

**Table 11 : Low vegetation leaf area index given by LANDPINE system**

| Value | Description |
|---|---|
| 1 | Prairie/Tundra |
| 1-3 | Small Bushes |
| 0-1 | Marshes |
| 0 | Bare rock/Lake |
| 5 | Cornfield |
| 4 | Potato field |
| 5 | Farmland (Grass) |

Depending upon the above table, a value of 1 has been assigned for marshes and small bush with different types, 3 for different types of forests, 0 for lakes and water bodies and 5 for the cultivated and farm lands and 0.5 for mountainous/Bare rock area.

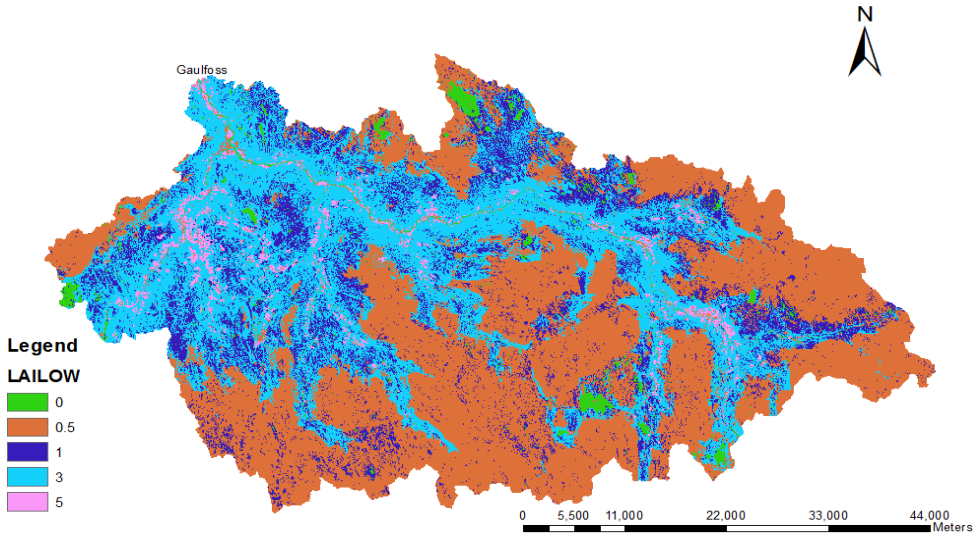


**Figure 22 : Leaf area index of low vegetation of the study catchment**

**SRFSTR**

The parameter is estimated by the land use map with the SRFSTR values given in **Table 9**. Since bare rocks are common in the study watershed and considering the hilly nature of the watershed, a value of zero has been assigned throughout the catchment.

**INFCAP**

As most of the catchment area is characterized by silty loam or loam (rough estimation), an infiltration capacity of 90 mm/day (**Table 10**) has been assigned for all land use types except for lakes and other water bodies. For lakes and other water bodies, a value of 0 has been assigned because of the fact that lakes and water bodies are not within the soil moisture computation zone.

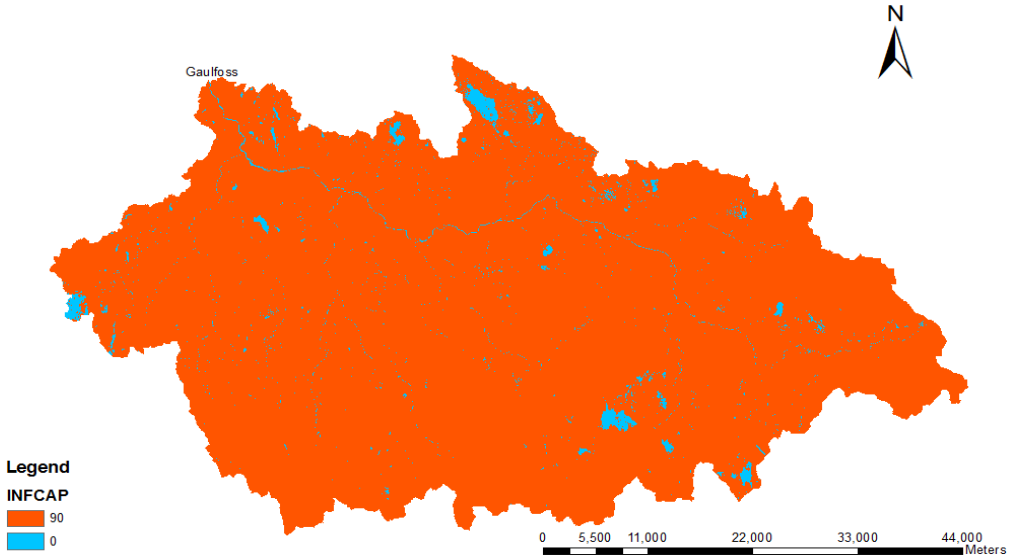


**Figure 23 : INFCAP map of the study catchment**

**FLDCAP**

Field capacity is defined as the maximum moisture holding capacity of the soil layer. The computation of field capacity is based on the estimation of depth of soil cover over the catchment. Deep soil cover depth is expected for marsh land use and shallow depth for forest. Assuming that the soil cover of Gaula catchment ranges from fine sand to sandy loam, an average FLDCAP of 150mm/m is selected for the whole catchment except for lakes and other water bodies of which a zero value has been assigned.

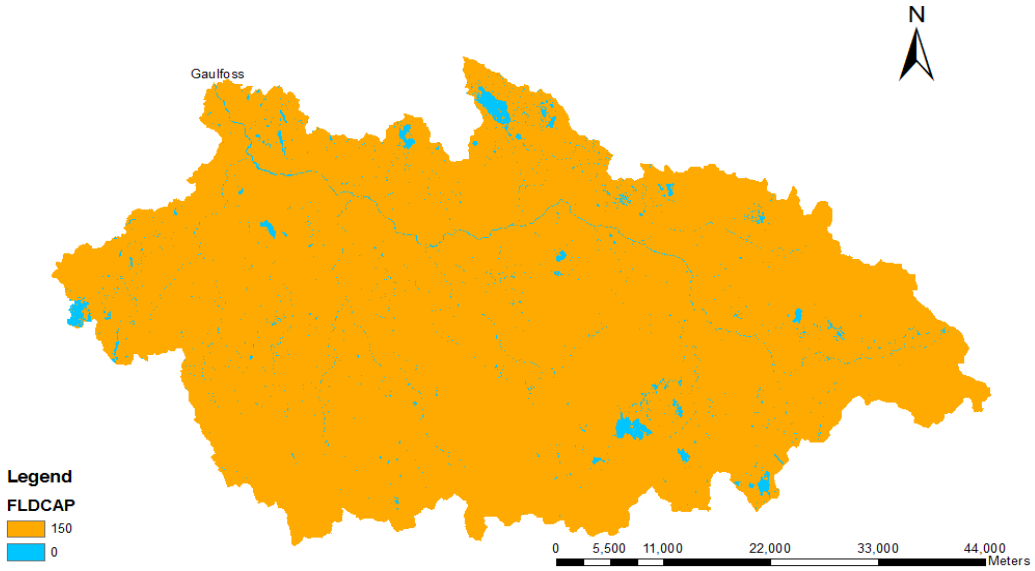


**Figure 24 : Field capacity map of the study catchment**

**INITIALSOLSAT**

The initial soil saturation describes the moisture conditions of the soil at the start of simulation. The model is set up to start simulation for the event that is prceeded by relatively dry periods (periods of low or minimum precipitation). To represent such conditions, a relatively small value (0.1) is assumed for forest and other non-water body land uses. A value of zero has been assigned for lake and other water bodies

**INITIALACCTMP**

The initial accumulated temperature is set to be 100 for all areal elements within the catchment. This value represents the ACCTMP beyond which the LAI is equal to LAIMAX.

**SNOW PARAMETERS**

Since all the simulation events have been selected from July event, all the snow has been assumed to melt during May. Therefore, all the initial snow parameters are set to be zero.

**STREAM LINK MAP**

The stream link map of the study catchment is an intermediate result of terrain pre-processing of arc hydro function. The function creates a grid of streams that have a unique identification number. The stream link segment may be either a head segment or defined as a segment between two segment junctions. In arc hydro analysis, a total of 45 stream link grids have been calculated. Since some sub catchments are big, further subdivision into a total of 50 stream link grids has been done. All the cells in a particular segment have the same grid code that is specific to that segment.

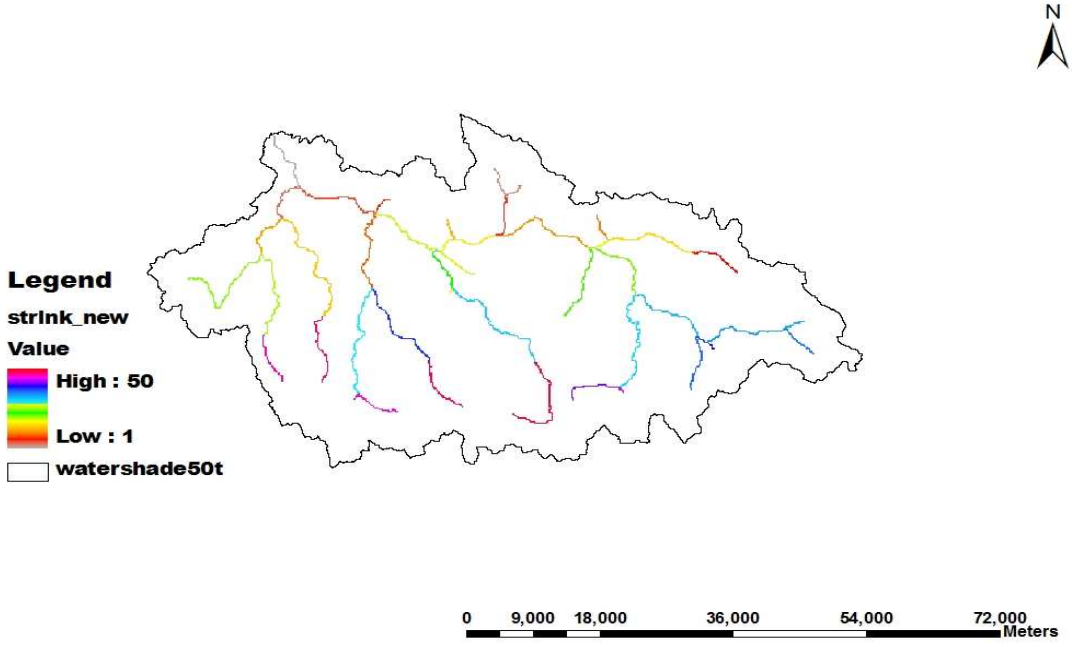


**Figure 25: Stream Link map of the study catchment**

**SUB- CATCHMENT MAP**

Like the stream link grid map, sub catchment map is an intermediate result of arc hydro preprocessing function. This function creates a grid in which each cell carries a value (grid code) indicating to which catchment the cell belongs.The value corresponds to the value carried by the stream segment that drains that sub catchment area, defined in the stream segment link grid. Refer to **Fig.9** for the sub-catchment map that has been divided.

**TOPOGRAPHIC INDEX MAP**

Topographic index map has been generated by Terrain Analysis Using Digital Elevation Models (TauDEM) software (Tarboton, 2002). For the detail description of topographic index, refer to section 4.1. Refer to **Fig.27** for the topographic index map of the study catchment.

# 4. DETERMINATION OF TOPOGRAPHIC INDEX AND TOPMODEL PARAMETER 'M'

## 4.1 TOPOGRAPHIC INDEX (TI)

### *4.1.1 GENERAL DESCRIPTION*

The topographic index, which combines local upslope contributing area and slope, is commonly used to quantify topographic control on hydrological processes. Topography is a first-order control on spatial variation of hydrological conditions. It affects the spatial distribution of soil moisture, and saturated zone flow often follows surface topography (Burt and Butcher, 1985; Seibert et al., 1997; Rodhe and Seibert, 1999; Zinko et al., 2005). Topographic indices have therefore been used to describe spatial soil moisture patterns (Burt and butcher, 1985, Moore et al., 1991). One such index is the topographic index ( $TI$ ) developed by Beven and Kirkby (1979) with in the runoff model TOPMODEL. From the assumption in TOPMODEL that later transmissivity decreases exponentially with depth, topographic index is defined as $ln\left({}^{a}/_{tan\beta}\right)$.

$$TI = ln\left({}^{a}/_{tan\beta}\right) \qquad \text{(Eq. 4.1)}$$

Where, a, is the local upslope area draining through $a$ certain point per unit contour length and $tan\beta$ is the local slope.

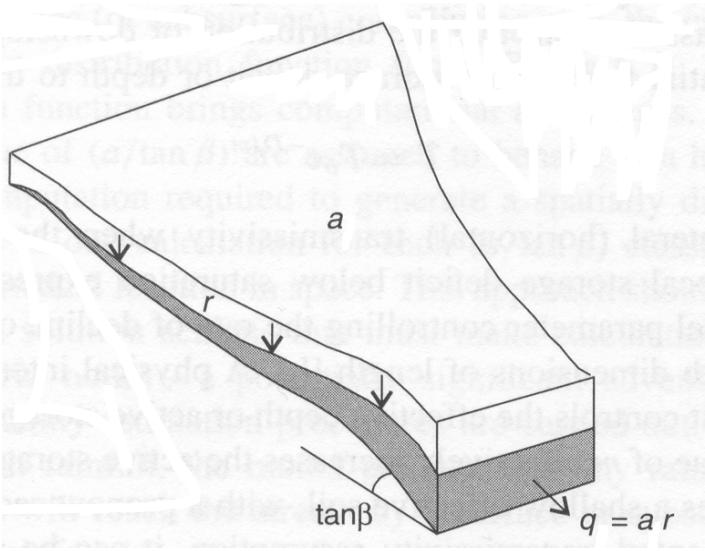


**Figure 26 : Definition of upslope area draining through point within the catchment**

***( Beven, 2000)***

Under uniform recharge, steady state condition, high a means more runoff and low a means less runoff. High $tan\beta$ means higher hydraulic gradient means that there is less back up of water and low $tan\beta$ means lower hydraulic gradient means that greater back up of water. Topographic index increases towards the stream indicating areas of topographic convergence and areas where the water table intersects the soil zone.

### *4.1.2 COMPUTATION OF TOPOGRAPHIC INDEX FOR THE STUDY SITE*

Computation of the topographic index for a catchment is a key problem (Beven and Kirkby, 1979; Deng and Li, 2002) for TOPMODEL performance because its distribution is affected by the resolution of the topography and the channel initiation threshold (CIT).

Topographic index of the 50m DEM has been computed by Terrrain Analysis Using Digital Elevation Models (TauDEM) software (Tarboton, 2002). In the software, $tan\beta/\mathrm{a}$ has been computed to avoid divide by zero error when slope is zero.

To calculate $\mathrm{a}/tan\beta$, the software uses DInf. slope grid (slp) and DInf. specific catchment grid (sca) but when the slope of the pixle is zero, connectivity in Topmodel will be lost. To avoid such problem, the input DInf. slope grids (slp) have been adjusted by assigning the minimum positive slope to zero slopes. The adjusted $tan\beta/\mathrm{a}$ output of TauDEM computation is re-computed by raster calculator to come up with the actual definition and formula of topographic index, $i.e.\ TI = ln\left(\mathrm{a}/tan\beta\right)$.

Topographic Index map of the Gaula catchment for 50m DEM is presented in **Fig.27.** The drawback of calculating topographic index using TauDEM software is that, it calculates specific catchment area using contributing area from all pixels upstream. The accumulated contributing area from an upstream stream cell is routed down slope , because the DInf. specific catchment area grid (Sca ) algorithm does not examine whether a given cell is on the stream or not. Therefore, this method gives unrealistic high result of topographic index along the stream pixels.

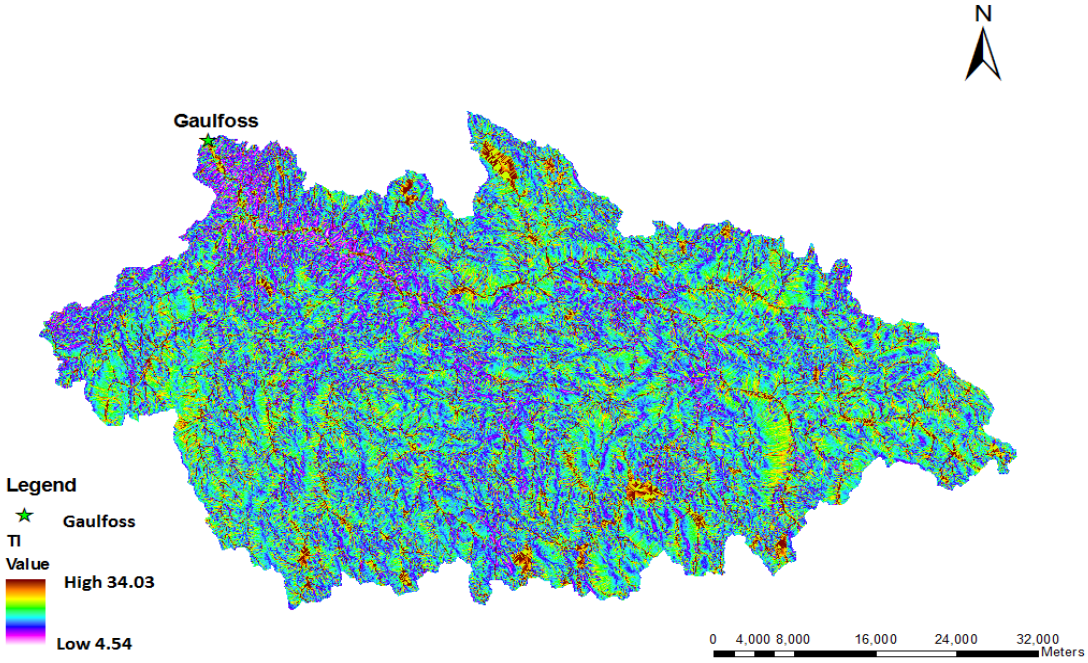


**Figure 27: Topographic index map of Gaula catchment for 50m Dem.**

### *4.1.3 UPSLOPE CONTRIBUTING AREA*

Calculation of upslope area depends on the way the accumulated area of upstream cells is routed to downstream cells. TauDEM software estimation of upslope contributing areas for the pixels along the stream link is simply routing of all upstream area to downstream (**A of Fig.28** used for this study) which gives relatively high upslope area that actually do not belong to these cells. The basic assumptions of topographic index do not hold when there is stream and, thus pixels along the stream need to be considered explicitly. The correct definition of upslope area but not used for this study is shown in **B of Fig.28.**

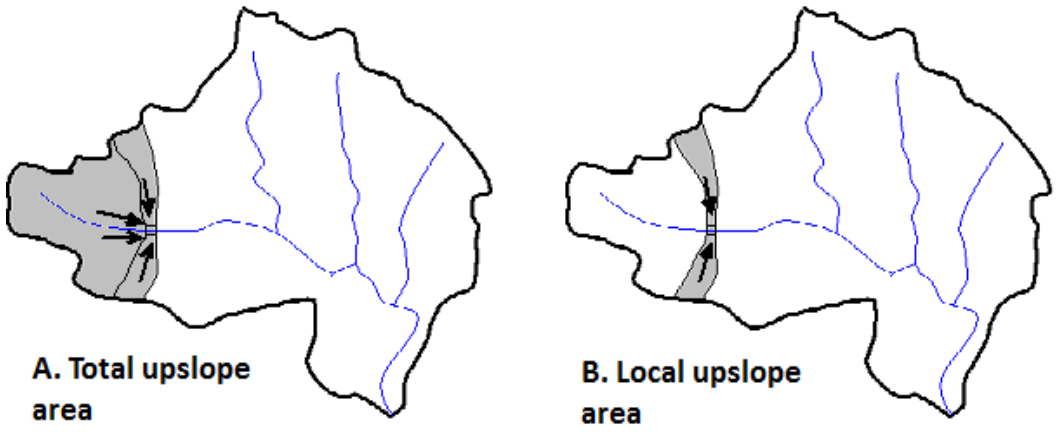


**Figure 28 : Alternative methods of calculating upslope area ( SAULNIER, 1996)**

## 4.2 ESTIMATION OF BASE FLOW RECESSION PARAMETER 'M'

### *4.2.1 GENERAL DESCRIPTION*

The base flow recession curve of a catchment, which expresses the way in which the base flow $Q_b$ decreases naturally during periods without recharge or large evaporation effects, can take varies forms depending on the nature and complexity of the catchment. Decrease in lateral transmissivity can be expressed by one of the following equations;

I. Exponential equation (in which TOPMODEL originally developed) and leads to first order-hyperbolic base flow Master Recession Curve.

II. Parabolic equation which leads to second-order hyperbolic base flow Master Recession Curve.

III. Linear equation leads to exponential base flow Master recession curve.

One of the parameters that control the base flow component of the TOPLAND, is the recession parameter 'm'. The parameter tells us about the storage properties of a catchment and how the discharge from the ground storage depletes gradually during little or no precipitation time. It is determined from the recession curve of the hydrographs using already recorded flow data by recession analysis.

The recession curve tells us in a general way about the natural storages feeding the stream. It contains valuable information concerning storage properties and aquifer characteristics. Recession analysis has been useful in many areas of water resource planning and management including rainfall-runoff models such us TOPLAND.

The base flow recession parameter 'm' at four upstream gauge sub-catchments has been analyzed to see the variation of the parameter in the sub–catchments. At gauging stations of Killingidal, Egafoss and Lillibudal a similar result has been obtained and at HugdalBru a slightly higher result is observed.

### *4.2. 2 RECESSION ANALYSIS*

#### *4.2.* 2.1 Elements of Recession Analysis

Analysis of recession curves, taken from periods of relatively unaffected by evapotranspiration, rainfall or snowmelt inputs, will reveal which of the functions will be best suited to modeling a particular catchment and provide estimates of the constant slope of a linear transform of a recession curve against time.

The recession curve has two major components; linear components of surface flow and, recession segment of base flow.

The main elements of recession analysis are presented below.

**I**. The three analytical expressions used to fit the recession segment includes; exponential, first-order hyperbola and second -order hyperbola. To know which analytical expression fits best for the data at varies gauging stations is the question that has been answered in this paper.

**II**. In humid climate like Norway, rainfall frequently interrupts the recession period. As a result, each discharge series produces a series of recession segments. The method and criteria to select individual recession segment and finding characteristic recession segment from the recession curve has been presented to treat the high variability encountered in the recession behavior of individual segments in a manageable way.

**III**. There are different methods available to optimize the recession parameters and the matching strip method has been utilized to do so.

#### 4.2.2.2 Characteristic curve

If there are n recession segments, then the recession characteristic, $C_P$, can be obtained either from the master recession curve ( a single representative curve for n segments) or from the mean of each segment calculated separately. **Fig.29** illustrates the two methods. Both methods have been done and comparable results have been obtained. Since the master recession curve is selected as the method, only analysis results of Master recession curve is included.

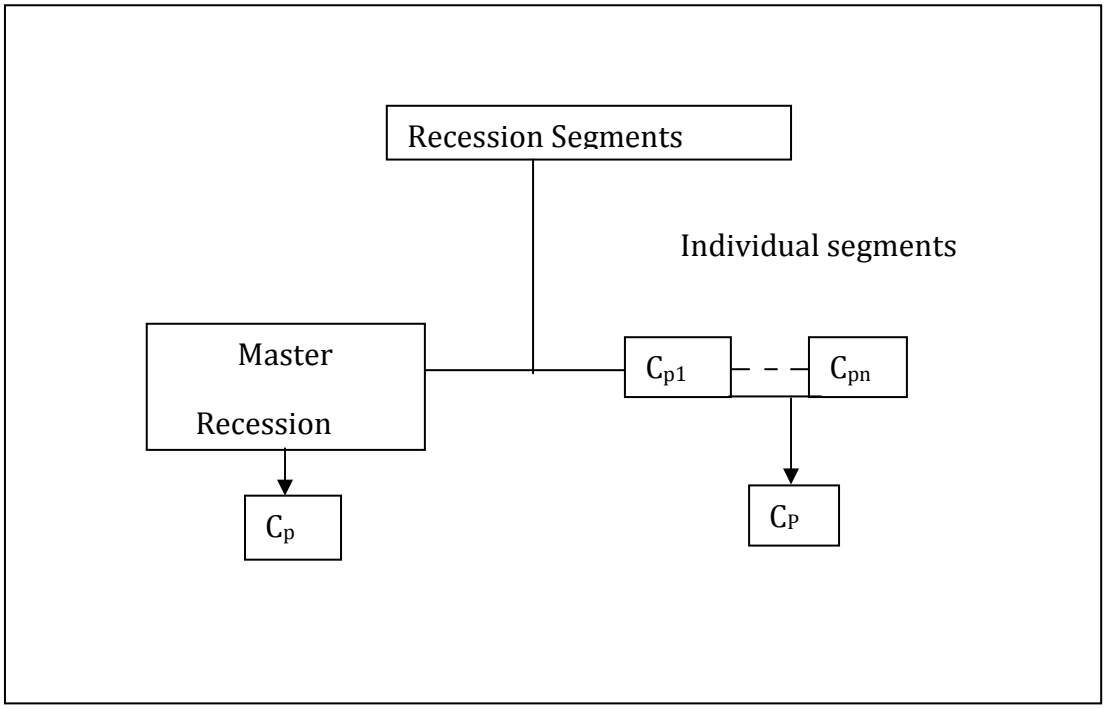


**Figure 29: Recession characteristic, $C_P$, estimation methods**

### *4.2.3 MASTER RECESSION CURVE - MATCHING STRIP METHOD*

#### 4.2.3.1 Segment Selection Criteria

The first step in constructing Master Recession Curve is to select appropriate recession segments from the hydrograph. If all recessions below a given threshold are used, there is a significant correlation between m – value and both starting value ($Q_o$) and length of recession (length). A decrease in ($Q_o$) and an increase in length involve an increase in m-value. In order to remove this influence, a standard recession selection criterion has been used. The principles of standard recession selection criteria are listed below.

I. The recession segments are selected from the set of recession periods of minimum 10 years flow data and 20 years flow data have been used for selection of recession segments.

II. $Q_o$ is limited to be the first value below an upper limit ($Q_{UL}$).

III. The upper limit ($Q_{UL}$) is used as 0.75*ADF (Lena Tallaksen, 1989) where ADF is the mean annual runoff.

As a principle, flow data in combination with precipitation and temperature records are used as a first step to define the recession periods. A minimum length of recession is (4-10) days are required and 10 days have been used for the construction of the Master Recession Curve.

#### 4.2.3.2 Matching Strip Method

Even if there are varies methods used to construct a Master Recession Curve including correlation method which require uninterrupted recessions data which is difficult to get in the flow data record. Matching Strip Method have been adopted which is flexible to handle interrupted recessions. It is a graphical technique that relies on subjective visual assessment to select the best recession curves and manually shift them to prepare the Master Recession curve.

Steps involved in matching strip method:

**I**. The selected recession has been ranked based on their last value or tail end flow, i.e. the recession that takes the first rank is the one with the highest tail end flow.

**II**. To establish the position of each recession with respect to the others, a shifting process is adopted where recessions are considered in pairs starting with the last two recessions.

**III**. The lower curve of each pair is shifted in time to the point where one of its values is as near as possible to but less than, the tail-end discharge of the next recession. At this point, the curves are connected and the higher curve becomes the new lower recession for next pairing.

Precautions taken into consideration while doing matching strip methods:

**I**. The relative position of each recession pair has been maintained throughout the entire shifting process.

**II**. Equal tail-end values have been eliminated.

**III**. When two or more values are identified in the lower recession as the nearest to the tail-end of the higher curve, then the first of these values has been used to establish its position.

The analysis results of Killingidal gauging station is shown in **Fig.30** and **31**. Refer to **Appendix 5, 6** and **7** fo**r** HugdalBru, Lillebudal and Eggafoss gauging stations respectively.

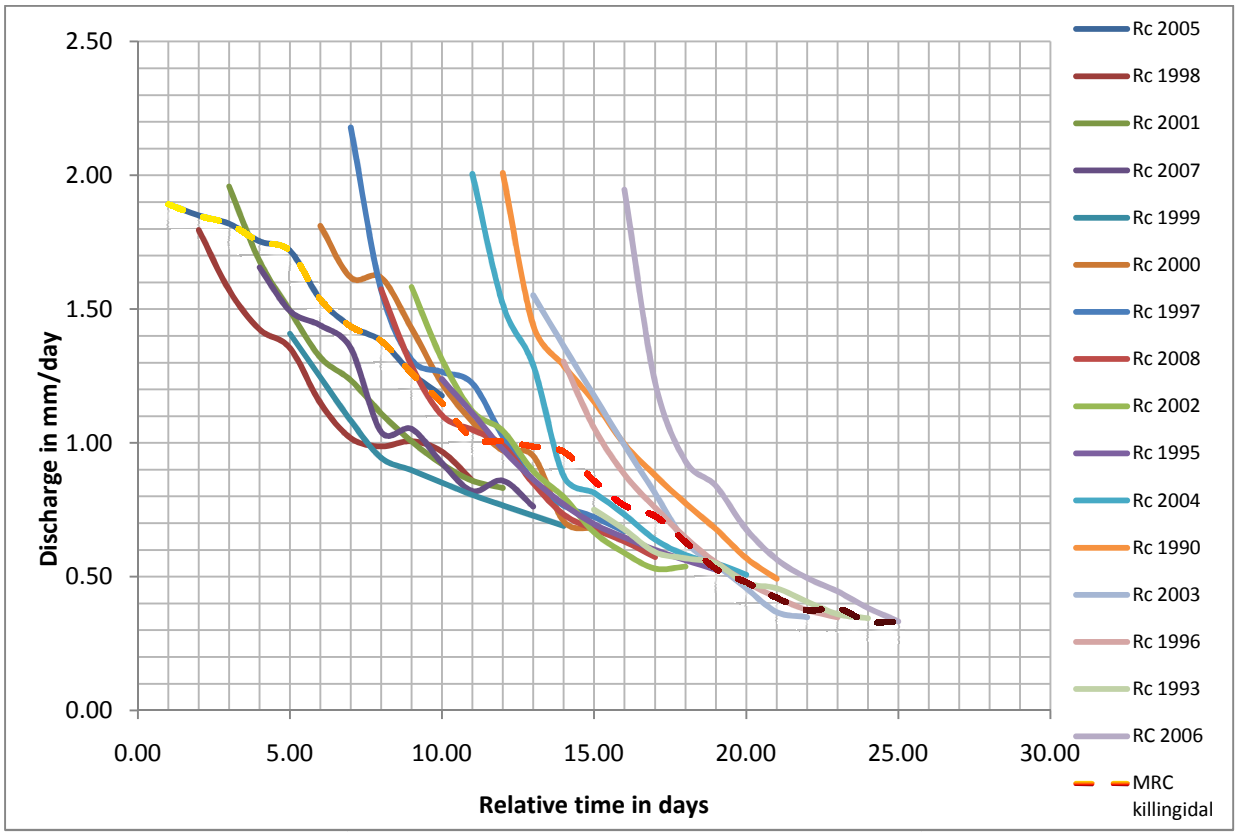


**Figure 30.: Master Recession Curve for Killingidal gauging station by matching strip method**

For linear transformation of MRC, **Equation 4.2** is used. **Fig.31** presents three method of linear transformation of MRC.

$$1/Q_b = 1/Q_0 + t/m \qquad \text{(Eq. 4.2)}$$

(Beven and Kirkby, 1979 ; Hornberger et al.,1985

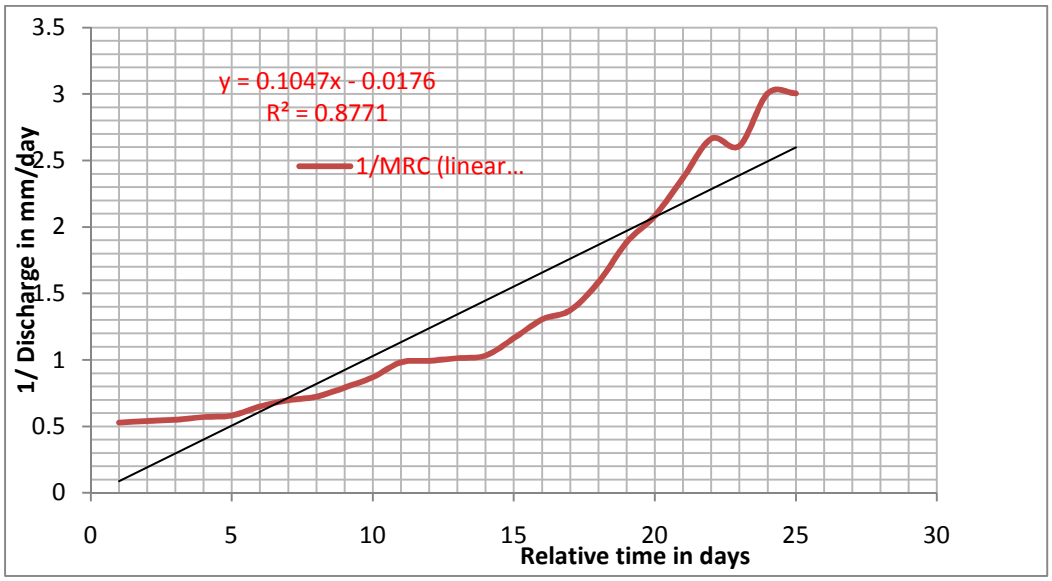


Where $\frac{1}{Q_b}$ = y; $\frac{1}{Q_o}$ = -0.0176; $t = x$; $\frac{1}{m} = 0.105 \rightarrow m$ =9.54mm

**a) Linear transformation of MRC using 1/Q (MRC fits first order hyperbola equation)**

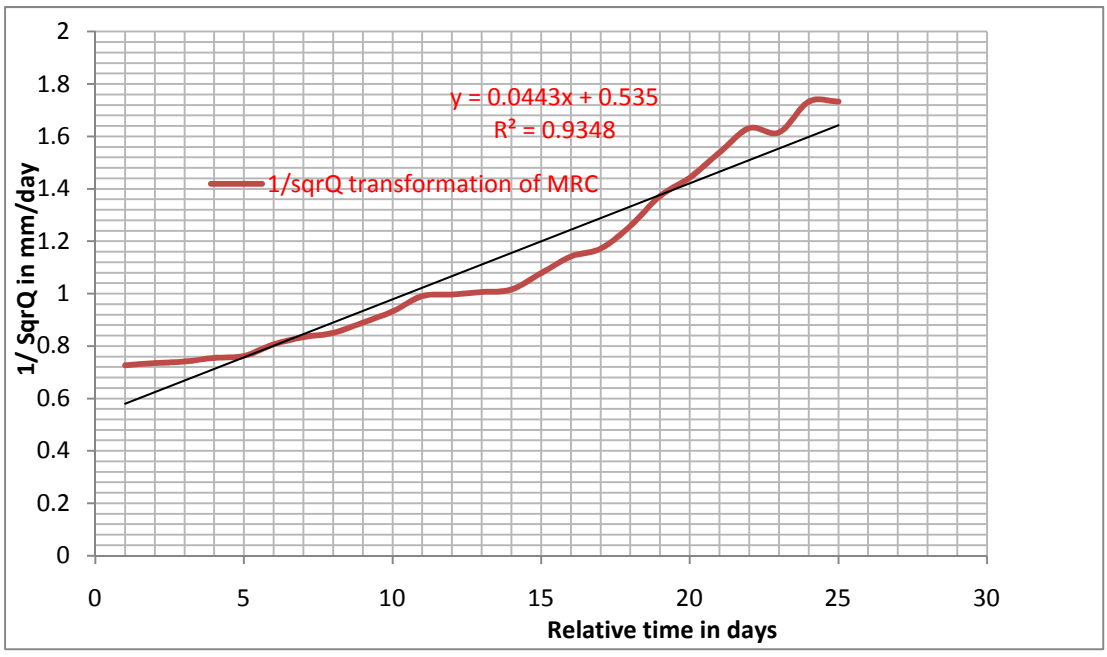


**c) Linear transformation of MRC using 1/sqrQ (MRc fits second order hyperbola)**

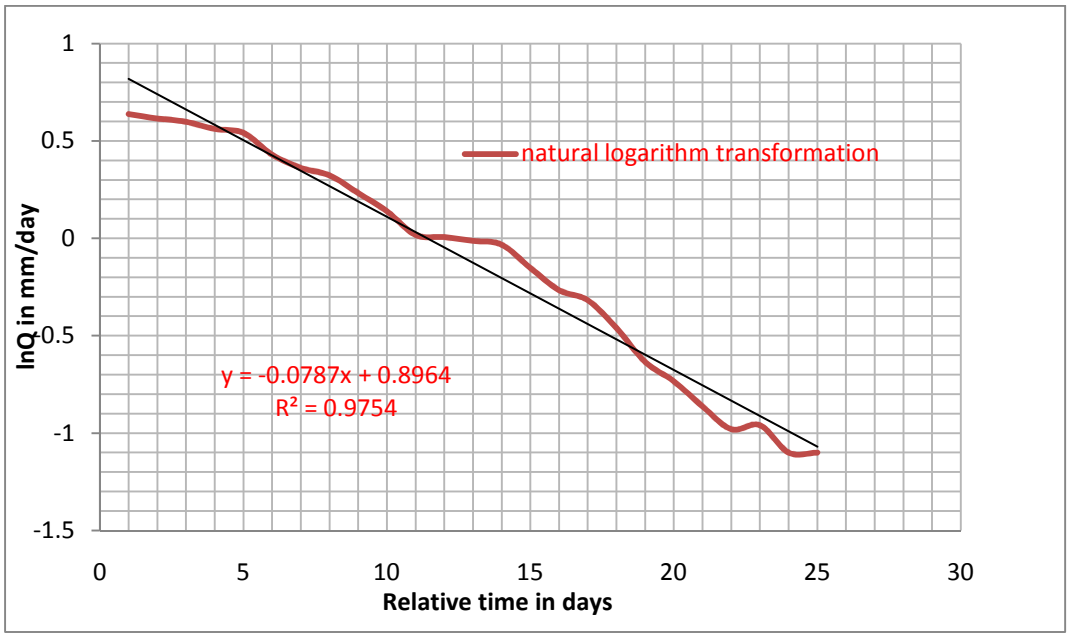


**c) Linear transformation of MRC using lnQ (MRC fits exponential equation)**

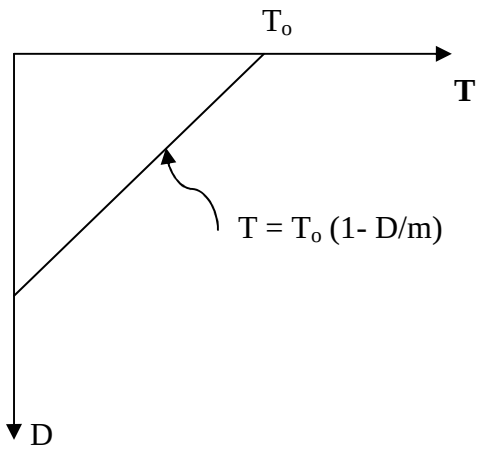


**D) Linear decrease of lateral transmissivity with depth**

**Figure 31: Different methods of linear transformation of MRC**

As it is observed from **Fig.31**, the natural logarithm (***ln*Q )** linear transformation gives the best correlation ($R^2$) than other methods, which gives preliminary indication that lateral transmissivity decrease linearly with depth as shown in **D of Fig.31.** This preliminary result contradicts with the original assumption of TOPMODEL (lateral transmissivity decreases exponentially with depth) and therefore, further analysis has to be done.

# 5. SHORT TERM EVENT SELECTION AND CALIBRATION

## 5.1 EVENT SELECTION CRITERIA

Depending upon the purpose of simulation and the requirement of the model, there are different criterion for different time resolution and hydrological modeling. For the TOPLAND hydrological model with time resolution of one hour, the following selection criteria have been applied. Radar, gauge or gauge simulated precipitation that can satisfy one or more of the criterion mentioned below has been selected for calibration at Gaulfoss gauging station and for assessing of the model performance at the interior uncalibrated gauging stations. There is no event that is selected as validation period event; because events selected for calibration are also used as validation at internal uncalibrated gauging stations.

**Criterion 1**

TOPMODEL, that controls the soil hydrology of TOPLAND model, is initialized by assuming that the simulation begins after a long dry period, i.e. the start time of the simulation period has to be preceded by a number of no or little precipitation periods so that the contributions of flow in the streams comes only from ground water.

This criterion comes from the assumption that contribution of each sub-catchments for initial discharge is obtained by proportioning area of each sub-catchment to the total drainage area at calibration point (Gaulfoss). The proportioning assumption will be true if the total initial discharge source is only ground water. Therefore, the catchment should not be saturated fully at the start of simulation period.

**Criterion 2**

Since one of the objectives of this paper is to tryout the model for short-time resolution events (hourly basis), which are potentially hazardous to the local environment, the mean of the selected event flow shall be higher than the mean flow of the corresponding year. E.g.July 2009 event.

**Criterion 3**

Since some events are highly localized and some are evenly distributed throughout a water shade, it is important to assess the applicability of the model for such events. e.g July 2006 event.

## 5.2 CRITERIA AND METHODS OF RESULT COMPARISON

The process of calibration is the comparison of two data sets. In this case it is comparison of time series of measured and simulated stream flow. It is done by selecting short term events and comparing simulated results with the selected subset. When comparing model prediction with observed data, objective as well as hydrograph techniques should be employed. Hydrograph techniques are based on visual inspection of the results; the objective techniques express the agreement between model and measured data using mathematical model performance measures. In this thesis the Nash Sutcliff Index, NS, Correlation coefficient, $R^2$, and Percent Deviation, PBIAS, were used to evaluate the utility of the model. These indices are represented by the following equations.

1. Nash Sutcliff Index (Nash and Sutcliffe 1970)

$$NS = 1 - \frac{\sum_{i=1}^{n}(O_i - P_i)^2}{\sum_{i=1}^{n}(O_i - \overline{O})^2} \qquad \text{(Eq. 5.1)}$$

2. Correlation coefficient ($R^2$)

$$R^2 = \left[\frac{\sum_{i=1}^{n}(O_i - \overline{O})\,(P_i - \overline{P})}{\left(\sqrt{\sum_{i=1}^{n}(O_i - \overline{O})^2}\right)\left(\sqrt{\sum_{i=1}^{n}(P_i - \overline{P})}\right)^2}\right]^2 \qquad \text{(Eq. 5.2)}$$

3. Percent Deviation (PBIAS)

$$PBIAS = \frac{\sum_{i=1}^{n}(O_i - P_i)}{\sum_{=1}^{n}(O_i)} * 100 \qquad \text{(Eq. 5.3)}$$

$\mathbf{P_i}$ and $\mathbf{O_i}$ denote the simulated value and observed value respectivelyy at time step $\boldsymbol{i}$, and n represents the number of observations. The coefficient of efficiency, i.e. Nash-

Sutcliffe index quantifies the relative performance of the employed model. A Nash-Sutcliffe index of unity means that the model produces discharge data which are exactly coinciding with the measured data. The correlation coefficient $R^2$ can be used to compare the model prediction and the observation. The deviation of correlation $R^2$ from one is an indication for the poor performance of model. The PBIAS gives an estimate of the deviation of predicted stream flow from observed stream flow. $R^2$ Values closer to unity and PBIAS value closer to zero represent good performance of the model.

## 5.3 CALIBRATION AND CALIBRATION PARAMETERS

The TOPLAND model includes a number of parameters which describe the different hydrological conditions in the catchment. The parameters are adjusted during calibration so that attained model results approximate measured results closely. The simulated discharge at the interior gauging stations with the calibration point parameters have been used as the validation of the model. **Table 12** lists some of TOPLAND parameters. However, for this thesis not all the parameters were calibrated and calibration was limited to m, $t_d$, v, Rzini., Rzmax., and $T_o$ Parameters (**Table 12**). These is because according to the simulation for Sagelva catchment (3.14km$^2$), these were found to be the most important parameters which played a major part in influencing simulated stream flow. In this thesis, calibration is done manually by trial and error.

Calibration of the model has been done for two typical events (localized July 2006 event and evenly distributed July 2009 event) using three different precipitation input methods, i.e. gauge, gauge simulated and radar precipitation. For the July 2009 event (19-07-2009 05:00 to 25-07-2009 20:00), all the three methods of precipitation input are used. For the July 2006 event (27-07-2006 00:00 to 29-07-2006 23:00), only radar precipitation method has been used.

There are five interior discharge gauging stations for the Gaula catchment. For the July 2009 event, three out of the five gauging stations has been used as a validation of the model because of the fact that Killingidal gauging station has no reading for the above mentioned period and Hagabru is very close to the calibration point (Gaulfoss) gauging station. For the July 2006 event, all but Hagabru, internal gauges have been used for the validation of the model.

**Table 12 *:* Some of the TOPLAND model parameters**

| Parameters | Symbol(units) | Description |
|---|---|---|
| Saturated store sensitivity | m(mm) | Describes decrease of lateral transmissivity with depth. |
| Saturated lateral transmissivity at saturation | $T_o$($mm^2$/hr) | Lateral transmissivity when the saturated deficit is zero (the soil is fully saturated). |
| Time constant | $t_d$ (hr/m) | Expresses a mean residence time for vertical flow per unit of moisture deficit. |
| Overland delay velocity | v(m/s) | The velocity that the overland flow has before it joins the stream. |
| Initial root zone storage | RZinit.,(mm) | The water depth equivalent that the soil has in it before the simulation starts. |
| Maximum root zone storage | RZmax.(mm) | The maximum water depth equivalent that the soil can store to its field capacity. |
| Storage capacity per unit leaf area index | Laicap ($mm/m^2$) | The depth of precipitation intercepted per unit leaf area index. |
| Reach length | L (m) | Stream length |
| Reach slope | $S_o$ | Stream bed slope |
| Reach manning's number | n | The roughness characteristic of the stream |
| Hydraulic geometric parameters | $a_o$, $b_o$ | coefficients that relate top width with flow cross sectional area |

## 5.4 CALIBRATION AND FINDINGS OF 2009 EVENT (19-07-2009 05:00 TO 25-07-2009 20:00)

During the precipitation period of the 2009 selected event, the spatial distribution of precipitation is relatively uniform within the study catchment, i.e. there is precipitation throughout the catchment. The contribution of flow at the calibration point from different gauging is proportional to their catchment area. This can be justified by looking at the shape of the hydrographs at the gauging stations. **Fig.32** elaborates this statement.

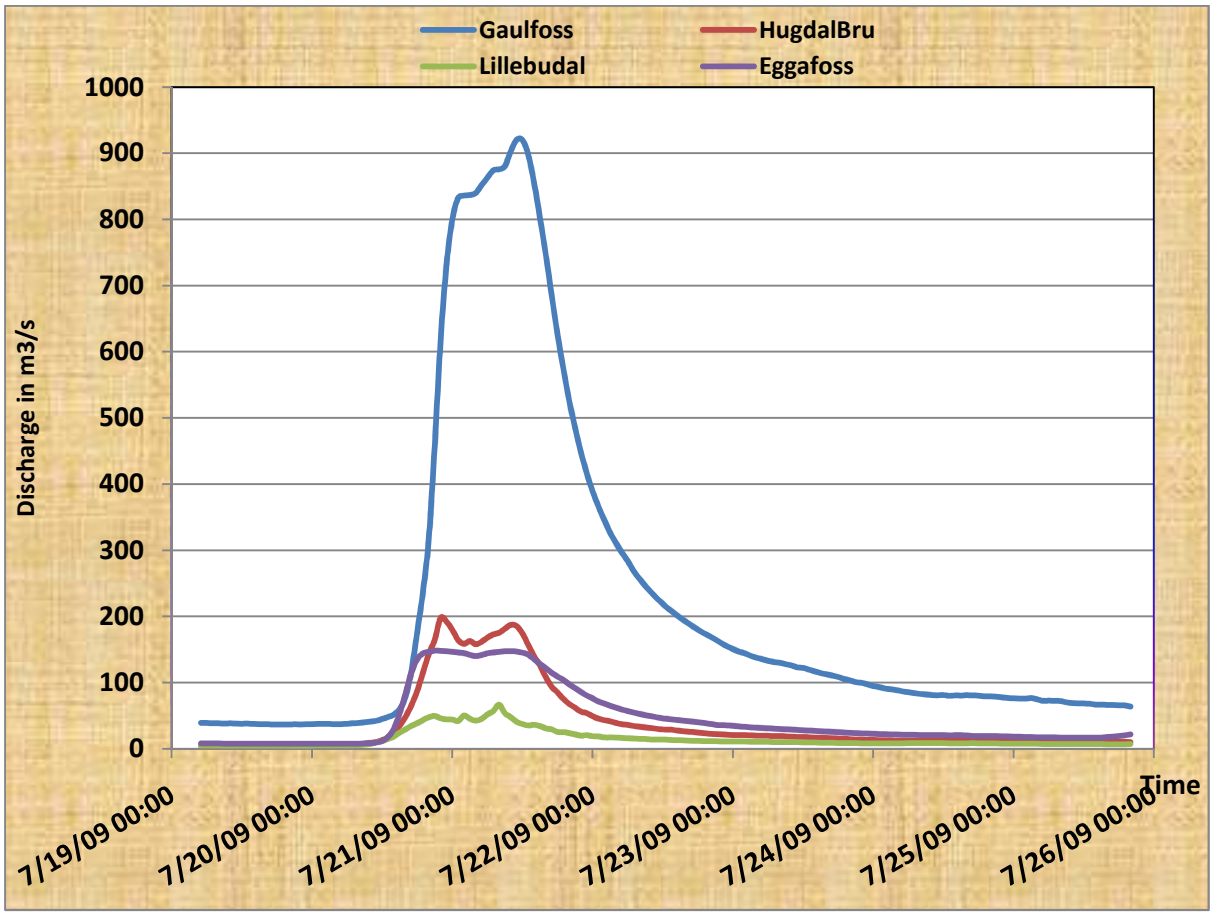


**Figure 32: Hydrographs observed at the calibration point (Gaulfoss) and uncalibrated interior gauging stations for 2009 event**

From the figure it is clear that almost 20% of the total peak at the Gaulfoss gauging station is contributed by HugdalBru gauging station that covers 20% of the total catchment area. Other gauging stations also contributed flow which is proportional to their catchment area. From the figure, it can be concluded that precipitation has occurred throughout the total catchment.

### *5.4.1 Model Calibration Using Gauge IDW Precipitation Input Method*

The model is calibrated using manual method of trial and error calibration. The calibration point for all calibrations is the Gaulfoss gauging station. To get the best calibration parameters, different components of the water balance have been used as a control to know which parameter has to be altered at each calibration process so that the number of trials is reduced. Finally, the objective and hydrograph method of result comparison is used to arrive at the final calibration parameters.

**Table 13: Summary of final calibration parameters for different precipitation input methods**

| Precipitation input methods | Calibration parameters | | | | | |
|---|---|---|---|---|---|---|
| | **m** (mm) | **$T_o$** ($mm^2$/hr) | **V** (m/s) | **$t_d$** (hr/mm) | **RZmax.** (mm) | **RZinit.** (mm) |
| Gauge IDW interpolation | 25 | 18000 | 0.25 | 0.0002 | 10 | 0.0002 |
| Bias corrected radar | 15 | 10000 | 0.25 | 0.0005 | 5 | 0.0002 |
| Gauge simulated | 29 | 10000 | 0.25 | 0.0005 | 12 | 0.0002 |

### 5.4.1.1 Objective Results

The objective results of both at calibration and uncalibrated internal discharge gauging stations are presented in **Fig.33 and 34.**

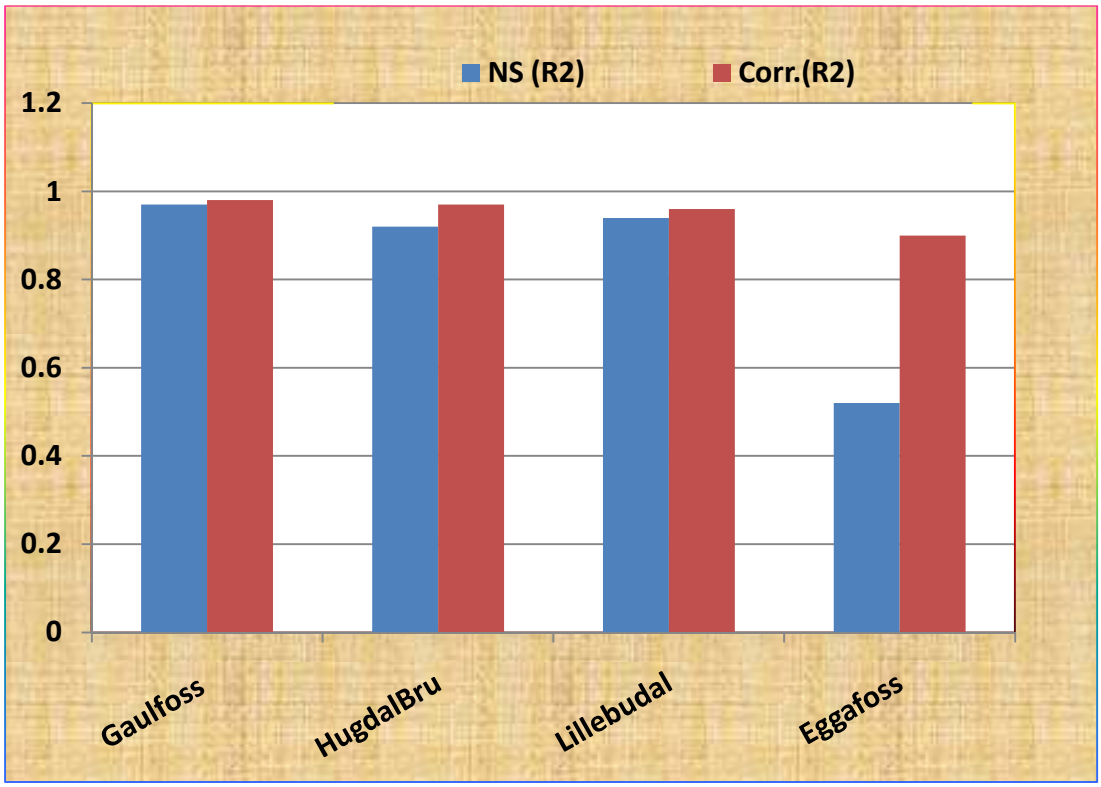


**Figure 33 : Nash Sutcliff Index (NS) and Correlation coefficient results of the calibration point and uncalibrated internal discharge gauging stations using gauge IDW method**

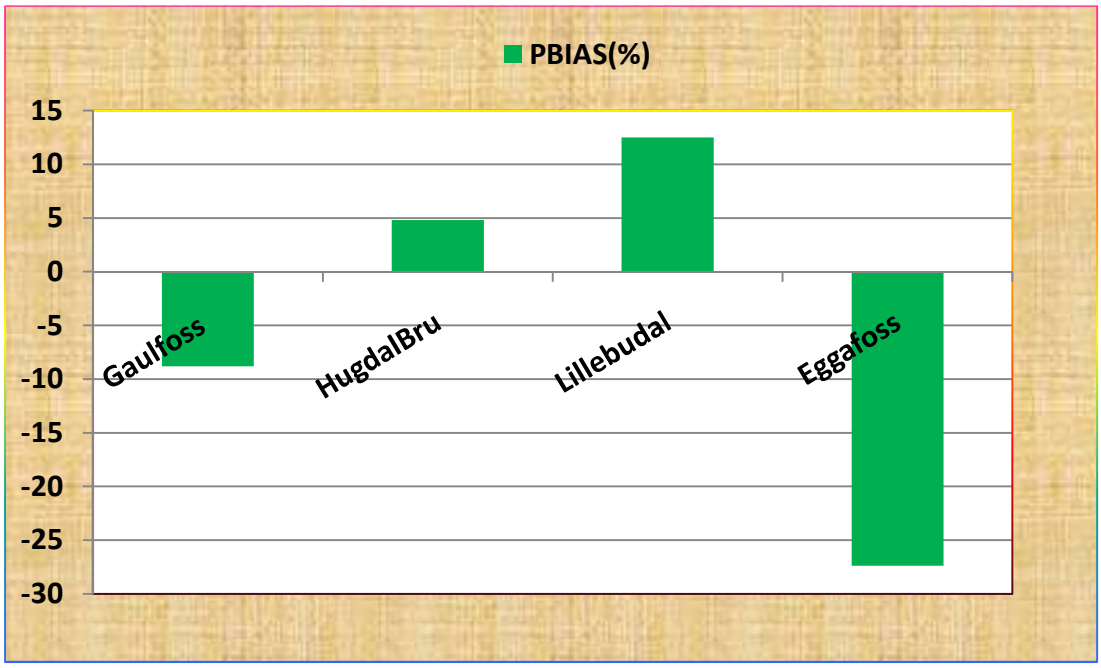


**Figure 34 : Percent deviation results of the calibration point and uncalibrated internal gauging stations using gauge IDW method**

**Table 14: Summary of statistics for the calibration point and uncalibrated interior discharge gauging stations using gauge IDW precipitation input method.**

| Objective methods of result comparison | At calibration Gauging station (Gaulfoss) | Uncalibrated interior gauging stations | | |
|---|---|---|---|---|
| | | HugdalBru | Lillebudal | Eggafoss |
| Average measured flow ($m^3/s$) | 216.2 | 39.1 | 15.1 | 45.2 |
| Average simulated flow ($m^3/s$) | 235.1 | 37.3 | 13.2 | 57.6 |
| Nash Sutcliff index (NS. $R^2$) | 0.97 | 0.92 | 0.94 | 0.52 |
| Correlation (Corr.$R^2$) | 0.98 | 0.97 | 0.96 | 0.92 |
| Percent deviation (PBIAS , %) | -8.8 | 4.8 | 12.5 | -27.4 |

### 5.4.1.2 Hydrographs

Hydrograph method of result comparison have to be evaluated because of the fact that if the objective result shows a very good result, it does not necessarily means that the observed and simulated values are matched well at all flows of simulation. This can be illustrated with Nash Sutcliff Index (NS) which is sensitive at peak flows. If NS has a very good result it may have poor fit of the low flows when we look at the hydrograph method.

In the following figures, hydrographs for calibration parameters and other precipitation input parameters are presented for the calibration point and uncalibrated interior discharge gauging stations. Calibration at the calibration point gauging station (Gaulfoss) has been done independently for different precipitation inputs. The calibration parameters of one precipitation input method is used for another method to have a preliminary insight whether the same parameters can be used for all precipitation input methods or not.

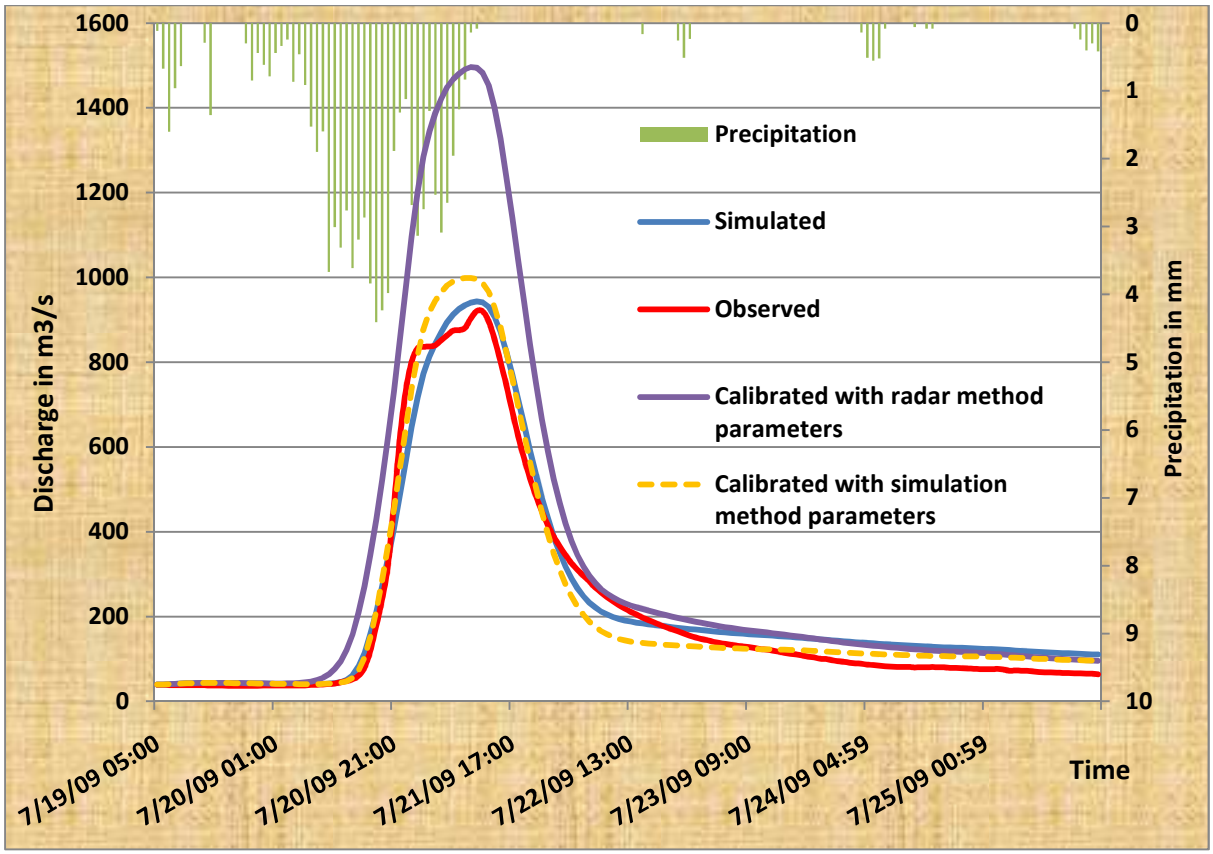


**Figure 35 : Hydrographs at the calibration point using gauge IDW precipitation input with different parameters**

**Note:-** The precipitation values are averages of the distributed input values. They indicate only the period on which precipitation has occurred. It has nothing to do with the precipitation input magnitudes of the model.

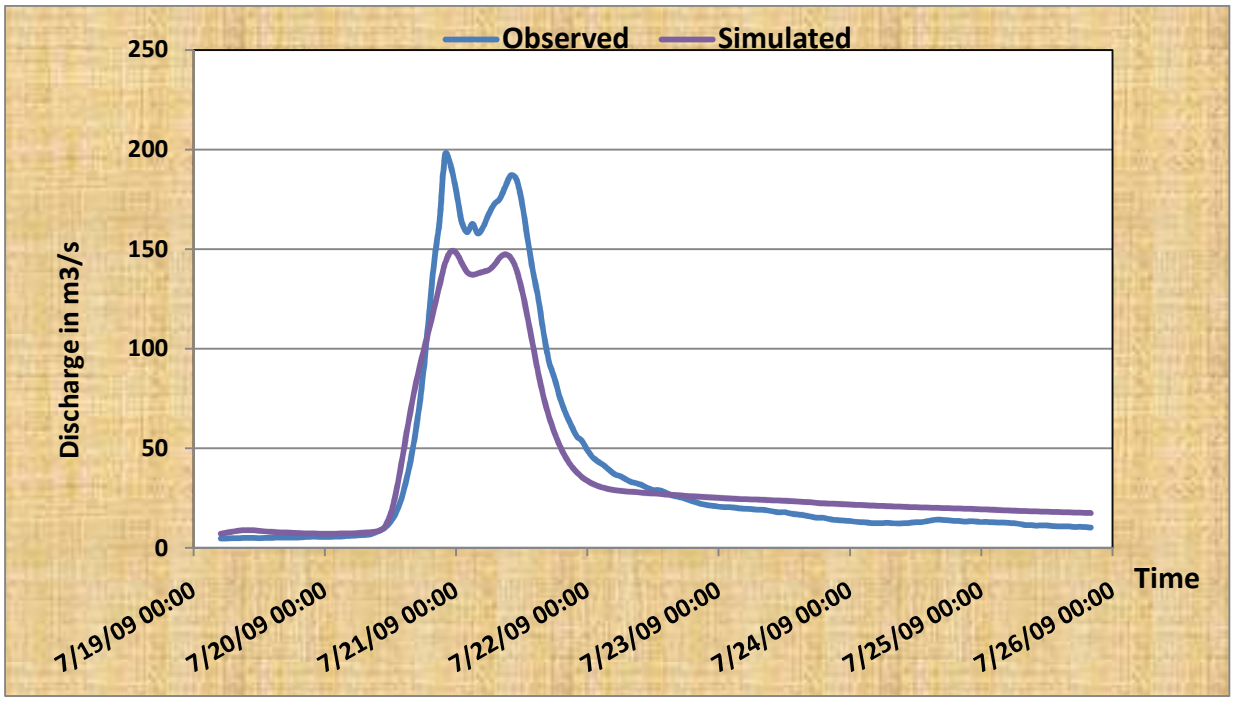


**Figure 36: Hydrographs at the HugdalBru gauging station (uncalibrated interior gauging station) using gauge IDW precipitation input method.**

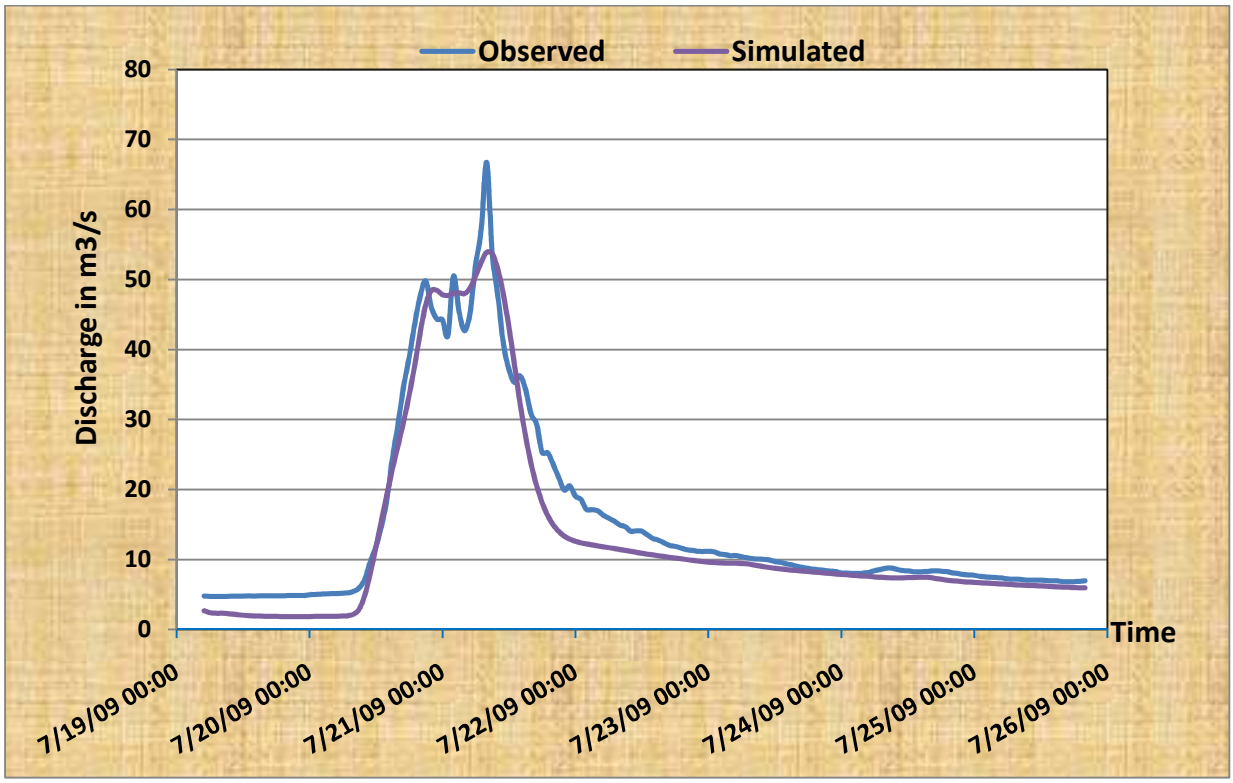


**Figure 37: Hydrograph sat Lillebudal gauging station (uncalibrated interior station) using gauge IDW precipitation input method**

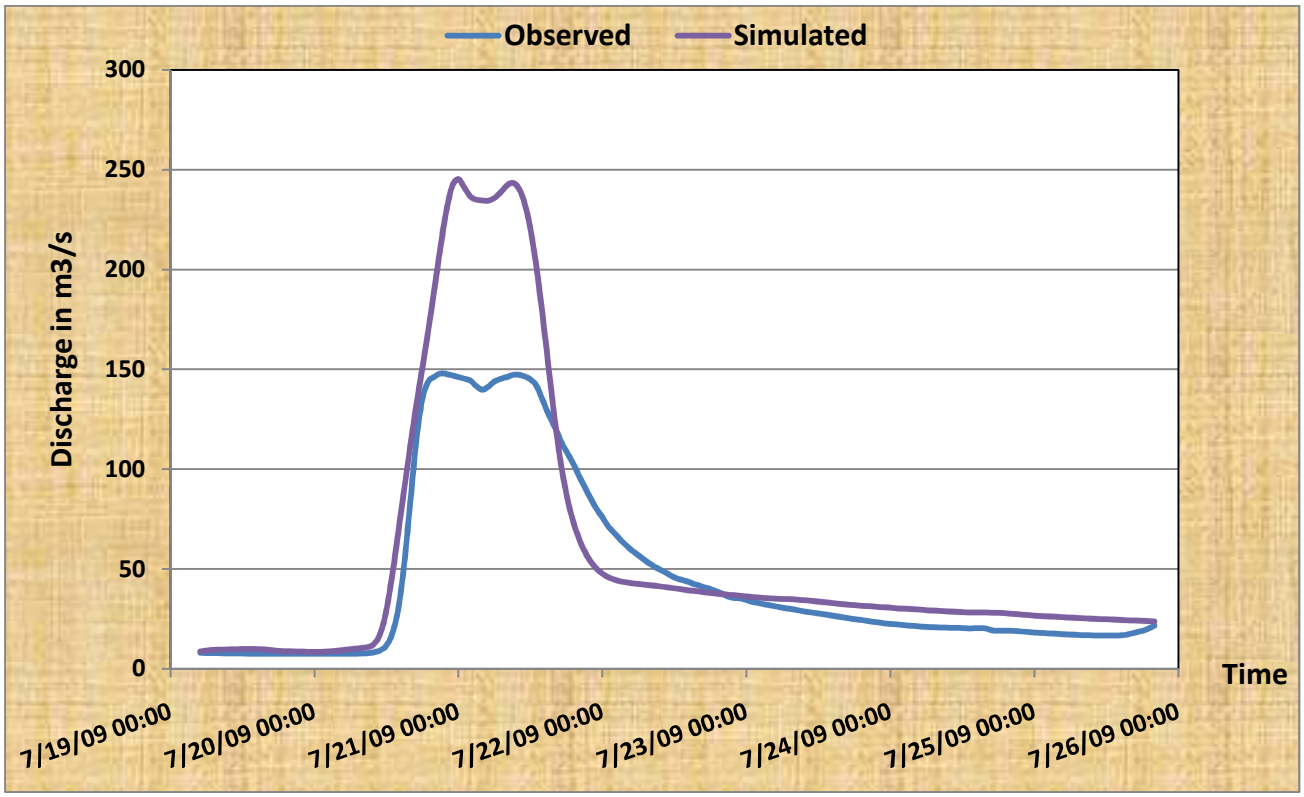


**Figure 38 : Hydrographs at Eggafoss gauging station (uncalibrated interior station) using gauge IDW precipitation input method.**

### 5.4.1.3 Discussions

Generally, objective calibration results using Inverse Distance Weighting (IDW) precipitation input method shows a good performance of the model both at calibration and uncalibrated interior gauging stations. Internal discharge gauging stations, (Hugdalbru and Lillebudal) close to the rain gauge stations, gave better result than the farther gauging station (Eggafoss). The negative percent deviation indicates the overestimation of the model and positive percent deviation shows the underestimation of the model. Van Liew et al. (2005) states that PBIAS values of up to $\pm 25\%$ are considered satisfactory. Nash Sutcliff index and correlation coefficient values $\geq 0.8$ are taken has satisfactory. The high values of NS ($R^2$) and corr. ($R^2$) generally show that the model is able to predict stream flows effectively in periods of low and high flows.

Eggafoss gauging station shows poor results of NS ($R^2$) and PBIAS. This may be due to uncertainties resulting from Inverse Distance Weighting method of precipitation interpolation at farther gauging stations.

In the hydrograph of **Fig.38**, it is clear that simulated hydrograph using bias corrected radar parameters over estimates much the observed discharge and this is an indication that parameters used for calibrating radar precipitation input may not be used for gauge IDW precipitation input method. But parameters used for calibrating gauge simulated precipitation input estimates the observed well and this is an indication that parameters used for calibrating gauge simulated precipitation input can be used for gauge IDW precipitation input method.

The overestimations and underestimations shown by the objective method also reflected well in the hydrograph method. All the simulated hydrographs show a special trend in the recession part that shows abrupt change from high flow to low flow while the observed hydrograph shows a smooth transition.

### *5.4.2 Model Calibration Using Bias Corrected Radar Precipitation Input Method*

#### 5.4.2.1 Objective Results

The bias corrected radar precipitation has been used to calibrate the model since the bias uncorrected radar data under-estimates the simulated hydrograph. The objective results have been shown in the following figures.

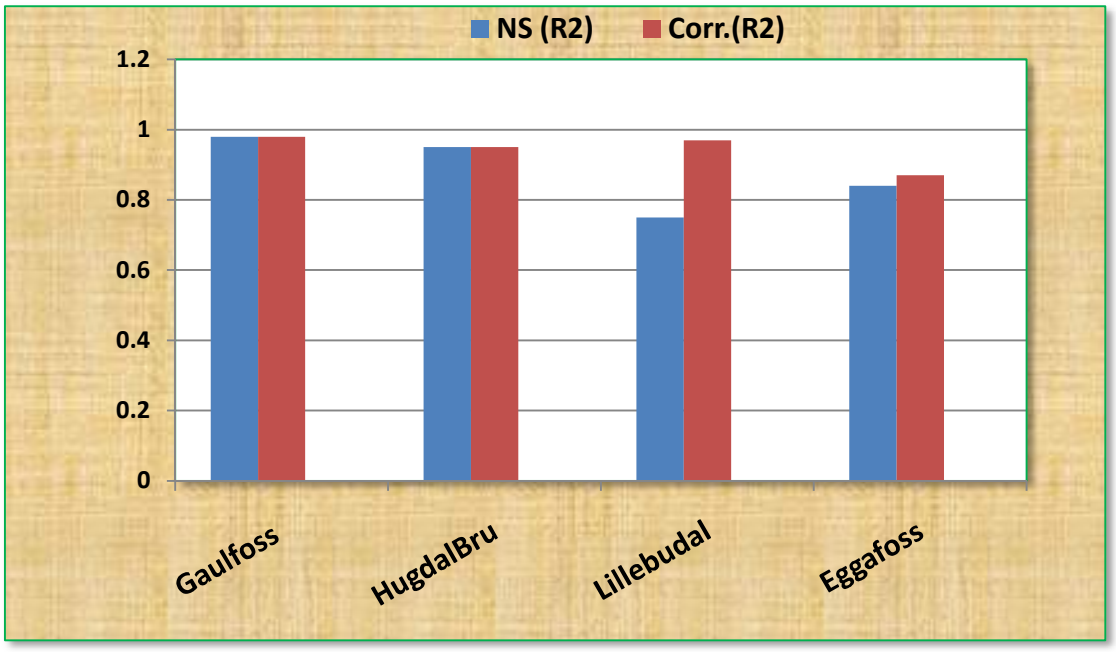


**Figure 39 : Nash Sutcliff Index (NS) and Correlation coefficient results of the calibration point and uncalibrated internal gauging stations using bias corrected radar data**

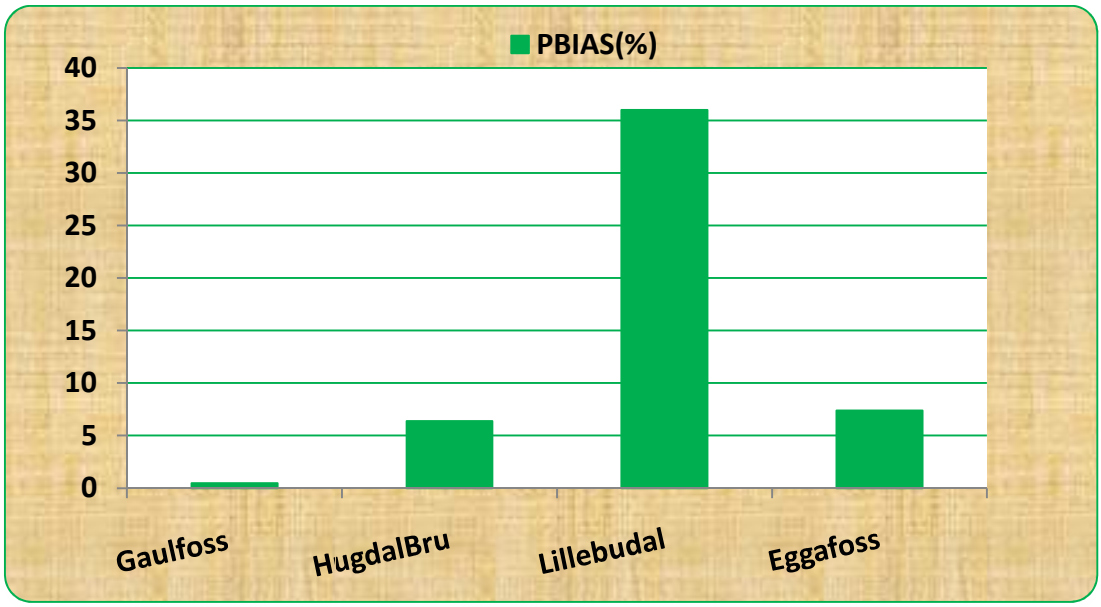


**Figure 40 : Percent Deviation results of the calibration point and uncalibrated internal gauging stations using bias corrected radar data**

**Table 15 *:* Summary of statistics for the calibration point and uncalibrated interior gauging stations using bias corrected radar precipitation input method**

| **Objective methods of result comparison** | **At calibration Gauging station (Gaulfoss)** | **Uncalibrated interior gauging stations** | | |
|---|---|---|---|---|
| | | **HugdalBru** | **Lillebudal** | **Eggafoss** |
| Average measured flow ($m^3/s$) | 216.2 | 39.1 | 15.1 | 45.2 |
| Average simulated flow ($m^3/s$) | 215.1 | 41.6 | 9.6 | 41.9 |
| Nash Sutcliff index NS ( $R^2$) | 0.98 | 0.95 | 0.75 | 0.84 |
| Correlation Corr.($R^2$) | 0.98 | 0.95 | 0.97 | 0.87 |
| Percent deviation (PBIAS %) | 0.48 | 6.4 | 36 | 7.4 |

### 5.4.2.2 Hydrographs

Hydrographs of the calibration point and uncalibrated internal gauging stations has been shown in following figures. For the calibration gauging station, bias uncorrected and bias corrected radar precipitation data has been plotted to see how bias uncorrected radar precipitation data under estimates simulated flow.

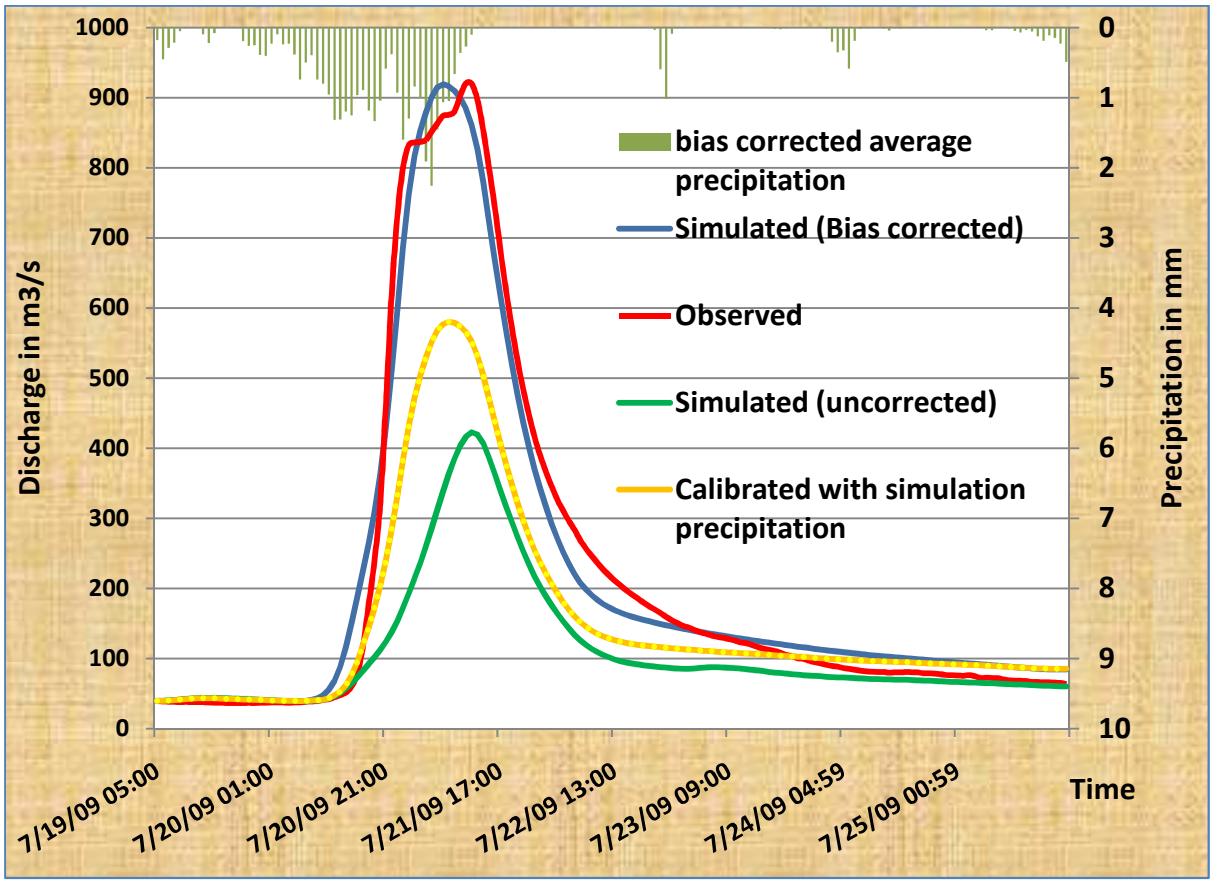


**Figure 41 : Hydrographs at the calibration point using bias corrected radar precipitation input with different parameters**

Note:- The precipitation values are averages of the distributed input values. They indicate only the period on which precipitation has occurred. It has nothing to do with the precipitation input magnitudes of the model.

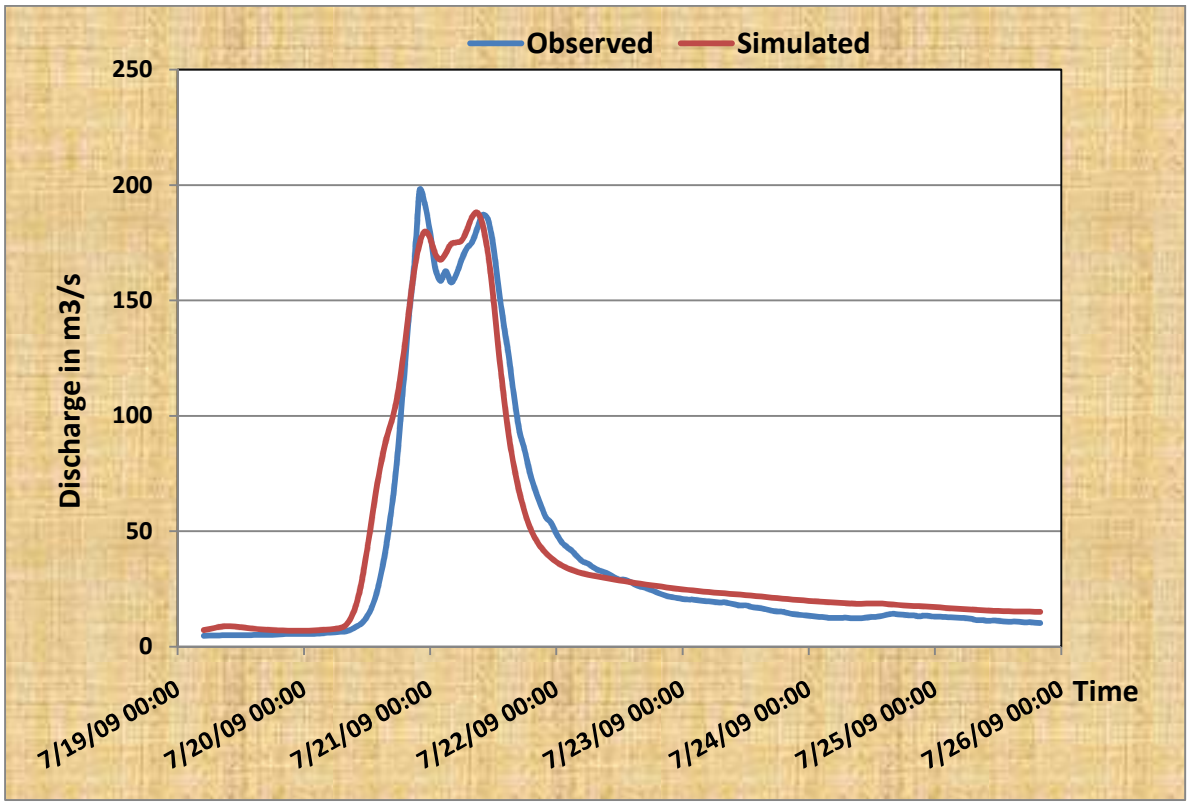


**Figure 42 : Hydrograph at the HugdalBru gauging station (uncalibrated interior gauging station) using bias corrected precipitation input method**

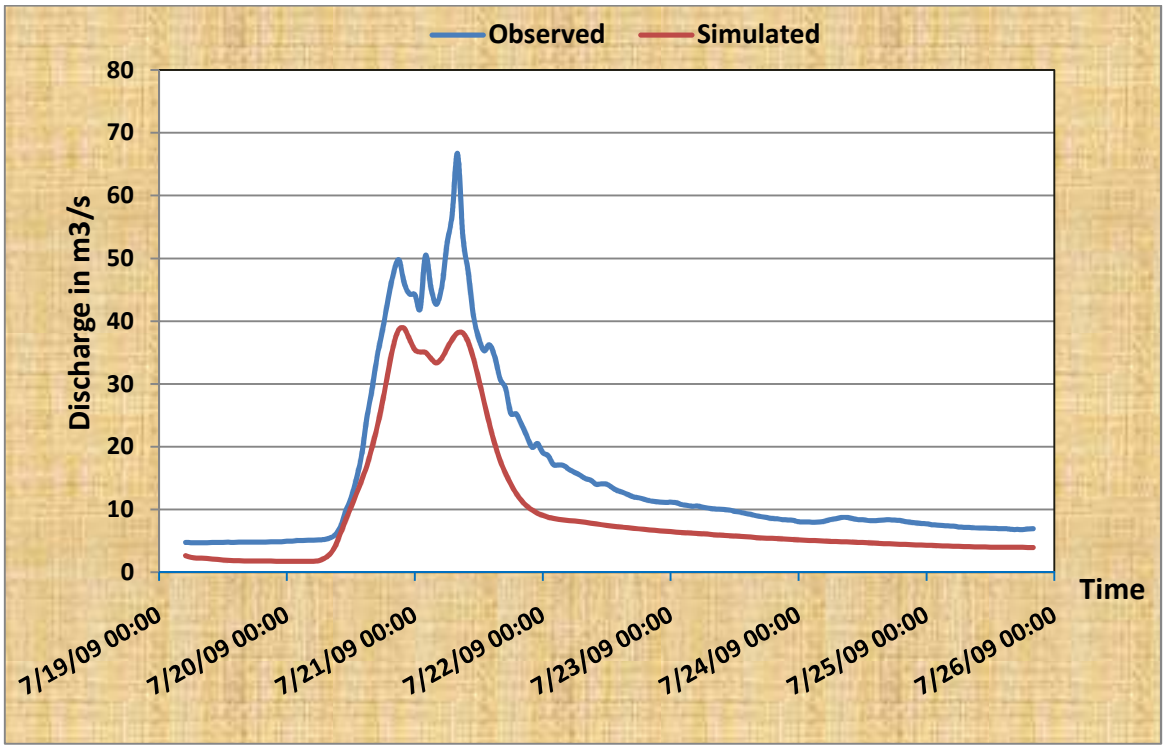


**Figure 43: Hydrograph at Lillebudal gauging station (uncalibrated interior station) using bias corrected radar precipitation input method**

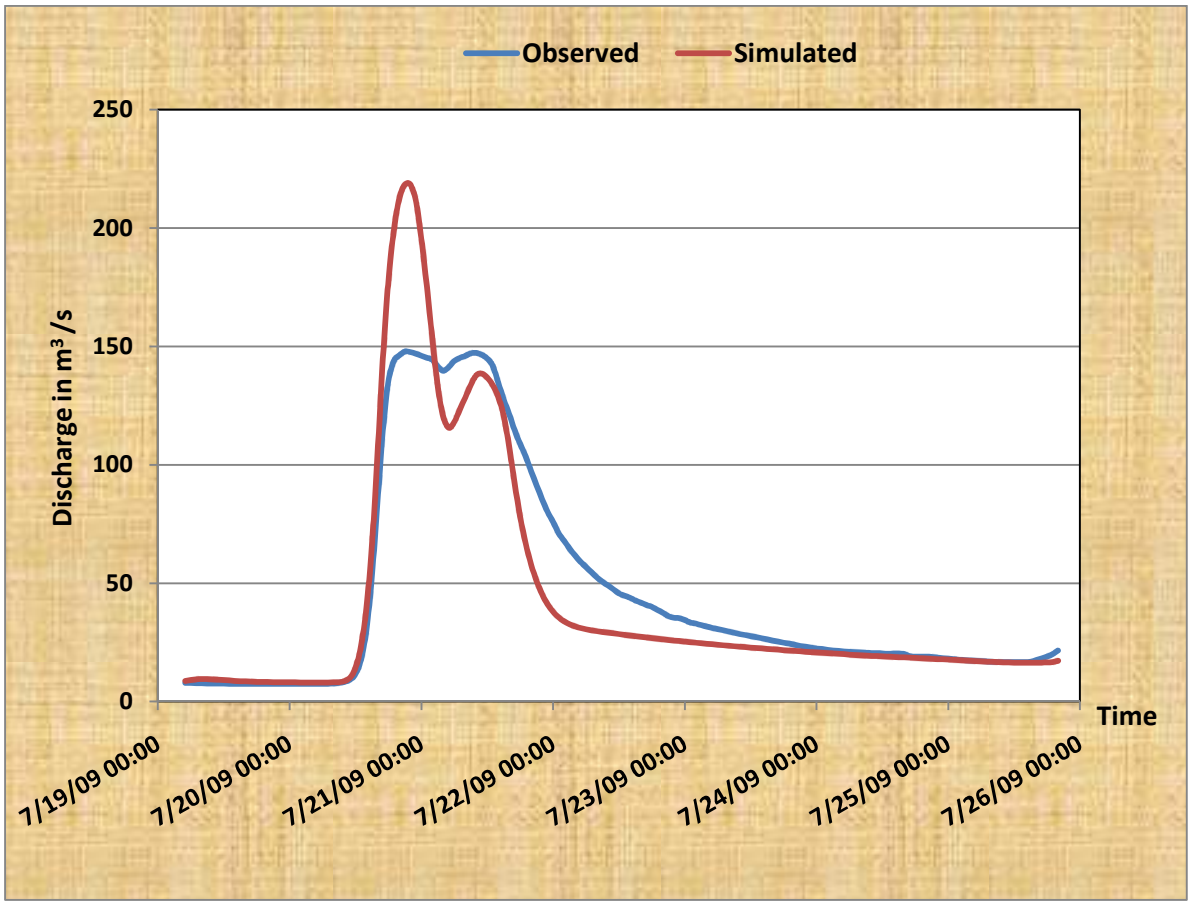


**Figure 44: Hydrograph at Eggafoss gauging station (uncalibrated interior station) using bias corrected precipitation input method.**

### 5.4.2.3 Discussions

The objective method of result comparison, for bias corrected radar precipitation, shows a very nice performance of the model both at the calibration point and uncalibrated interior gauging stations. From the result, it is also clear that the calibrated model underestimated stream flows especially for Lillebudal gauging station. As outlined by Bandaragoda et al. (2004), TOPMODEL, on which TOPLAND is based, has a single function that models saturated zone flow recession. Therefore, calibration of the model results in the adjustment of the sensitivity parameter, 'm', to match high flow recessions rather than low flow recessions. This under-estimation is also reflected in the positive values of PBIAS.

Model underestimation may also be caused by uncertainties resulted from bias correction method, since the sources of error in radar precipitation is complex in structure. It may also have been resulted from rough estimation of distributed and initial state variables due to lack of detail soil map of the catchment.

From the hydrograph of **Fig.41,** it is clear that bias uncorrected radar precipitation underestimates the simulated flow and it is a must that appropriate bias adjustment has to be carried out before using raw radar precipitation as input to the model.

The hydrograph also shows that, calibrating bias corrected precipitation input using parameters from gauge simulated precipitation, underestimates the simulated flow. Therefore, calibration parameters from simulated precipitation input cannot be used for bias corrected precipitation input method.

### *5.4.3 Model Calibration Using Gauge Simulated Precipitation Input Method*

#### 5.4.3.1 Objective results

Figures 45 and 46 show the objective results obtained during the calibration of the model.

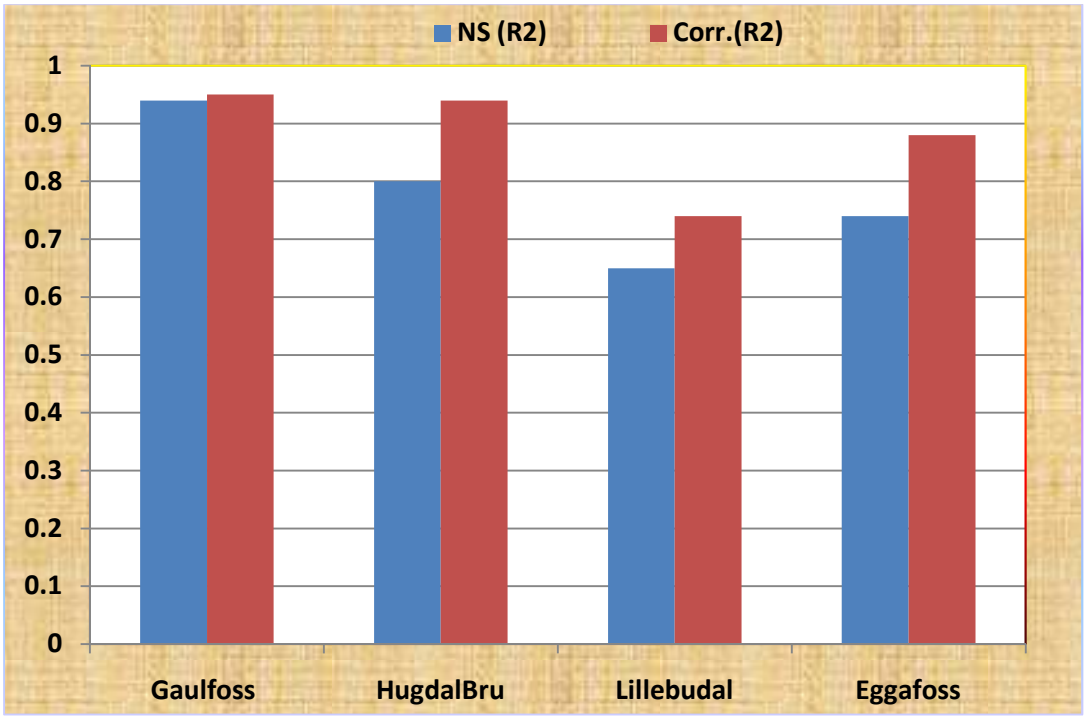


**Figure 45: Nash Sutcliff Index (NS) and Correlation coefficient results of the calibration point and uncalibrated internal gauging stations using gauge simulated precipitation**

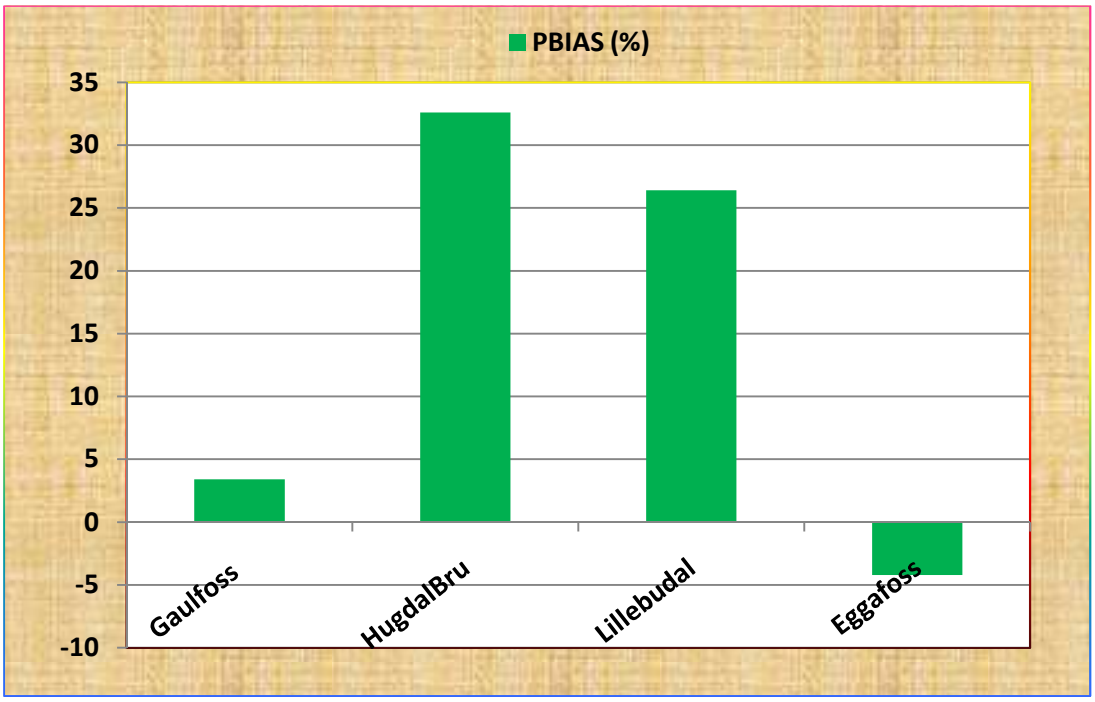


**Figure 46 : Percent Deviation results of the calibration point and uncalibrated internal gauging stations using gauge simulated gauging stations**

**Table 16 : Summary of statistics for the calibration point and uncalibrated interior gauging stations using gauge simulated precipitation input method**

| **Objective methods of result comparison** | **Calibration point Gauging station (Gaulfoss)** | **Uncalibrated interior gauging stations** | | |
|---|---|---|---|---|
| | | **HugdalBru** | **Lillebudal** | **Eggafoss** |
| Average Measured flow ($m^3/s$) | 216.2 | 39.1 | 15.1 | 45.2 |
| Average Simulated flow ($m^3/s$) | 208.7 | 26.4 | 11.1 | 47.1 |
| Nash Sutcliff Index (NS. $R^2$) | 0.94 | 0.8 | 0.67 | 0.74 |
| Correlation (Corr.$R^2$) | 0.95 | 0.94 | 0.74 | 0.88 |
| Percent Deviation (PBIAS %) | 3.4 | 32.6 | 26.4 | -4.2 |

### 5.4.3.2 Hydrographs

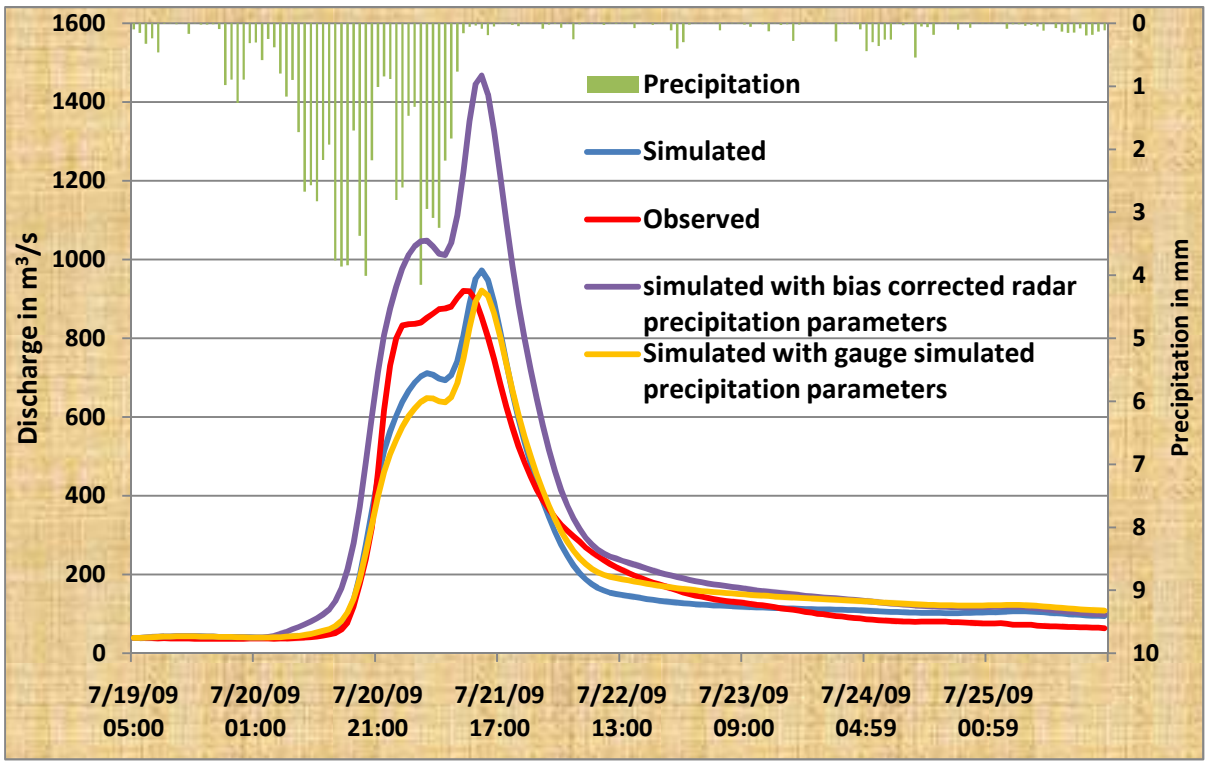


**Figure 47: Hydrographs at the calibration point (Gaulfoss) using gauge simulated precipitation input with different parameters**

**Note:-** The precipitation values are averages of the distributed input values. They indicate only the period on which precipitation has occurred. It has nothing to do with the precipitation input magnitudes of the model.

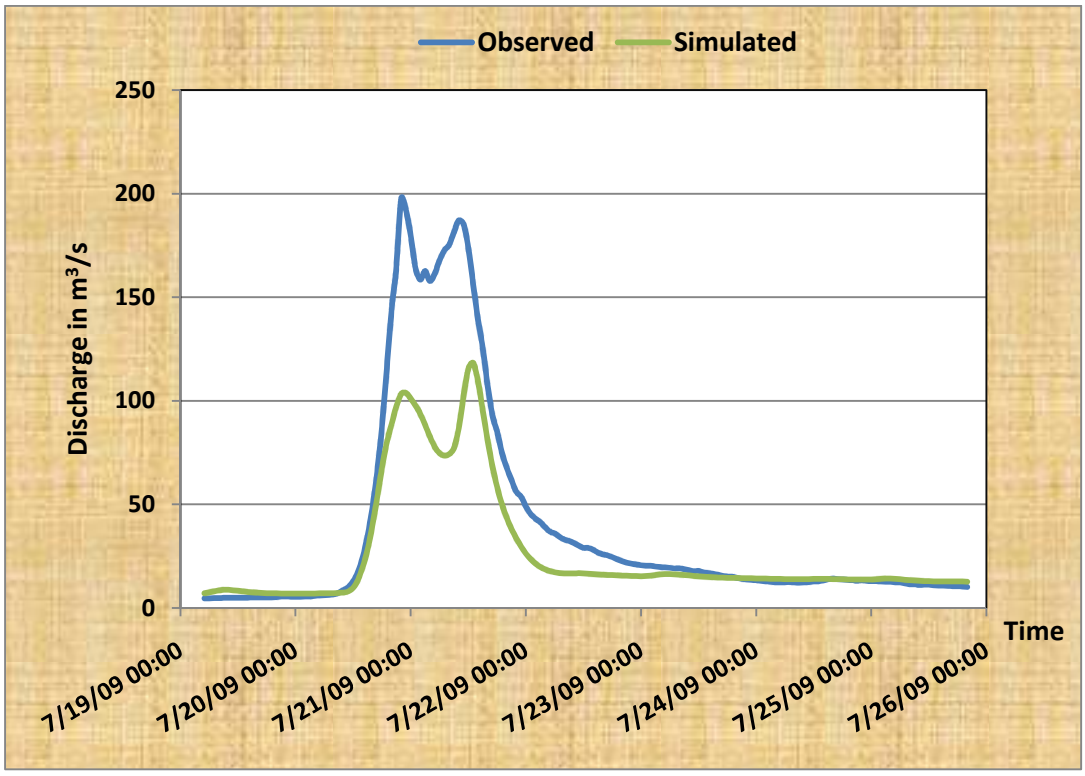


**Figure 48: Hydrographs at the HugdalBru gauging station (uncalibrated interior gauging station) using gauge simulated precipitation input method**

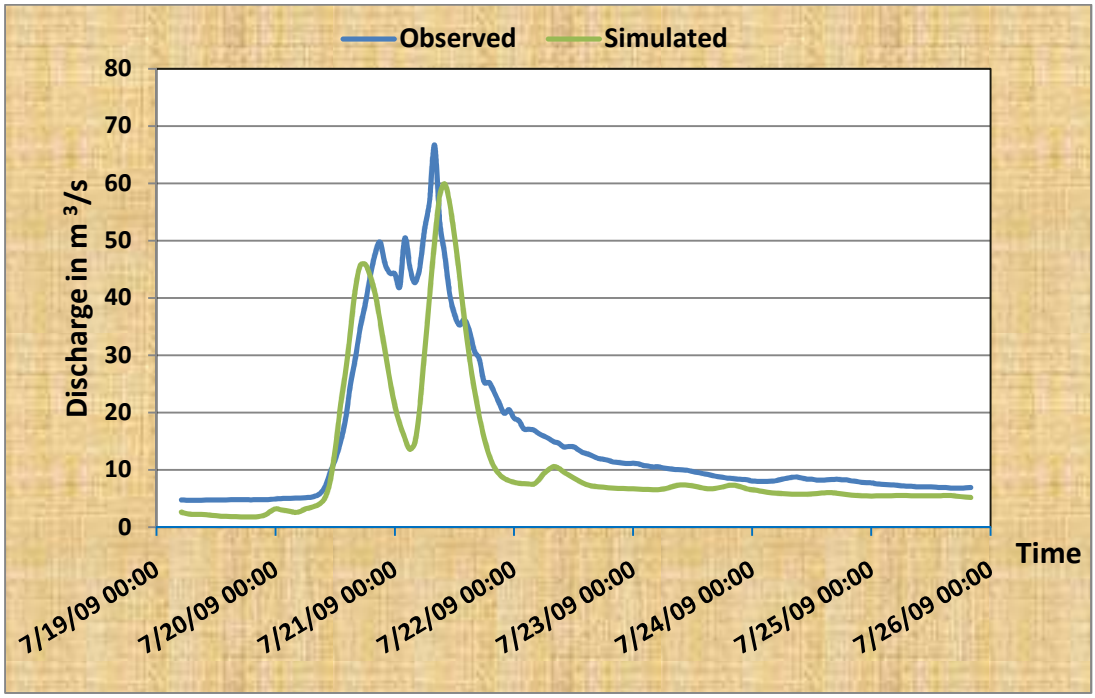


**Figure 49:Hydrographs of Lillebudal gauging station (uncalibrated interior station) using gauge simulated precipitation input method.**

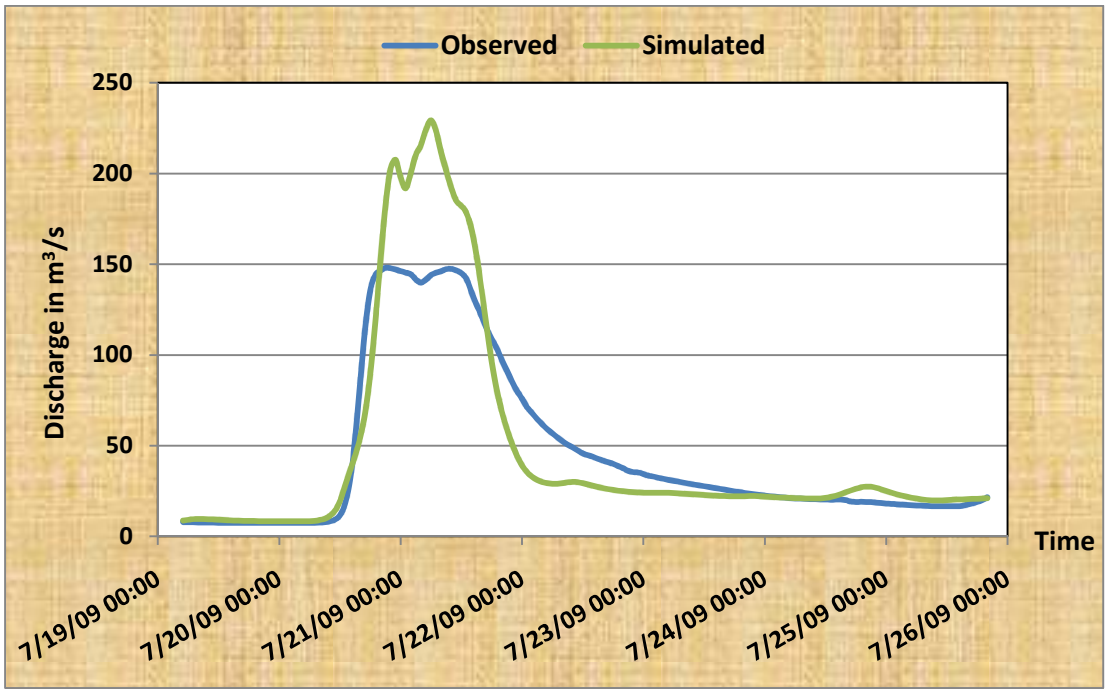


**Figure 50 : Hydrographs at Eggafoss gauging station (uncalibrated interior station) using gauge simulated precipitation input method**

### 5.4.3.3 Discussions

All the calibration point and uncalibrated interior gauging stations show a sharp peak with special shape of the simulated hydrograph that cannot handle some of the peak flows. At HugdalBru and Lillebudal gauging stations, underestimation of the simulated flow has been revealed both in objective and hydrograph methods of result comparison with a special trend at the Lillebudal gauging station that may require a further analysis of why gauge simulated precipitation input method show such trend.

Contrary to the gauge IDW precipitation input method, the gauge simulated precipitation input gave a very good result at the Eggafoss gauging station which is encouraging for its spatial representation than gauge IDW precipitation input method. Like the bias corrected radar precipitation and gauge IDW precipitation input methods, the recession hydrograph shows abrupt change from high to low flows.

## 5.5 Calibration and Findings of 2006 event (27-07-2006 00:00 to 29-07-2006 23:00)

During the precipitation period of the 2006 selected event, the spatial distribution of precipitation varies very much within the study catchment. There is precipitation in some part of the catchment and none in another part. The contribution of flow at the calibration point from different gauging stations is not proportional to their catchment area. This can be justified by looking at the shape of the hydrographs of the gauging stations. **Fig.51** elaborates this statement.

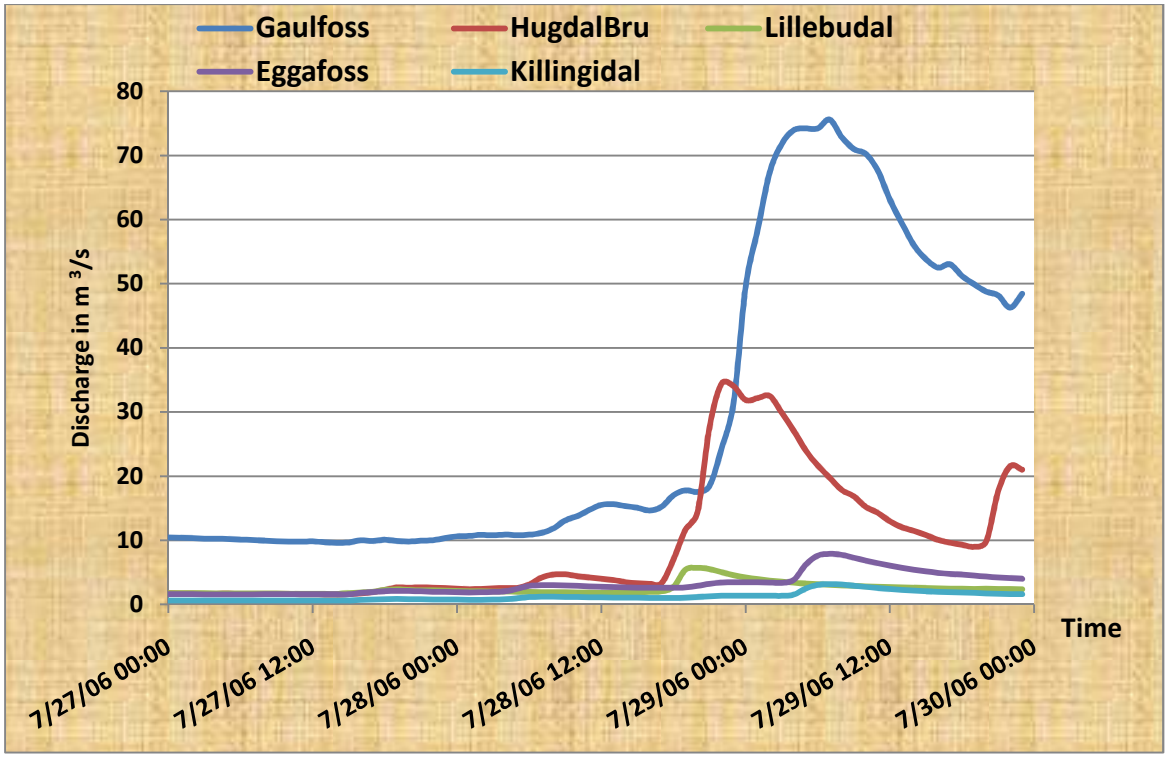


**Figure 51 : Hydrographs observed at the calibration point (Gaulfoss) and uncalibrated interior gauging stations**

Contrary to the 2009 event, it is clear that almost half of the total peak at the Gaulfoss gauging station is contributed by HugdalBru gauging station that covers only 20% of the total catchment area. During the peak period of the selected event, other gauging stations do not show any rise up of their hydrographs. Therefore, it can be concluded that most precipitation has occurred only to 20% of the total catchment and the event is a localized, low peak type.

### *5.5.1 Model Calibration Using Bias Corrected Radar Precipitation Input Method*

Since the 2006 event is localized, it is difficult to calibrate using gauge IDW and gauge simulated precipitation input methods because of the fact that gauges cannot capture precipitation which is confined to only some places of the study catchment while rain gauges are situated somewhere else. Therefore, only bias corrected precipitation input method has been used to tryout the performance of the model. The findings of the objective and hydrograph methods of result comparison have been presented in the following section.

**Table17 : Summary of final calibration parameters for different precipitation input methods**

| **Precipitation input method** | **Calibration parameters** | | | | | |
|---|---|---|---|---|---|---|
| | **m** (mm) | **$T_o$** ($mm^2$/hr) | **V** (m/s) | **$t_d$** (hr/mm) | **RZmax** (mm) | **RZinit.** (mm) |
| Bias corrected radar | 25 | 18000 | 0.1 | 0.0005 | 10 | 0.0002 |

#### 5.5.1.1 Objective Results

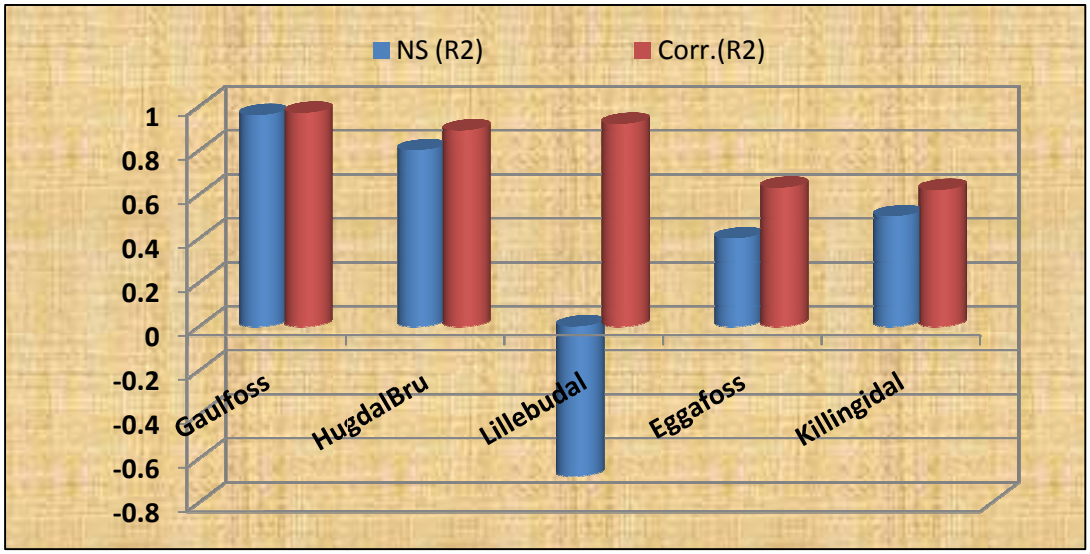


**Figure 52: Nash Sutcliff Index (NS) and Correlation coefficient results of the calibration point and uncalibrated internal gauging stations**

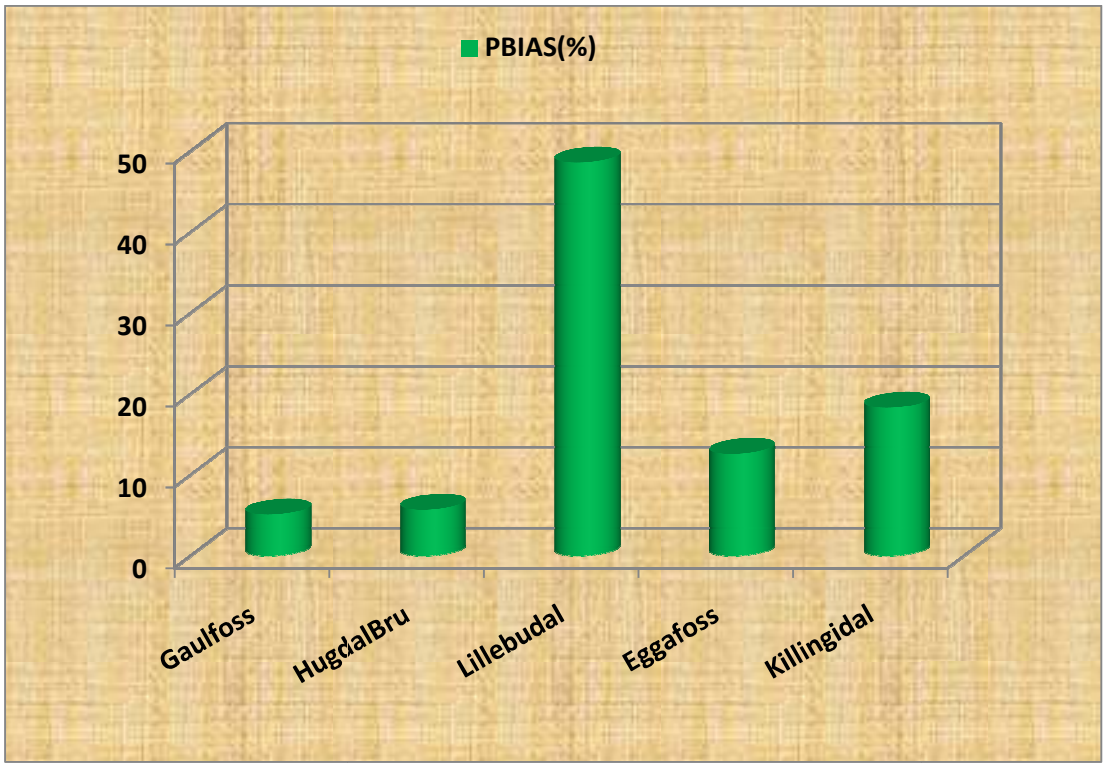


**Figure 53: Percent Deviation results of the calibration point and uncalibrated internal gauging stations**

**Table 18 : Summary of statistics for the calibration point and uncalibrated interior gauging stations using bias corrected precipitation input method.**

| **Objective methods of result comparison** | **Calibration point Gauging station (Gaulfoss)** | **Uncalibrated interior gauging stations** | | | |
|---|---|---|---|---|---|
| | | **HugdalBru** | **Lillebudal** | **Eggafoss** | **Killingidal** |
| Average measured flow ($m^3/s$) | 28.6 | 9.4 | 2.5 | 3.2 | 1.3 |
| Average simulated flow ($m^3/s$) | 27.1 | 8.8 | 1.3 | 2.8 | 1 |
| Nash sutcliff index (NS. $R^2$) | 0.96 | 0.87 | -0.68 | 0.4 | 0.5 |
| Correlation (Corr.$R^2$) | 0.97 | 0.89 | 0.92 | 0.63 | 0.62 |
| Percent deviation (PBIAS %) | 5.1 | 5.7 | 48.6 | 12.6 | 18.3 |

### 5.5.1.2 Hydrographs

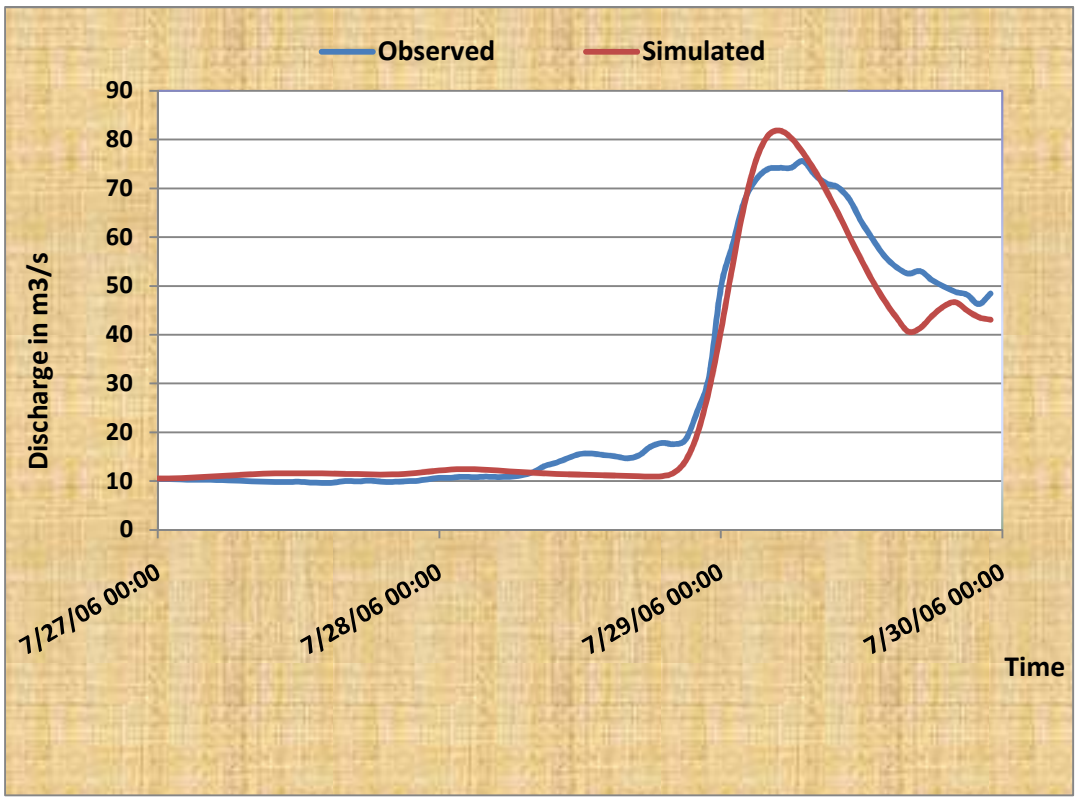


**Figure 54 : Hydrograph at the calibration point (Gaulfoss) using bias corrected radar precipitation input method**

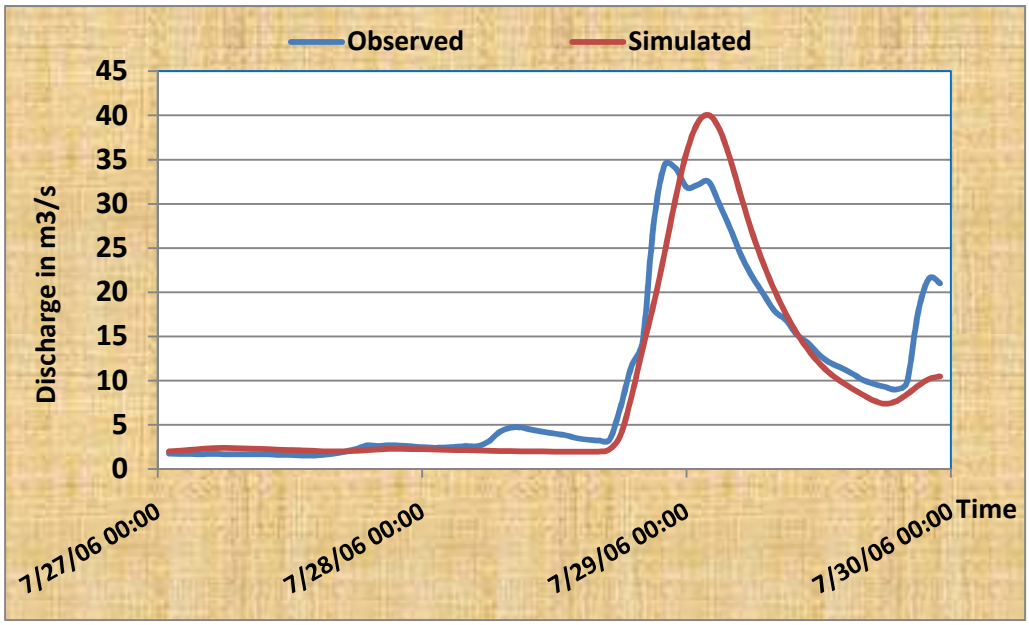


**Figure 55: Hydrograph at the HugdalBru gauging station (uncalibrated interior gauging station) using bias corrected radar precipitation input method**

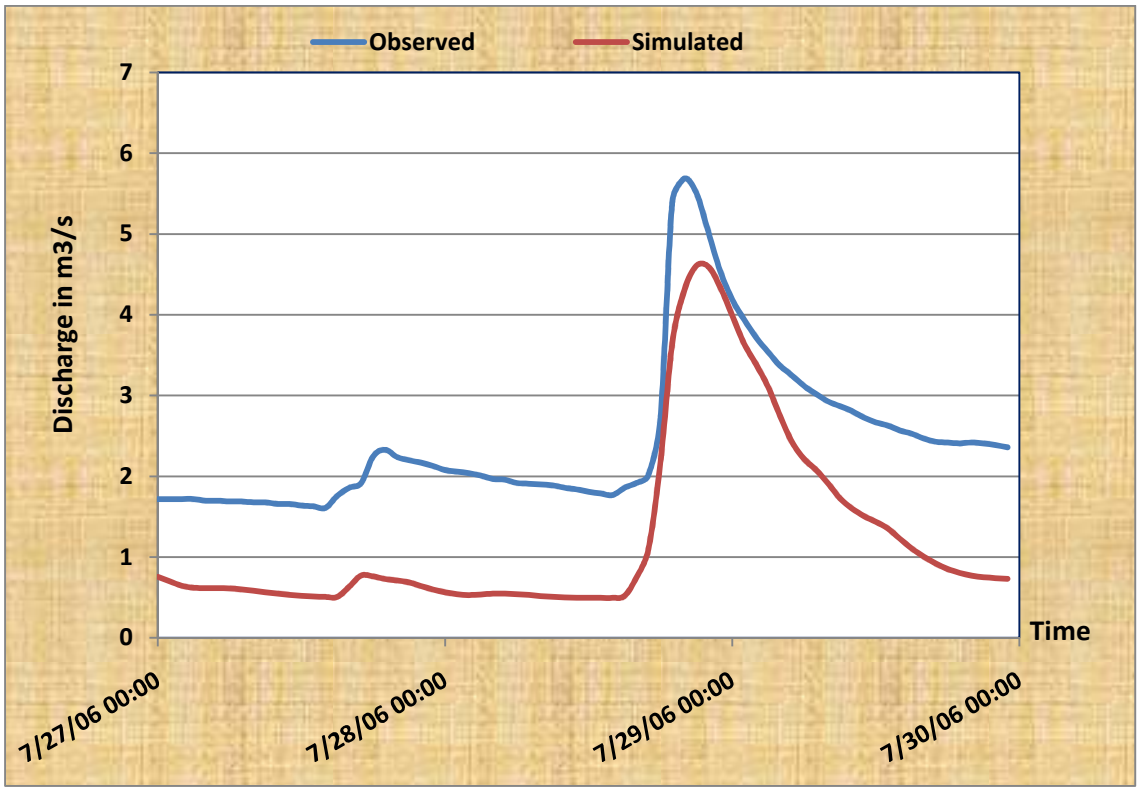


**Figure 56: Hydrographs at Lillebudal gauging station (uncalibrated interior station) using bias corrected radar precipitation input method**

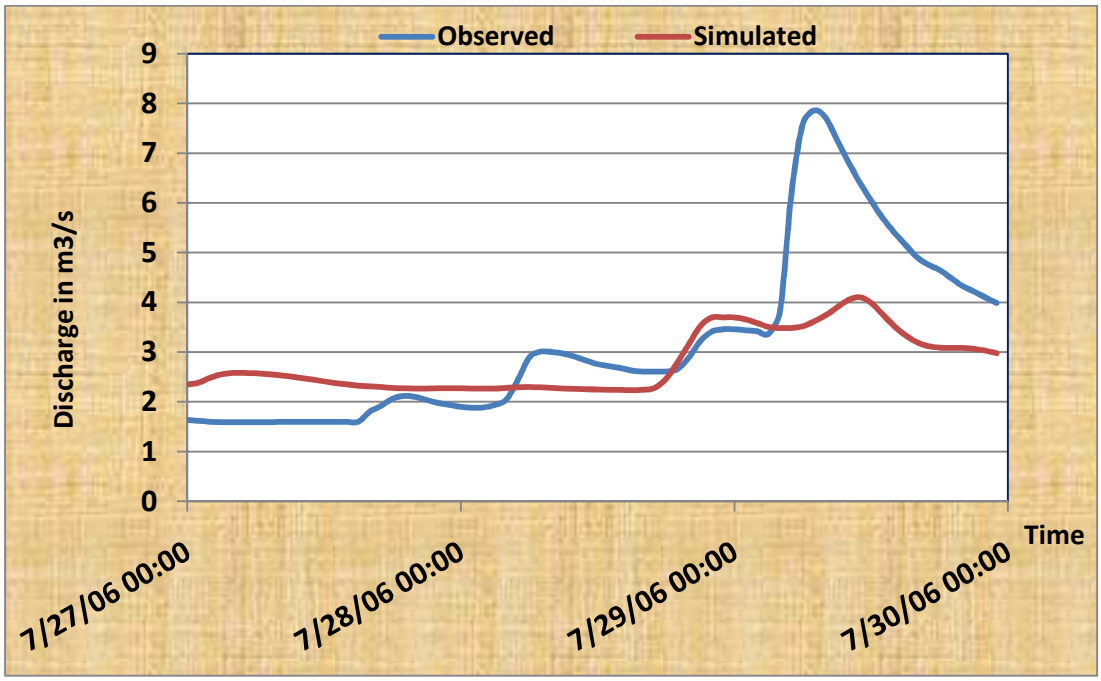


**Figure 57: Hydrographs at Eggafoss gauging station (uncalibrated interior station) using bias corrected radar precipitation input method**

#### 5.5.1.3 Discussions

For 2006 event, only bias corrected radar precipitation input method made possible the calibration process; because of the fact that calibration is difficult for events that confined only to some part of the catchment while rain gauge stations are located at non-precipitation part of the catchment. At the calibration point gauging station (Gaulfoss) and the HugdalBru interior gauging station, a very good performance of the model has been observed with a little overestimation of the peak flows and underestimation of low flows. At the Eggafoss and Lillebudal gauging stations, poor performance of the model has been observed. The poor performance of the interior unclibrated gauging stations may be resulted from the lumped input of some of the initial state and recession parameters due to lack of detail investigations or the poor bias correction method adopted or the combination of the two.

### *5.5.2 Sample Analysis of Highly Localized Event*

One of the objectives of this study is to assess the applicability of TOPLAND hydrological modelling in handling a short term events which are highly localized. The following figures illustrate the assessment using an hour precipitation event on a small sub- catchment of the study site (sub-catchment ID 24). **Fig. 58 A, B** & **C** shows the radar precipitation pattern for three consecutive hours and **Fig.60** shows the responses to these events at different selected locations.

A. Radar precipitation pattern over Gaula catchment in mm on 25-07-2006 15:00

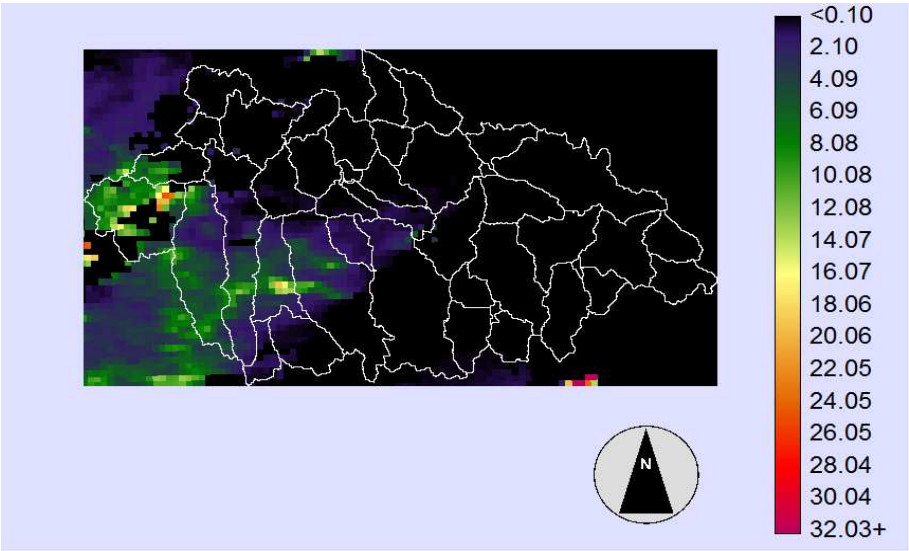

B. Radar precipitation pattern over Gaula catchment in mm on 25-07-2006 16:00

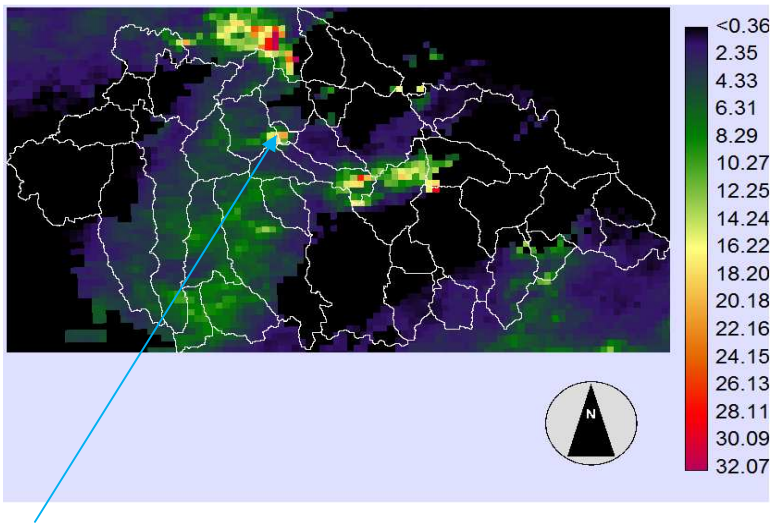


Location of Stream ID 24 (point of interest)

C. A radar precipitation pattern over Gaula catchment in mm on 25-07-2006 17:00

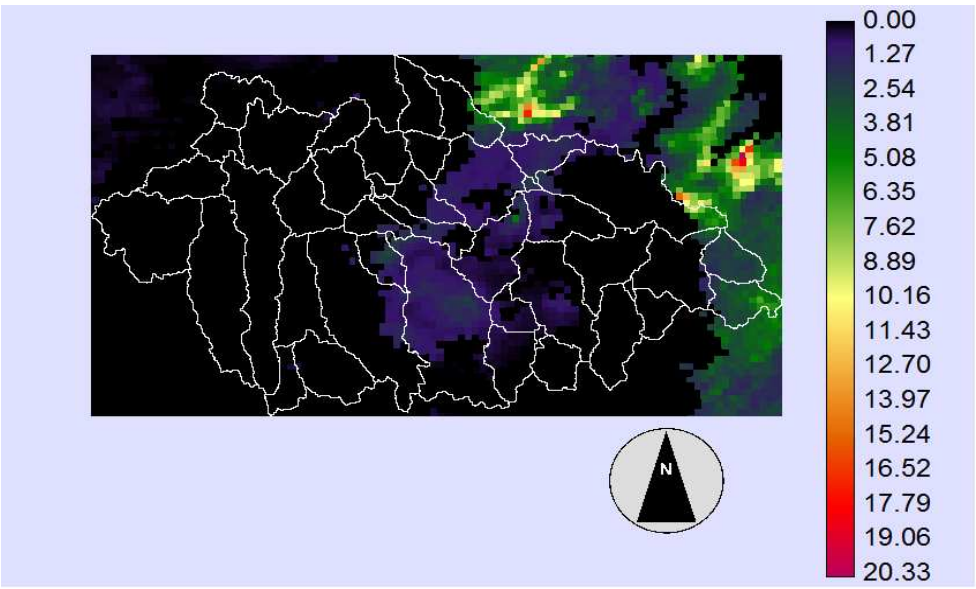


**Figure 58 : Radar precipitation distribution over gaula catchment for consecuative three hours of the 2006 event**

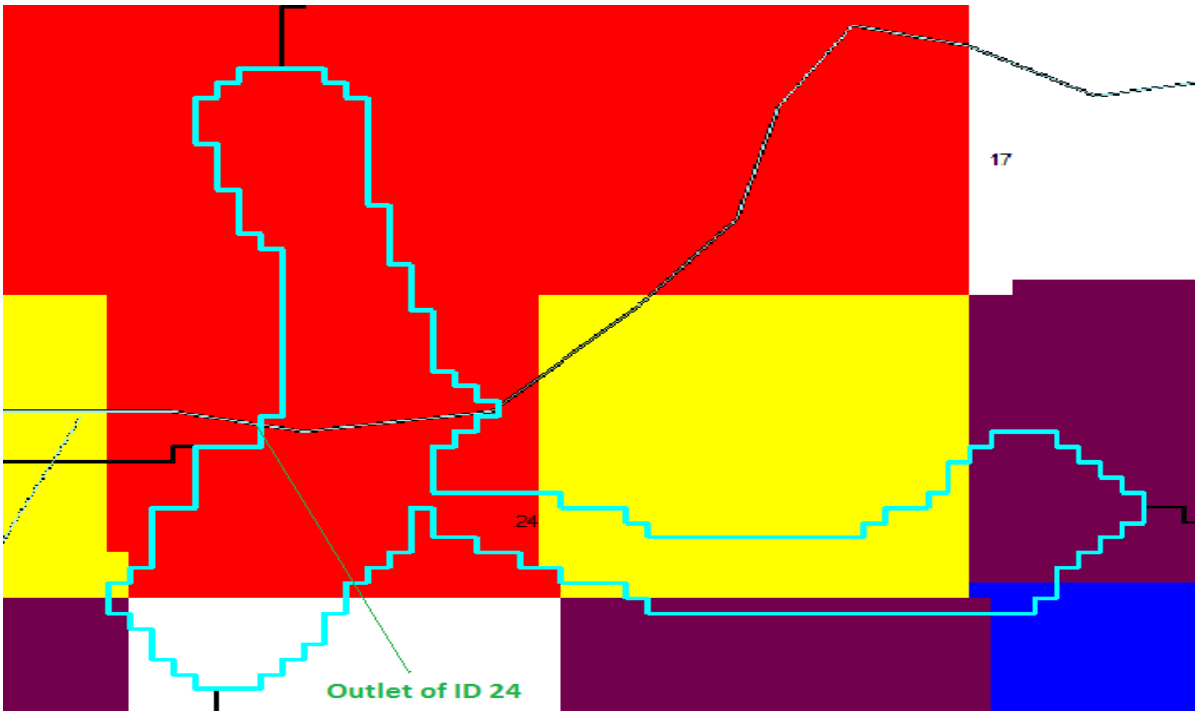


**Figure 59: Detail of sub-catchment ID 24 receiving a highly localized 18.5mm (red) high magnitude precipitation on 25-07-2006 16:00**

The response at the outlet of sub catchment ID 24 and other selected locations is shown in the following figure.

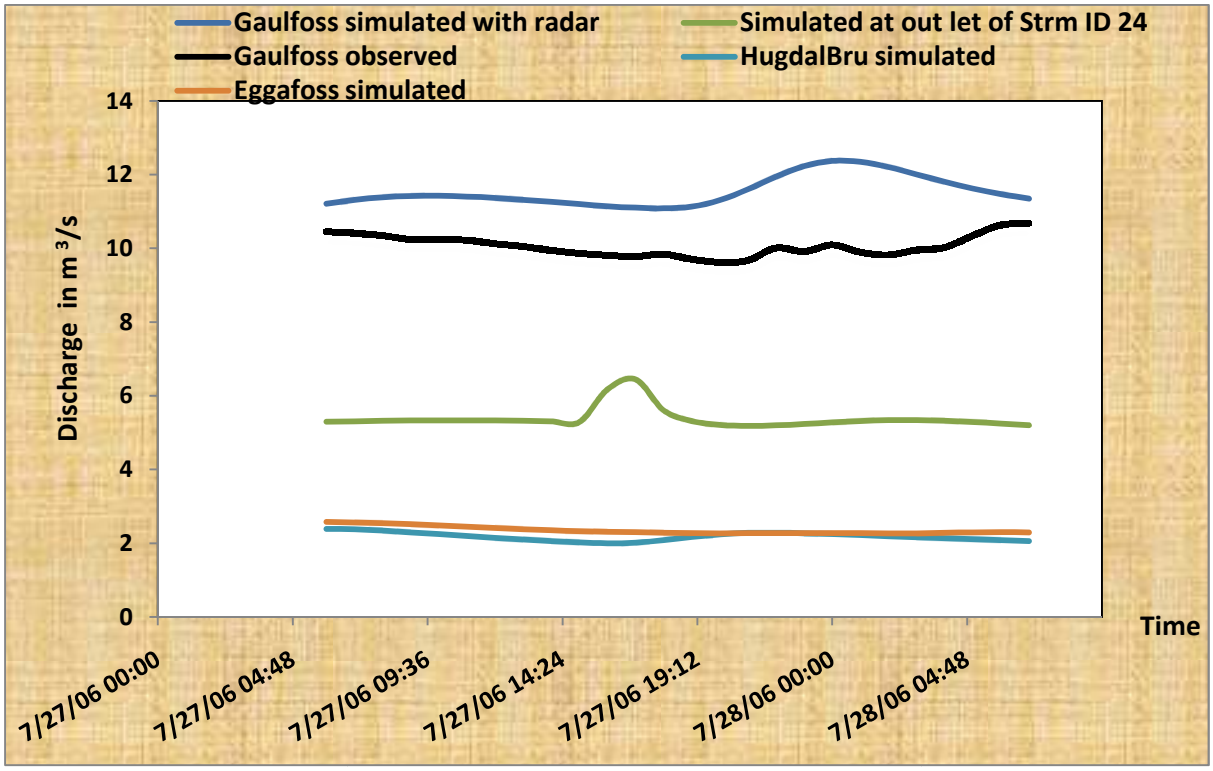


**Figure 60: Responses to the localized precipitation events at some selected locations**

From **Fig.60,** the outlet of sub-catchment with identification number 24 (ID 24) responds to the localized high precipitation event with a sharp peak while at the calibration point (Gaulfoss), this peak has been smoothed out. At the Hugdalbru and Eggafoss gauging stations, there is no rise of the simulated hydrograph during this period and the radar data also shows that there is no precipitation in these sub-catchments during the specified period.

The sample analysis confirms that highly localised events can be handled in the model and their local impact can be predicted. Literatures show that this specific localised event was a thunderstorm at the sub-catchment ID 24 and caused landslide to the local area.

# 6. CONCLUSIONS AND RECOMMENDATIONS

## 6.1 CONCLUSIONS

### *6.1.1 CONCLUSIONS FOR 2006 LOCALIZED AND LOW PEAK EVENT*

From the manual calibration results of the TOPLAND model on localized and low peak 2006 events, the following preliminary conclusions can be set:

- It is difficult to calibrate such localized event using either rain gauge or gauge simulated precipitation methods using TOPLAND model where the density of rain gauges inside the study area is poor, i.e. calibration is impossible while there is no precipitation in the rain gauges (there are only two rain gauges situated at downstream side of the catchment).
- Bias corrected radar precipitation is applicable both at calibration point and internal uncalibrated gauging stations with some limitations that may be caused by bias correction method, lack of spatially variability of initial state maps or combination of the two.
- Handling of peak flow from highly localized and short-term event, which cannot be handled with rain gauges, has shown a positive and encouraging result with bias corrected radar precipitation.
- For localized events, TOPLAND model can show a very good performance if appropriate bias correction method and appropriate spatial variations of the recession and distributed parameters are made possible.
- With the existing conditions, the TOPLAND model performance for the selected localized and low peak event is not as good as the uniformly distributed and high peak 2009 event.

### *6.1.2 CONCLUSIONS FOR 2009 DISTRIBUTED AND HIGH PEAK EVENT*

- All the three precipitation input methods, i.e. Gauge IDW interpolation, Gauge simulated and bias corrected radar precipitation can be used efficiently for stream flow prediction both at the calibration point and uncalibrated interior gauging stations especially if the event is preceded by dry periods,
- TOPLAND model has shown encouraging result for its applicability to a relatively uniform precipitation event in Gaula catchment.
- Flows can be predicted well with little or no calibration at the uncalibrated interior internal gauging stations.
- Bias corrected radar precipitation input method is the best of all precipitation input methods for TOPLAND model performance both at the calibration and uncalibrated interior gauging stations.
- The preliminary results indicate that, calibration parameters of gauge IDW interpolation can be used interchangeably with the gauge simulated calibration parameters with a little error.
- The preliminary investigation shows that, bias corrected radar precipitation parameters data cannot be used for calibration of gauge IDW interpolation or gauge simulated precipitation input methods.

## 6.2 OVER ALL RECOMMENDATIONS

**I**.Since the preliminary investigation of recession analysis shows that the lateral transmissivity decreases linearly with depth, detailed and automated recession analysis has to be carried out, since this is one of the factors that determine whether the original TOPMODEL assumption has to be revised or not.

**II**. The Master Recession Curve analysis has been done using daily flow data by assuming that recession analysis does not depend much on the time scale variation. The calibration parameter 'm' of the TOPMODEL gave a higher result than what has been computed. Therefore, further analysis on the dependency of recession analysis on time scale should be done.

**III**. The possibility of development of perched saturated zone (local saturated zone before the infiltrated water reaches ground water) has to be assessed so that modification of the original TOPMODEL –TOPLAND may be possible.

**IV**. Detailed soil map of some representative sites has to be prepared so that initial state maps and other input parameters like saturated lateral transmissivity (To) can be handled by the model in distributed or semi-distributed manner.

**V**. Appropriate method to handle pixels of zero slope and upslope contributing area has to be searched for computation of topographic index of the catchment.

**VI**. Appropriate method of computation for longitudinal slope, that used for kinematic routing, has to be used to avoid negative and zero slope problems.

**VII**. A defined relation between cross sectional area versus top width has to be developed by appropriate methods for a range of discharges at different representative locations of the Gaula River.

**VIII**. Since sources of errors in radar data has a complex nature, appropriate method of correction has to be implemented.

# REFERENCES

A.GÜntner, S. Uhlenbrook, J. Seibert and Ch. Leibundgut, 1999: Multi-criterial validation of TOPMODEL in a mountainous catchment. Hydrological processes; Hydrol. Process.13, 1603-1620.

Alphonce Chenjerayi Gusha.T.B. Hardy, 2009: Application of the distributed hydrological model, TOPNET, to the Big Darby Creek Watershed, Ohio, USA

Andreas Schild, Pratap Singh, Johannes HÜbl, 1998: Application of GIS for hydrological modelling in high mountain areas of the Austrian Alps. Hydrology, Water resources and Ecology in headwaters. IAHS Publ.no.248.

Beven, K.J., Kirkby, M.J., 1979: A physically based variable contributing area model of basin hydrology. Hydrological Sciences Bulletin 24(1), 43-69.

Bruno Ambroise, Keith Beven and Jim Freer,1996: Toward a generalization of the TOPMODEL concepts: Topographic indices of hydrological similarity. Water Resources research 95WR03716.

Christina Banedaragoda, David G. Tarboton, Ross Woods , 2004: Application of TOPNET in the distributed model intercomparison project. Journal of Hydrology 298 (2004) 178 - 201

David Maidment and Oscar Robayo, 2002: Arc hydro tutorial prepared by ESRI.

David G. Tarboton, 2008: Terrain Analysis Using Digital Elevation Model (TauDEM).

David G. Tarboton, 1997: A new Method for the Determination of Flow directions and Upslope areas in grid digital elevation models. Water resources research, 33(2): 309-319.

David Kinner[1.2],Helena Mitasova, Robert Stallard, Russell S. Harmon, and Laura Toma, 2005. GIS -based stream network analysis for the upper Río Chagres basin, Panama.

David Nagel, 2005: Using TauDEM streams to generate a Stream gradient profile.

David Nagel, Richard Cissel, Sharon Parks, 2008: TauDEM procedures and notes.

Héctor D. Rivera – Ramírez, Glenn S. Warner,and Frederick N. Scatena, 2002: Prediction of master recession curves and base flow recessions in the Luquillo Mountains of Puerto rico. Journal of the American Water Resource Association.

Iwan Holleman, 2007: Bias adjustment and long-term verification of radar-based precipitatiin estimates. Royal Netherlands Meteorological Institute (KNMI), The Netherlands.

J. G. Arnold, P.M.Allen, R.Muttiah, and G.Bernhardt, 1995: Automated base flow and recession analysis techniques.

John B. Lindsay, 2005: The terrain analysis system: a tool for hydro-geomorphic applications. Hydrological processes; Hydrol.Process.19, 1123-1130.

John Snell [a], Murugesu Sivapalan, Bryson Bates, 2004: Non-linear kinematic dispersion in channel network response and scale effects: application of the meta-channel concept. Advances in Water Resources 27, 141-154.

Keith J. Bven ,2002: Rainfall – Runoff Modelling, The Primer.Chichester: John Wiley &Sons.

Keith Beven, 1997: TOPMODEL: A critique. Hydrological processes. Vol.11, 1069-1085

Kohei Matsunaga, Toshihiko Sugai, Tomoki Nakaya. 2009. Simple DEM-Based methods to delineate Channel Network for Hydrogeomorphological Mapping.

L.M. Tallaksen, 1995: A review of baseflow recession analysis. Journal of Hydrology 165, 349-370.

Lena Tallaksen, 1989: Analysis of time variability in recessions.

Luis S. Pereira, Hans M, keller, 1982: Recession characterization of small mountain basins, derivation of master recession curves and optimization of recession parameters. IAHS Pub1.no. 138.

Madhusudan B. Shrestha and Toshitaka Miyazaki, 2006: GIS application on drainage network extraction.

Martyn P.Clark, David E. Rupp, Ross A.Woods, Xiaogu Zheng ,Richard P. Ibbitt, Andrew G. Slater, Jochen Schmidt, Michael J.Uddstrom, 2008: Hydrological data assimilation with the ensemble Kalman filter: Use of stream flow observations to update states in a distributed hydrological model. Advances in Water Resources 31, 1309-1324.

Newsha K. Ajami , Hoshin Gupta, Thorsten Wagener, Soroosh Sorooshian, 2004: Calibration of a semi–distributed hydrological model for stream flow estimation along a river system. Journal of Hydrology 298, 112-135.

Richard M. Vogel, Charles N. Kroll, 1996: Estimation of base flow recession constants. Water resource management 10: 303-320.

R.Sørensen , U.Zinko, and J.Seibert , 2005: On the calculations of the topographic wetness index: evaluation of different methods based on field observations.

Robert Lamb and Keith Beven, 1997: Using interactive recession curve analysis to specify a general catchment storage model. Hydrology and Earth System Sciences,1, 101-113.

Scann Reed, Victor Koren , Ziya Zhang, Michael Smith, Dong-June Seo, 1994: Hydrology Laboratory, Office of Hydrologic Development, National wether Service, NOAA 1492

Seibert, J., 1999: Conceptual models – fiction or representation of reality? Acta Univ. Ups., Compressive Summaries of UPPsala Dissertations from the Faculty of Science and Technology 436.52 pp. Uppsala.ISBN 91 – 554-4402-4.

Stefan Uhlenbrook, Stefan Roser, Nils Tilch, 2004: Hydrological process at the meso-scale: the potential of a distributed, conceptual catchment model. Journal of Hydrology 291, 278-296.

Sun Shufen, Deng Huiping, 2004: A study of Rainfall-Runoff response in a catchment using TOPMODEL. Advances in atmospheric Sciences, Vol.21, no.1, 87-95.

Trond Rinde, 1998: LANDPINE – A Hydrological model to simulate the influence of Land – use changes on runoff.

US Army Corps of Engineers, 1993: Introduction and Application of Kinematic Wave Routing Techniques Using HEC-1.

Yisak Sultan Abdella, June2005: Application and Comparison of a Distributed Hydrological Model for a Tropical and Temperate Catchment. M.Sc.Thesis, Norwegian University of Science and Technology.

# APPENDIX

## APPENDIX 1: BIAS CORRECTION FACTORS FOR 2006 RADAR PRECIPITATION

| Date | Gauge data | Radar data | correction factor | Date | Gauge data | Radar data | correction factor |
|---|---|---|---|---|---|---|---|
| 27/07/2006 00:00 | 0.00 | 0.00 | 1.00 | 28/07/2006 12:00 | 0.00 | 0.00 | 1.00 |
| 27/07/2006 01:00 | 0.00 | 0.00 | 1.00 | 28/07/2006 13:00 | 0.00 | 0.00 | 1.00 |
| 27/07/2006 02:00 | 0.00 | 0.00 | 1.00 | 28/07/2006 14:00 | 2.08 | 3.59 | 0.58 |
| 27/07/2006 03:00 | 0.00 | 0.00 | 1.00 | 28/07/2006 15:00 | 0.29 | 0.96 | 0.30 |
| 27/07/2006 04:00 | 0.00 | 0.00 | 1.00 | 28/07/2006 16:00 | 10.25 | 9.63 | 1.06 |
| 27/07/2006 05:00 | 0.00 | 0.00 | 1.00 | 28/07/2006 17:00 | 7.30 | 18.12 | 0.40 |
| 27/07/2006 06:00 | 0.00 | 0.00 | 1.00 | 28/07/2006 18:00 | 18.37 | 19.62 | 0.94 |
| 27/07/2006 07:00 | 0.00 | 0.00 | 1.00 | 28/07/2006 19:00 | 15.77 | 13.10 | 1.20 |
| 27/07/2006 08:00 | 0.00 | 0.00 | 1.00 | 28/07/2006 20:00 | 4.06 | 8.95 | 0.45 |
| 27/07/2006 09:00 | 0.00 | 0.00 | 1.00 | 28/07/2006 21:00 | 5.85 | 4.53 | 1.29 |
| 27/07/2006 10:00 | 0.00 | 0.00 | 1.00 | 28/07/2006 22:00 | 0.10 | 0.30 | 0.33 |
| 27/07/2006 11:00 | 0.00 | 0.00 | 1.00 | 28/07/2006 23:00 | 0.00 | 0.00 | 1.00 |
| 27/07/2006 12:00 | 0.00 | 0.00 | 1.00 | 29/07/2006 00:00 | 0.00 | 0.00 | 1.00 |
| 27/07/2006 13:00 | 0.00 | 0.00 | 1.00 | 29/07/2006 01:00 | 0.00 | 0.00 | 1.00 |
| 27/07/2006 14:00 | 0.00 | 0.00 | 1.00 | 29/07/2006 02:00 | 0.00 | 0.00 | 1.00 |
| 27/07/2006 15:00 | 35.96 | 24.52 | 1.47 | 29/07/2006 03:00 | 0.00 | 0.00 | 1.00 |
| 27/07/2006 16:00 | 5.15 | 5.10 | 1.01 | 29/07/2006 04:00 | 0.02 | 0.35 | 0.06 |
| 27/07/2006 17:00 | 6.34 | 10.29 | 0.62 | 29/07/2006 05:00 | 0.00 | 0.00 | 1.00 |
| 27/07/2006 18:00 | 0.81 | 1.55 | 0.52 | 29/07/2006 06:00 | 0.00 | 0.00 | 1.00 |
| 27/07/2006 19:00 | 0.42 | 1.09 | 0.38 | 29/07/2006 07:00 | 0.00 | 0.00 | 1.00 |
| 27/07/2006 20:00 | 0.62 | 2.75 | 0.23 | 29/07/2006 08:00 | 0.00 | 0.00 | 1.00 |
| 27/07/2006 21:00 | 3.97 | 6.27 | 0.63 | 29/07/2006 09:00 | 0.00 | 0.00 | 1.00 |
| 27/07/2006 22:00 | 0.13 | 0.40 | 0.33 | 29/07/2006 10:00 | 0.00 | 0.00 | 1.00 |
| 27/07/2006 23:00 | 0.00 | 0.00 | 1.00 | 29/07/2006 11:00 | 0.02 | 0.88 | 0.02 |
| 28/07/2006 00:00 | 0.00 | 0.00 | 1.00 | 29/07/2006 12:00 | 0.00 | 0.00 | 1.00 |
| 28/07/2006 01:00 | 0.00 | 0.00 | 1.00 | 29/07/2006 13:00 | 0.00 | 0.00 | 1.00 |
| 28/07/2006 02:00 | 0.00 | 0.00 | 1.00 | 29/07/2006 14:00 | 1.14 | 2.56 | 0.44 |
| 28/07/2006 03:00 | 0.00 | 0.00 | 1.00 | 29/07/2006 15:00 | 1.00 | 5.31 | 0.19 |
| 28/07/2006 04:00 | 0.00 | 0.00 | 1.00 | 29/07/2006 16:00 | 0.85 | 1.64 | 0.52 |
| 28/07/2006 05:00 | 0.00 | 0.00 | 1.00 | 29/07/2006 17:00 | 0.00 | 0.00 | 1.00 |
| 28/07/2006 06:00 | 0.00 | 0.00 | 1.00 | 29/07/2006 18:00 | 0.47 | 5.07 | 0.09 |
| 28/07/2006 07:00 | 0.00 | 0.00 | 1.00 | 29/07/2006 19:00 | 1.29 | 4.39 | 0.29 |
| 28/07/2006 08:00 | 0.00 | 0.00 | 1.00 | 29/07/2006 20:00 | 2.80 | 2.75 | 1.02 |
| 28/07/2006 09:00 | 0.00 | 0.00 | 1.00 | 29/07/2006 21:00 | 2.50 | 3.23 | 0.77 |
| 28/07/2006 10:00 | 0.00 | 0.00 | 1.00 | 29/07/2006 22:00 | 0.00 | 0.00 | 1.00 |
| 28/07/2006 11:00 | 0.00 | 0.00 | 1.00 | 29/07/2006 23:00 | 0.00 | 0.00 | 1.00 |

## APPENDIX 2: BIAS CORRECTION FACTORS FOR 2009 RADAR PRECIPITATION

| Date | Gauge data (mm) | Radar data (mm) | correction factor | Date | Gauge data (mm) | Radar data (mm) | correction factor |
|---|---|---|---|---|---|---|---|
| 19/07/2009 05:00 | 0.00 | 0.00 | 1.00 | 20/07/2009 21:00 | 41.48 | 24.99 | 1.66 |
| 19/07/2009 06:00 | 0.76 | 3.24 | 0.23 | 20/07/2009 22:00 | 33.03 | 21.57 | 1.53 |
| 19/07/2009 07:00 | 5.30 | 5.55 | 0.96 | 20/07/2009 23:00 | 32.47 | 21.15 | 1.53 |
| 19/07/2009 08:00 | 7.05 | 7.83 | 0.90 | 21/07/2009 00:00 | 34.10 | 25.99 | 1.31 |
| 19/07/2009 09:00 | 7.31 | 7.32 | 1.00 | 21/07/2009 01:00 | 39.03 | 30.61 | 1.28 |
| 19/07/2009 10:00 | 2.85 | 1.85 | 1.54 | 21/07/2009 02:00 | 37.21 | 29.61 | 1.26 |
| 19/07/2009 11:00 | 0.00 | 0.00 | 1.00 | 21/07/2009 03:00 | 47.09 | 34.96 | 1.35 |
| 19/07/2009 12:00 | 0.00 | 0.00 | 1.00 | 21/07/2009 04:00 | 50.13 | 41.31 | 1.21 |
| 19/07/2009 13:00 | 0.00 | 0.00 | 1.00 | 21/07/2009 05:00 | 42.67 | 36.31 | 1.18 |
| 19/07/2009 14:00 | 2.73 | 3.38 | 0.81 | 21/07/2009 06:00 | 37.77 | 30.59 | 1.23 |
| 19/07/2009 15:00 | 2.76 | 5.75 | 0.48 | 21/07/2009 07:00 | 26.06 | 21.39 | 1.22 |
| 19/07/2009 16:00 | 0.86 | 0.78 | 1.11 | 21/07/2009 08:00 | 16.54 | 14.47 | 1.14 |
| 19/07/2009 17:00 | 0.00 | 0.00 | 1.00 | 21/07/2009 09:00 | 12.83 | 10.49 | 1.22 |
| 19/07/2009 18:00 | 0.00 | 0.00 | 1.00 | 21/07/2009 10:00 | 8.25 | 5.59 | 1.48 |
| 19/07/2009 19:00 | 1.13 | 1.74 | 0.65 | 21/07/2009 11:00 | 3.89 | 4.29 | 0.91 |
| 19/07/2009 20:00 | 5.45 | 6.29 | 0.87 | 21/07/2009 12:00 | 0.53 | 1.19 | 0.44 |
| 19/07/2009 21:00 | 10.94 | 8.05 | 1.36 | 21/07/2009 13:00 | 0.10 | 0.26 | 0.38 |
| 19/07/2009 22:00 | 7.87 | 5.55 | 1.42 | 21/07/2009 14:00 | 0.00 | 0.00 | 1.00 |
| 19/07/2009 23:00 | 9.50 | 10.55 | 0.90 | 21/07/2009 15:00 | 0.00 | 0.00 | 1.00 |
| 20/07/2009 00:00 | 10.23 | 9.26 | 1.11 | 21/07/2009 16:00 | 0.00 | 0.00 | 1.00 |
| 20/07/2009 01:00 | 10.59 | 9.84 | 1.08 | 21/07/2009 17:00 | 0.00 | 0.00 | 1.00 |
| 20/07/2009 02:00 | 16.71 | 11.31 | 1.48 | 21/07/2009 18:00 | 0.00 | 0.00 | 1.00 |
| 20/07/2009 03:00 | 12.93 | 6.04 | 2.14 | 21/07/2009 19:00 | 0.00 | 0.00 | 1.00 |
| 20/07/2009 04:00 | 15.74 | 11.45 | 1.37 | 21/07/2009 20:00 | 0.00 | 0.00 | 1.00 |
| 20/07/2009 05:00 | 27.01 | 15.01 | 1.80 | 21/07/2009 21:00 | 0.00 | 0.00 | 1.00 |
| 20/07/2009 06:00 | 36.85 | 18.91 | 1.95 | 21/07/2009 22:00 | 0.03 | 0.03 | 1.06 |
| 20/07/2009 07:00 | 36.45 | 13.88 | 2.63 | 21/07/2009 23:00 | 0.00 | 0.00 | 1.00 |
| 20/07/2009 08:00 | 34.99 | 13.92 | 2.51 | 22/07/2009 00:00 | 0.20 | 0.02 | 8.18 |
| 20/07/2009 09:00 | 42.28 | 17.25 | 2.45 | 22/07/2009 01:00 | 0.00 | 0.00 | 1.00 |
| 20/07/2009 10:00 | 40.80 | 14.92 | 2.73 | 22/07/2009 02:00 | 0.04 | 0.03 | 1.59 |
| 20/07/2009 11:00 | 44.41 | 18.51 | 2.40 | 22/07/2009 03:00 | 0.00 | 0.00 | 1.00 |
| 20/07/2009 12:00 | 56.78 | 33.68 | 1.69 | 22/07/2009 04:00 | 0.00 | 0.00 | 1.00 |
| 20/07/2009 13:00 | 63.98 | 27.61 | 2.32 | 22/07/2009 05:00 | 0.00 | 0.00 | 1.00 |
| 20/07/2009 14:00 | 82.99 | 32.17 | 2.58 | 22/07/2009 06:00 | 0.00 | 0.00 | 1.00 |
| 20/07/2009 15:00 | 80.57 | 29.46 | 2.74 | 22/07/2009 07:00 | 0.00 | 0.00 | 1.00 |
| 20/07/2009 16:00 | 72.44 | 25.85 | 2.80 | 22/07/2009 08:00 | 0.00 | 0.00 | 1.00 |
| 20/07/2009 17:00 | 75.82 | 26.07 | 2.91 | 22/07/2009 09:00 | 0.00 | 0.00 | 1.00 |
| 20/07/2009 18:00 | 74.17 | 31.05 | 2.39 | 22/07/2009 10:00 | 0.00 | 0.00 | 1.00 |
| 20/07/2009 19:00 | 75.50 | 35.53 | 2.12 | 22/07/2009 11:00 | 0.00 | 0.00 | 1.00 |
| 20/07/2009 20:00 | 61.35 | 34.01 | 1.80 | 22/07/2009 12:00 | 0.00 | 0.00 | 1.00 |

# APPENDIX 3: SUB CATCHMENT AND STREAM REACH PROPERTIES FROM ARC HYDRO

| Sub-cat ID | Next Down ID | number of pixles | Sub-catchment area ($m^2$) | Stream length (m) | Bed slope (%) | Sub-cat ID | Next Down ID | number of pixles | Sub-catchment area ($m^2$) | Stream length (m) | Bed slope (%) |
|---|---|---|---|---|---|---|---|---|---|---|---|
| 1 | -1 | 23206 | 58015000 | 10665.86 | 0.12 | 26 | 12 | 45165 | 112912500 | 24714.75 | 2.28 |
| 2 | 6 | 21118 | 52795000 | 5101.65 | 1.86 | 27 | 24 | 17239 | 43097500 | 6481.549 | 6.50 |
| 3 | 6 | 22680 | 56700000 | 3373.833 | 2.08 | 28 | 23 | 15541 | 38852500 | 1107.843 | 14.60 |
| 4 | 1 | 10951 | 27377500 | 7830.509 | 0.91 | 29 | 9 | 34412 | 86030000 | 20537.36 | 1.61 |
| 5 | 1 | 39259 | 98147500 | 13265.43 | 0.37 | 30 | 21 | 50854 | 127135000 | 20003.05 | 1.95 |
| 6 | 16 | 12521 | 31302500 | 8035.534 | 3.10 | 31 | 23 | 49063 | 122657500 | 37706.53 | 2.43 |
| 7 | 8 | 14716 | 36790000 | 3522.056 | 9.58 | 32 | 21 | 36528 | 91320000 | 13262.49 | 0.68 |
| 8 | 5 | 33 | 82500 | 262.132 | 1.05 | 33 | 34 | 18286 | 45715000 | 3389.214 | 0.62 |
| 9 | 5 | 25695 | 64237500 | 15116.04 | 1.82 | 34 | 37 | 37973 | 94932500 | 13286.14 | 2.15 |
| 10 | 18 | 16880 | 42200000 | 4729.163 | 4.90 | 35 | 34 | 19839 | 49597500 | 5922.971 | 1.32 |
| 11 | 16 | 48466 | 121165000 | 16538.83 | 0.37 | 36 | 32 | 30964 | 77410000 | 9743.377 | 2.67 |
| 12 | 4 | 23187 | 57967500 | 8163.351 | 1.23 | 37 | 32 | 1240 | 3100000 | 1769.239 | 4.17 |
| 13 | 17 | 20655 | 51637500 | 3865.254 | 5.54 | 38 | 9 | 51515 | 128787500 | 26611.81 | 1.36 |
| 14 | 4 | 39427 | 98567500 | 35193.79 | 2.04 | 39 | 37 | 13205 | 33012500 | 1575.305 | 3.92 |
| 15 | 18 | 43137 | 107842500 | 21945.82 | 1.63 | 40 | 42 | 12645 | 31612500 | 226.7767 | 0.00 |
| 16 | 17 | 18284 | 45710000 | 6911.27 | 0.30 | 41 | 42 | 22840 | 57100000 | 6803.122 | 0.42 |
| 17 | 24 | 3171 | 7927500 | 2717.767 | 0.75 | 42 | 30 | 1578 | 3945000 | 2248.528 | 4.01 |
| 18 | 11 | 1516 | 3790000 | 3789.949 | 2.01 | 43 | 30 | 16353 | 40882500 | 1149.264 | 2.52 |
| 19 | 8 | 24373 | 60932500 | 12289.7 | 0.32 | 44 | 29 | 12886 | 32215000 | 1113.173 | 6.51 |
| 20 | 11 | 32 | 80000 | 141.4214 | 0.00 | 45 | 29 | 30609 | 76522500 | 6960.839 | 2.10 |
| 21 | 20 | 28537 | 71342500 | 12948.28 | 0.37 | 46 | 26 | 23779 | 59447500 | 8914.35 | 2.41 |
| 22 | 20 | 36682 | 91705000 | 13652.87 | 3.35 | 47 | 14 | 32637 | 81592500 | 12783.57 | 2.41 |
| 23 | 19 | 13074 | 32685000 | 8018.377 | 2.15 | 48 | 38 | 36227 | 90567500 | 81605284 | 1.76 |
| 24 | 19 | 532 | 1330000 | 662.132 | 0.15 | 49 | 31 | 48793 | 121982500 | 17134.34 | 1.38 |
| 25 | 12 | 59156 | 147890000 | 19850.54 | 1.58 | 50 | 15 | 30436 | 76090000 | 8178.25 | 0.49 |

## APPENDIX4: CROSS-SECTIONAL PROFILE DATA CLOSE TO THE GAULFOSS GAUGING STATIONS

| Distance from bank (m) | Elevation (m) | Distance from bank (m) | Elevation (m) |
|---|---|---|---|
| 0 | 62 | 164.03 | 41.45 |
| 3 | 60 | 166.12 | 41.1 |
| 6 | 57 | 166.73 | 41.1 |
| 10 | 55 | 174.59 | 40.7 |
| 14 | 53 | 175.3 | 40.7 |
| 21 | 50 | 182.99 | 41.72 |
| 24 | 49 | 183.7 | 41.72 |
| 31 | 48 | 186.43 | 41.93 |
| 54 | 47 | 187.14 | 41.93 |
| 63 | 54.8 | 189.19 | 42.38 |
| 71 | 54.8 | 189.62 | 42.38 |
| 82 | 47 | 190.3 | 42.92 |
| 87 | 46.57 | 190.71 | 42.92 |
| 87.35 | 46.57 | 194.48 | 42.54 |
| 96.7 | 44.86 | 197.57 | 42.79 |
| 104.47 | 43.33 | 198.42 | 42.48 |
| 106.34 | 43.24 | 202.19 | 42.5 |
| 111.25 | 43.29 | 205.55 | 43.17 |
| 118.18 | 44.06 | 211.6 | 44.85 |
| 118.89 | 44.06 | 211.79 | 45.25 |
| 121.17 | 45.12 | 212.05 | 45.25 |
| 122.57 | 44.98 | 214.04 | 45.87 |
| 125.42 | 43.63 | 214.75 | 45.87 |
| 126.13 | 43.63 | 220.85 | 48.25 |
| 128.25 | 42.35 | 221.56 | 48.25 |
| 129.83 | 42.15 | 227.59 | 49.65 |
| 133.7 | 42 | 228.3 | 49.65 |
| 137.09 | 42.15 | 233.15 | 50.63 |
| 138.84 | 42.39 | 233.5 | 50.63 |
| 139.55 | 42.39 | 243 | 52 |
| 143.93 | 42.79 | 249 | 54 |
| 144.64 | 42.79 | 251 | 55 |
| 155.42 | 42.11 | 254 | 58 |
| 156.13 | 42.11 | 258 | 59 |
| 159.51 | 42.07 | 264 | 62.5 |
| 160.22 | 42.07 | 346.46 | 63.68 |
| 163.07 | 41.49 | 460 | 65 |

## APPENDIX 5: MRC AND ITS LINEAR TRANSFORMATION FOR HUGDALBRU GAUGING STATION

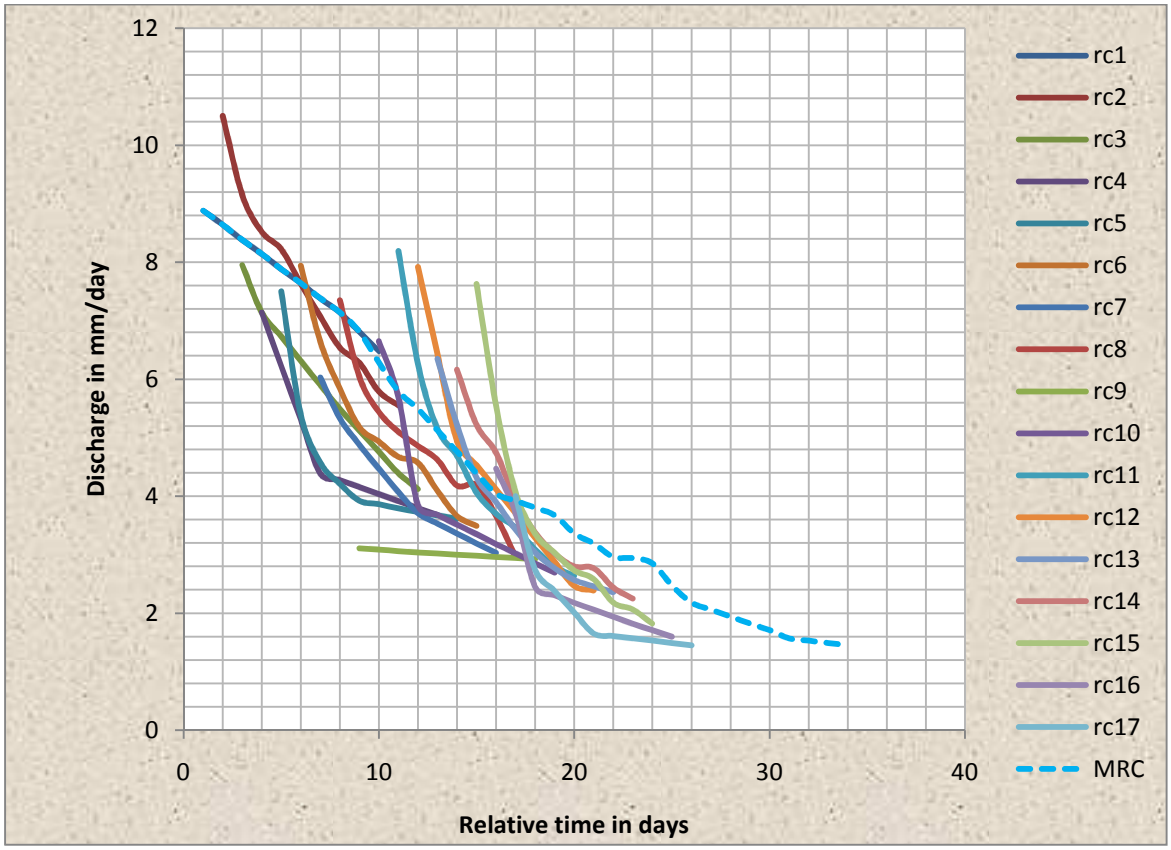


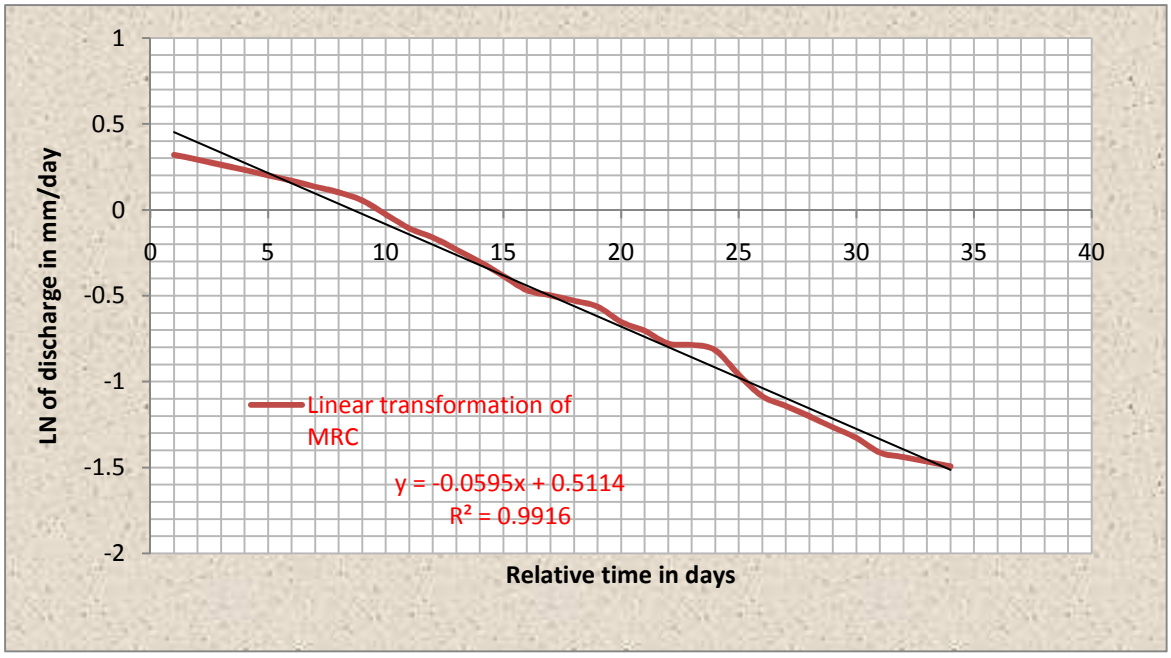

## APPENDIX 6: MRC AND ITS LINEAR TRANSFORMATION FOR LILLEBUDAL GAUGING STATION

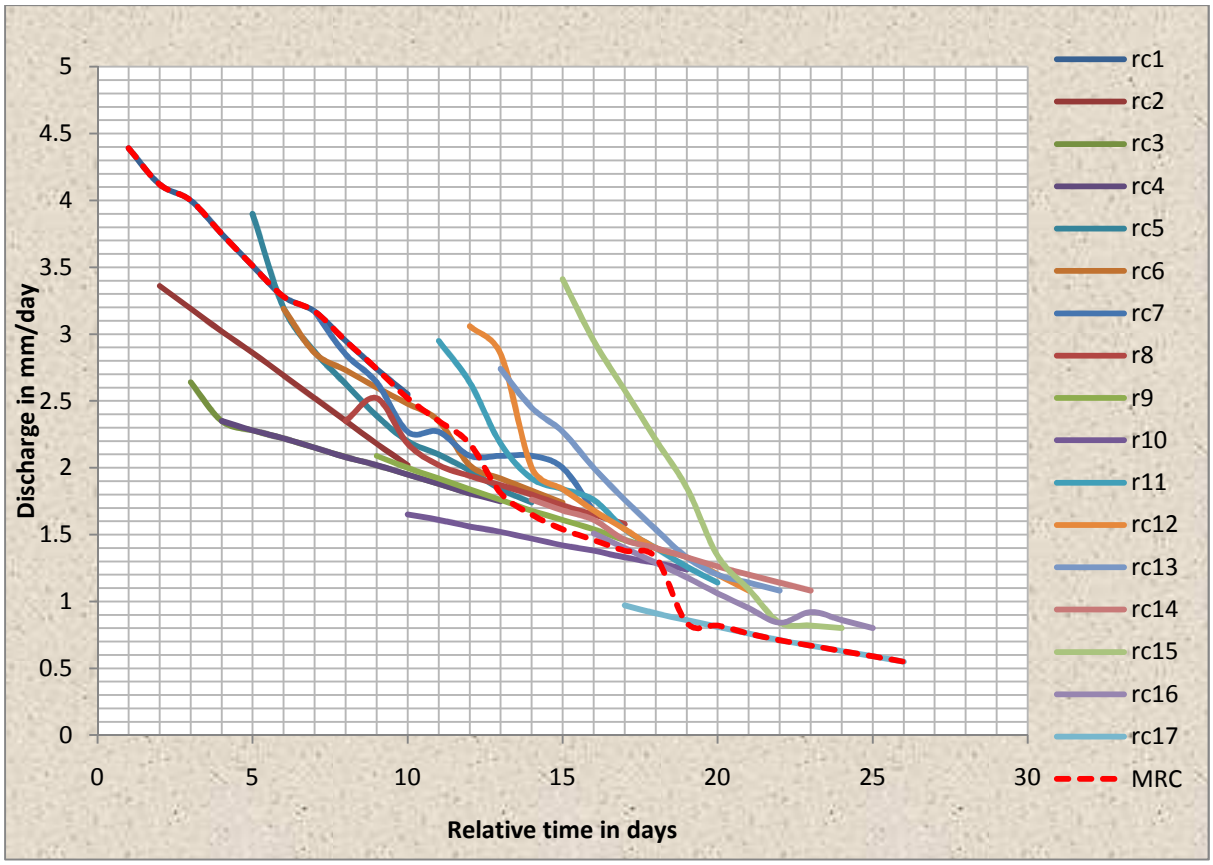


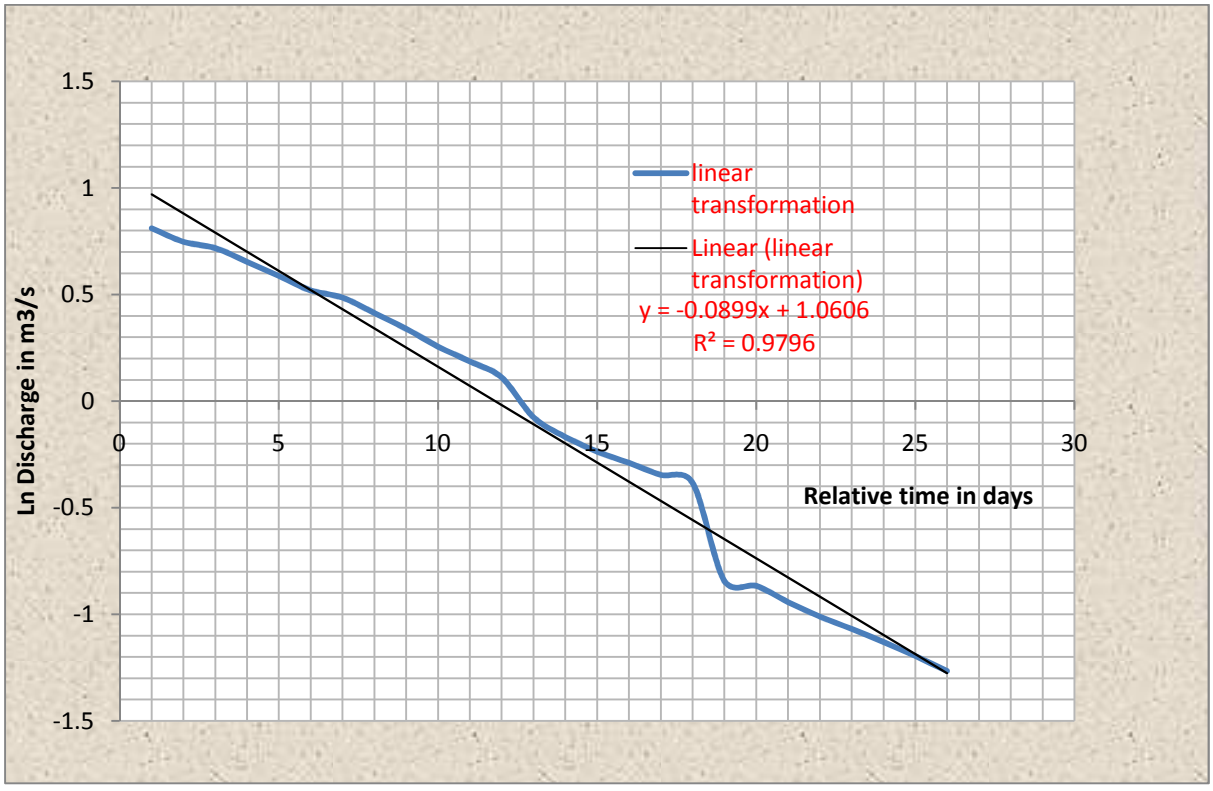

## APPENDIX 7: MRC AND ITS LINEAR TRANSFORMATION FOR EGGAFOSS GAUGING STATION